Aus dem Zentrum für Innere Medizin der Universität Heidelberg

Abteilung Innere Medizin V

Hämatologie, Onkologie und Rheumatologie

Ärztlicher Direktor: Prof. Dr. med. Carsten Müller-Tidow

Reshape of CAR-T cells by overexpression of TCF-1

Inauguraldissertation

zur Erlangung des Doctor scientiarum humanarum

an der

Medizinischen Fakultät Heidelberg

der

Ruprecht-Karls-Universität Heidelberg

vorgelegt von

Hao Yao

aus

dem Taizhou

VR China

2023

Dekan: Prof. Dr. Michael Boutros
Doktorvater: Prof. Dr. med. Michael Schmitt

This thesis is dedicated to my family.

CONTEXT

LIST OF TABLES V
LIST OF FIGURES VI
LIST OF ABBREVIATIONS X
1. INTRODUCTION 1
1.1 Chimeric antigen receptor T cell therapy 1
1.1.1 Chimeric antigen receptor structure 1
1.1.2 Evolution of CAR constructs 3
1.1.2.1 CARs based on scFv 3
1.1.2.1 Novel CARs 4
1.1.3 Production chain of CAR-T cell therapy 5
1.1.4 Commercial CAR-T cell products and clinical response 6
1.2 Limitations of CAR-T cell therapy 9
1.2.1 *Ex vivo* manipulation 10
1.2.2 Disease relapse 10
1.2.2.1 Antigen-positive relapse 10
1.2.2.2 Antigen downregulation or modulation relapse 11
1.2.3 Cytokine release syndrome and neurotoxicity 12
1.2.4 Immunosuppressive microenvironment 12
1.2.5 Lymphoma subtypes 13
1.3 TCF-1 in T cell immunity 13
1.3.1 Overview of TCF-1 13
1.3.2 Role of TCF-1 in the thymus 14
1.3.3 TCF-1 determines $CD4^+$ T helper cell differentiation. 15
1.3.4 TCF-1 as a master regulator of $CD8^+$ T cell fate. 17
1.3.5 The application of TCF-1 in immunotherapy. 19
1.4 Aim of the study 21

2. METHODS AND MATERIALS 22

2.1 Materials 22

2.1.1 Consumables 22

2.1.2 Media, Solutions and Buffers 24

2.1.3 Reagents and chemicals 25

2.1.4 Antibodies 26

2.1.5 Equipment 28

2.1.6 Software 29

2.1.7 Cell lines 30

2.1.8 Healthy donors' samples 30

2.2 Methods 31

2.2.1 Tcf-7 plasmid DNA production 31

2.2.1.1 Transformation 31

2.2.1.2 Growth of bacterial cultures 31

2.2.1.3 Purification of plasmid DNA 31

2.2.1.4 Restriction cloning 32

2.2.1.5 Gel extraction 32

2.2.1.6 DNA fragment extraction from polyacrylamide gels 33

2.2.1.7 Infusion cloning 33

2.2.2 Generation of CAR-T cells and DT.CAR-T cells 34

2.2.2.1 Preparation of plasmid DNA 34

2.2.2.2 Production of retrovirus 34

2.2.2.3 Isolation of peripheral blood mononuclear cells 35

2.2.2.4 Cryopreservation of peripheral blood mononuclear cells 36

2.2.2.5 Thawing of peripheral blood mononuclear cells 36

2.2.2.6 Activation of T cells 36

2.2.2.7 Retroviral transduction of T cells 37

2.2.2.8 Expansion of CAR-T cells and DT.CAR-T cells 37

2.2.3 Western blot 37
2.2.3.1 Cell lysis and protein extraction 37
2.2.3.2 Western blot 38
2.2.4 Killing assay 38
2.2.4.1 Short-term killing assay 39
2.2.4.2 Long-term co-culture assay 39
2.2.5 Flow cytometry 39
2.2.5.1 Cell surface staining 40
2.2.5.2 Intracellular cytokine staining 40
2.2.5.3 Cytokine detection 41
2.2.5.4 Sorting of CAR-T cells and DT.CAR-T cells 41
2.2.6 Elimination of dead cells 41
2.2.7 RNA isolation 42
2.2.8 FACS data mining 42
2.2.8.1 Cell cluster-based algorithm 42
2.2.8.2 Antigen-based algorithm 43
2.2.9 Machine learning-based advanced analysis 43
2.2.9.1 Unsupervised dimensional reduction 43
2.2.9.2 Unsupervised clustering 44
2.2.9.3 Correlation analysis 45
2.2.10 Statistical analysis 45
3. RESULTS 46
3.1 Successful generation of TCF-1$^+$CAR$^+$ T cells 46
3.2 No alteration of the CD4/CD8 component in the final products 48
3.3 Apoptosis resistance contributed to the higher number of DT.CAR-T cells 49
3.4 Modulation of CAR-T cell surface protein expression by overexpression of TCF-1 51

3.4.1 Reduction of apoptosis by overexpression of TCF-1 56

3.4.2 Maintaining of naïve status by overexpression of TCF-1 61

3.4.3 Modulation of CAR-T cell activation by overexpression of TCF-1 65

3.4.4 Modulation of co-stimulatory signal with a trend to inhibition by TCF-1 overexpression 68

3.5 Moderate cytokine release capacity of DT.CAR-T cells correlated with a low CAR density.....72

3.6 Stable short-term killing capability of TCF-1 overexpressed CAR-T cells.....78

3.7 Superior persistence of TCF-1 overexpressed CAT-T cells.....80

3.8 Upregulation of killing related cytokines by DT.CAR-T cells in long-term killing.....85

3.9 Reduction of multiple exhaustion markers in long-term killing. 86

4. DISCUSSION..... 92

5. SUMMARY..... 99

6. DIE ZUSAMMENFASSUNG..... 100

7. REFERENCES 101

8. APPENDIX..... 115

CURRICULUM VITAE 129

ACKNOWLEDGMENT 131

EIDESSTATTLICHE VERSICHERUNG 133

LIST OF TABLES

Table 1: Landmark clinical trials of CAR-T cell products. 8

Table 2. Infusion cloning reaction.....34

Table 3. Retrovirus production reaction. 35

LIST OF FIGURES

Figure 1: Chimeric antigen receptor structure. 2

Figure 2: Single-chain variable fragment (scFv) based chimeric antigen receptor (CAR) 4

Figure 3: Novel chimeric antigen receptors (CARs) 5

Figure 4: Production chain of CAR-T cell therapy 6

Figure 5： An overview of limitations of CAR-T cell therapy 9

Figure 6: T cell development in thymus depends on T cell factor 1 (TCF-1) 15

Figure 7: T cell factor 1 controls T helper cell differentiation 17

Figure 8: $CD8^+$ T cell development depends on T cell factor 1 18

Figure 9: Tex-stem cells response to immune checkpoint blockade (ICB) 20

Figure 10: The expression of CAR and TCF-1 on CAR-T cells and DT.CAR-T cells. 46

Figure 11: The composition of DT.CAR-T cells and protein level of TCF-1 on non-T cells, CAR-T cells, and DT.CAR-T cells. 47

Figure 12: CD4/CD8 composition in CAR-T cells and DT.CAR-T cells 48

Figure 13: Proliferation dynamics of CAR-T cells and DT.CAR-T cells from Day 3 to Day 11 49

Figure 14: The expression of apoptotic proteins in non-transduced T cells, CAR-T cells and DT.CAR-T cells 50

Figure 15: The expression of Ki67 in non-transduced T cells, CAR-T cells and DT.CAR-T cells. 51

Figure 16: Workflow of data mining algorithm. 52

Figure 17: The intensity of apoptosis related proteins on CD19.CAR-T cells and DT19.CAR-T cells in t-SNE plot 53

Figure 18: The intensity of differentiation markers on CD19.CAR-T cells and DT19.CAR-T cells in t-SNE plot 54

Figure 19: The intensity of activation markers on CD19.CAR-T cells and DT19.CAR-T cells in t-SNE plot.....55

Figure 20: The intensity of co-stimulatory markers on CD19.CAR-T cells and DT19.CAR-T cells in t-SNE plot.....56

Figure 21: The dynamics of apoptotic marker expression on CAR-T cells and DT.CAR-T cells. 57

Figure 22: Cell clustering and PCA. 58

Figure 23: Dimension reduction by PCA. 59

Figure 24: Workflow of Venn diagram and clustering of common cell populations 60

Figure 25: Statistical analysis of key cell clusters in CD19.CAR-T cells and DT19.CAR-T cells. 60

Figure 26: Statistical analysis of key cell clusters in CD33.CAR-T cells and DT33.CAR-T cells. 61

Figure 27: Effect of overexpression of TCF-1 on CAR-T cell differentiation over the generation period. 62

Figure 28: Workflow of data mining algorithm. 63

Figure 29: Statistical analysis of key cell clusters. 64

Figure 30: Effect of overexpression of TCF-1 on activation markers (CD27, CD57, CD69) expression on CAR-T cells and DT.CAR-T cells from Day 5 to Day 14. ..65

Figure 31: Workflow of data mining algorithm. 66

Figure 32: Statistical analysis of key cell clusters in CD19.CAR-T cells and DT19.CAR-T cells. 67

Figure 33: Statistical analysis of key cell clusters in CD33.CAR-T cells and DT33.CAR-T cells. 68

Figure 34: Effect of overexpression of TCF-1 on co-stimulatory markers expression on CAR-T cells and DT.CAR-T cells from Day 5 to Day 14. 69

Figure 35: Workflow of data mining algorithm. 70

Figure 36: Statistical analysis of key cell clusters in CD19.CAR-T cells and DT19.CAR-T cells. 71

Figure 37: Statistical analysis of key cell clusters in CD33.CAR-T cells and DT33.CAR-T cells. 72

Figure 38: The relative change of cytokine secretion at different timepoint. 73

Figure 39: Statistical analysis of cytokine release of CAR-T cells and DT.CAR-T cells. 74

Figure 40: Effect of overexpression of TCF-1 on multi-functional CD19.CAR-T cells and DT19.CAR-T cells. 76

Figure 41: Statistical analysis of cytokine release of CD33.CAR-T cells and DT33.CAR-T cells. Effect of overexpression of TCF-1 on multi-functional CD33.CAR-T cells. 77

Figure 42: Statistical analysis of correlation of CAR expression density and quantity of cytokine production by CAR-T cells. 78

Figure 43: Representative dot plots and statistical analysis of killing efficiency of CD19.CAR-T cells and DT19.CAR-T cells after 24 hours in E:T ratio of 1:1 and 1:2. 79

Figure 44: Representative dot plots and statistical analysis of killing efficiency of CD33.CAR-T cells and DT33.CAR-T cells after 24 hours at E:T ratio of 1:1 and 1:2. 80

Figure 45： Workflow of long-term co-culture assay of CAR-T cells 81

Figure 46: Statistical analysis of proliferation of CD19.CAR-T, DT19.CAR-T cells and Raji cells in co-culture assay at E:T ratio of 1:1 and 1:2. 82

Figure 47: Statistical analysis of proliferation of CD19.CAR-T , DT19.CAR-T cells and Nalm6 cells in co-culture assay at E:T ratio of 1:1 and 1:2. 83

Figure 48: Statistical analysis of proliferation of CD33.CAR-T, DT33.CAR-T cells and Nalm6 cells in co-culture assay at E:T ratio of 1:1 and 1:2. 84

Figure 49: Radar plots of cytokines secretion in co-culture assay. 85

Figure 50: Workflow of cell clustering. 86

Figure 51: Locally estimated scatterplot smoothing (LOESS) regression line fitted to the data set from co-culture. 88

Figure 52: Workflow of cell clustering and locally estimated scatterplot smoothing (LOESS) regression line fitted to the data set from co-culture. 91

Appendix Figure 1: The intensity of apoptosis related proteins on CD33.CAR-T cells and DT33.CAR-T cells in t-SNE plot. 115

Appendix Figure 2: The intensity of differentiation markers on CD33.CAR-T cells and DT33.CAR-T cells in t-SNE plot. 116

Appendix Figure 3: The intensity of activation markers on CD33.CAR-T cells and DT33.CAR-T cells in t-SNE plot. 117

Appendix Figure 4: The intensity of co-stimulatory markers on CD33.CAR-T cells and DT33.CAR-T cells in t-SNE plot. 118

Appendix Figure 5: Cell clusters and filtering of apoptotic markers. 119

Appendix Figure 6: Cell clusters and filtering of differentiation markers. 121

Appendix Figure 7: Cell clusters and filtering of activation markers 123

Appendix Figure 8: Cell clusters and filtering of co-stimulatory markers 125

Appendix Figure 9: Workflow of cell clustering and locally estimated scatterplot smoothing (LOESS) regression line fitted to the data set from co-culture. 128

LIST OF ABBREVIATIONS

AMs	Adapter molecules
APCs	Antigen presenting cells
BBB	Blood-brain barrier
BCA	Bicinchoninic acid assay
Bcl11b	B-cell lymphoma/leukemia 11b
BCL6	B cell lymphoma 6
BCMA	B cell maturation antigen
BLIMP1	B lymphocyte induced maturation protein 1
CAR	Chimeric antigen receptor
CLL	chronic lymphocytic leukemia
CLPs	Common lymphoid progenitors
CR	Complete response
CRS	Cytokine Release Syndrome
CXCR5	C-X-C motif chemokinereceptor5
DARPs	Designed ankyrin repeats
DEGs	Differentially expressed genes
DN1	Double-negative $CD4^{-}CD8^{-}$
DP	Double positive
E:T	Effector to target
EMA	European Medicines Agency
Eomes	Eomesodermin
EPTs	Early progenitor thymocytes
FDA	Food and Drug Administration
FOXP3	Forkhead box protein P3
GATA3	GATA binding protein 3
GM-CSF	Granulocyte-colony stimulating factor
GMP	Good Manufacturing Practice
HDAC	Histone deacetylase
HEB	HeLa E-box binding protein
HGBCL	High grade B cell lymphoma
HMG	High-mobility group
ICANS	Immune effector cell-associated neurotoxicity syndrome
ICB	Immune checkpoint blockade
ID2	DNA binding protein 2
IFN-γ	Interferon-gamma
ILC	Innate lymphoid cell
iMFI	Integrated mean fluorescence intensity

IRF4	Interferon regulatory factor 4
ITAMs	Immunoreceptor tyrosine activation motifs
iTregs	Induced regulatory T cells
LAG3	Lymphocyte activation gene 3 protein
LCMV	Lymphocytic Choriomeningitis virus
LEF-1	Lymphoid enhancer binding factor 1
LOESS	Locally Weighted Scatterplot Smoothing
MCC	Maximum Clique Centrality
MDSCs	Myeloid-derived suppressor cells
MFI	Mean fluorescence intensity
MHC	Major histocompatibility complex
ORR	Overall response rate
OS	Overall survival
PARP	Poly (ADP-ribose) polymerase
PBMCs	Peripheral blood mononuclear cells
PCA	Principal component analysis
PCs	Principal components
PD-1	Programmed death 1
PMBCL	Primary Mediastinal B-Cell Lymphoma
PPI	Protein-protein interactions
Prdm1	PR domain zinc finger protein 1
R/R B-ALL	Relapsed/Refractory B-cell Acute Lymphoblastic Leukemia
R/R DLBCL	Relapsed/Refractory Diffuse Large B-cell Lymphoma
R/R FL	Relapsed/Refractory Follicular Lymphoma
R/R MM	Relapsed/Refractory multiple myeloma
RT	Room temperature
RUNX3	Runt related transcription factor 3
scFv	Single-chain variable fragment
SD	Standard deviation
sFas	Soluble Fas
sFasL	Soluble Fas ligand
SOM	Self-organizing maps
ssGSEA	Single-sample gene set enrichment analysis
STAT4	Transducer and activator of transcription factor 4
TAAs	Tumor-associated antigens
T-bet	T-box transcription factor
TBS-T	Tris-buffered saline with tween 20
Tc17	IL-17 producing $CD8^+$ T cells
TCF-1	T cell factor 1
TCR	T cell receptor
Teff	Effector T cell

Tex-term	Exhausted terminal T cell
Tfh cells	T follicular helper cells
Th	T helper
Th1 cells	T helper 1 cells
Th-POK	Th-inducing POZ-Kruppel factor
TIM3	T cell immunoglobulin 3
Tmem	Central memory T cell
Tmp	Memory precursor T cell
TNF-α	Tumor necrosis factor-alpha
Tregs	Regulatory T cells
TSAs	Tumor-specific antigens
t-SNE	T-distributed stochastic neighborhood embedding
ZEB2	Zinc finger E-box binding homeobox 2

1. INTRODUCTION

1.1 Chimeric antigen receptor T cell therapy

1.1.1 Chimeric antigen receptor structure

Over the last years, cellular immunotherapy has emerged as one of the leading areas of ongoing research and clinical therapy [1]. Chimeric antigen receptor (CAR) T cell therapy revolutionized the field of cellular immunotherapy as it demonstrated remarkable effectiveness. Strikingly, durable clinical responses were observed in patients with certain subsets of B-cell leukemia or lymphoma [2-4]. The production of CAR-T cells start with the collection of peripheral blood from patients or donors and subsequently T cells are isolated and genetically modified *in vitro* to express CARs [5]. T cells expressing CARs, are called CAR-T cells and recognize tumor-specific surface antigens. CAR-T cell antigen recognition is independent of major histocompatibility complex (MHC) restriction [6] and initiates immediate anti-tumor responses when the target antigen is detected. Following the introduction of the CAR construct, CAR-T cells are expanded to large numbers *ex vivo*. To support CAR-T cell persistence and treatment efficacy, patients first undergo a lymphodepleting chemotherapy to reduce tumor burden adverse immune effects before the cells are infused. Following their administration, CAR-T cells precisely identify tumor cells through the detection of specific antigens expressed on the surface of target cells , proliferate rapidly and eliminate the tumor *in vivo* [7].

CARs are modular synthetic receptors, which consist of four basic components. These components are: An extracellular antigen recognition domain, a hinge region, a transmembrane domain and one or more intracellular signaling domains [8]. The extracellular domain is usually represented by a single-chain variable fragment (scFv) and is the part of the CAR, which mediates the detection and binding of target antigens

[9]. The hinge region is a flexible linker that connects the extracellular antigen recognition domain (scFv) to the transmembrane domain. The hinge region provides flexibility to the CAR and allows CAR-T cells to effectively bind to target antigens on the surface of cancer cells [10]. The transmembrane domain is a hydrophobic region that spans the cell membrane and anchors the CAR to the T cell surface. It ensures the stable expression and localization of the CAR on the surface of the T cell, allowing for efficient signaling upon recognition and engagement with the antigen [11].

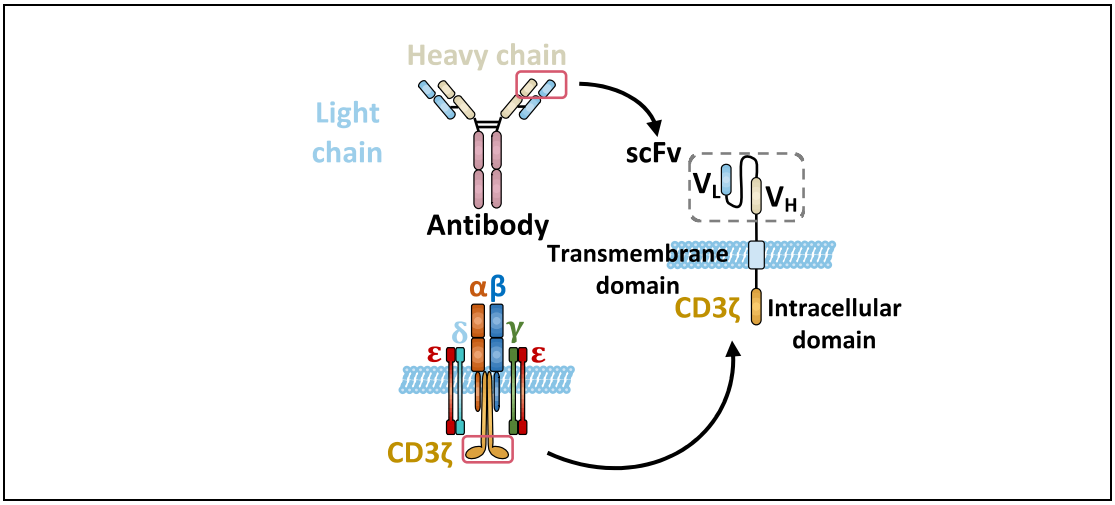

Figure 1: Chimeric antigen receptor structure. (Adapted from [12]).

The single chain variable fragment (scFv) of the CAR derived from heavy (V_H) and light (V_L) chains of the antibody. The CAR CD3ζ domain derived from the T cell receptor (TCR) intracellular signaling domain.

Binding of the scFv to tumor-associated antigens (TAAs) activates the CAR which induces a signaling cascade that is further propagated through the intracellular domain [13], which finally results in T cell activation and initiation of effector functions. The last component of CARs is a CD3 domain, which is usually derived from the CD3ζ subunit of the T cell receptor (TCR) complex. The CD3ζ domain contains immunoreceptor tyrosine activation motifs (ITAMs) which are crucial to initiate the intracellular signaling cascades following CAR stimulation [14]. Binding of TAAs to the scFv results in phosphorylation of the CD3ζ domain which in turn leads to the recruitment of intracellular signaling molecules and activates downstream signaling pathways (Figure 1).

1.1.2 Evolution of CAR constructs

1.1.2.1 CARs based on scFv

The first-generation CAR constructs only consisted of a scFv domain and an intracellular CD3ζ activation domain, while lacking additional costimulatory signals. This resulted in a limited proliferative capacity and a weaker anti-tumor effect of CAR-T cells. To overcome these limitations, second-generation CARs were developed, and these constructs included an additional costimulatory domain such as CD28, 4-1BB or ICOS. Incorporation of these costimulatory domains increased the proliferative capacity and release of cytokines of CAR-T cells, which greatly enhanced anti-tumor responses. Due to their outstanding performance, second-generation CAR-T cell constructs are currently used in many commercial CAR-T cell products [15-17]. To further enhance the activation and anti-tumor effects of CAR-T cells, third-generation CAR constructs were developed. These types of CARs incorporate two costimulatory domains, which are often 4-1BB and CD27 or OX40 [18,19]. Studies have shown that the use of two costimulatory domains can lead to more robust and durable responses [20]. Fourth-generation CAR constructs, also known as TRUCK or armored CAR [21,22], are the most recently developed CAR constructs used in CAR-T cell therapy. In addition to multiple costimulatory domains, the 4th generation CAR-T cells are modified to secrete specific cytokines such as IL-7, IL-12, IL-15, IL-21 or to express suicide genes like iCaspase-9. These modifications allow the 4th generation CAR-T cells both, to directly target tumor cells, and to activate the body's immune response. This increases their effectiveness to eliminate tumor cells [23,24] (Figure 2).

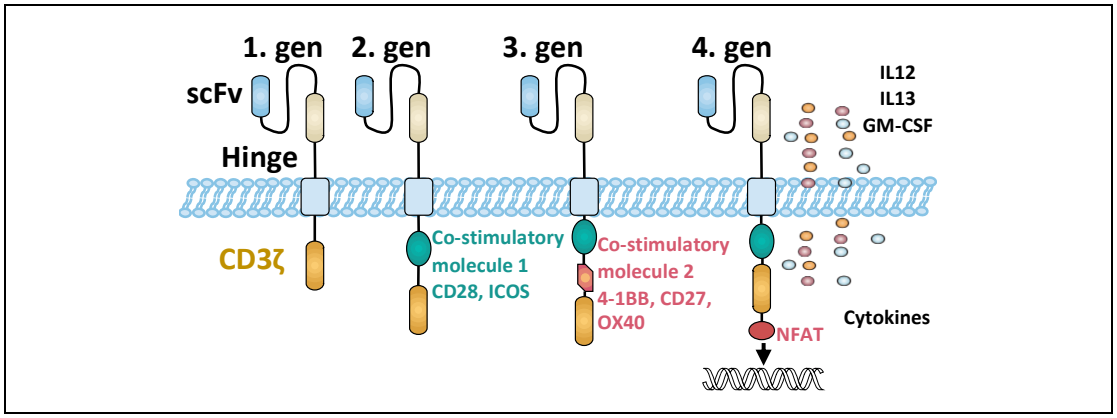

Figure 2: Single-chain variable fragment (scFv) based chimeric antigen receptor (CAR). (Adapted from [25]).

scFv: single-chain variable fragment; gen: generation; ICOS: Inducible T cell co-stimulator; IL12: Interleukin 12; IL13: Interleukin 13; GM-CSF: Granulocyte-Macrophage Colony-Stimulating Factor; NFAT: Nuclear factor of activated T cells.

1.1.2.1 Novel CARs

Ongoing advances in the field of CAR-T cell therapy further drives the development of CAR constructs with alternative targeting domains or modified costimulatory domains. While scFvs represented the most abundant type of targeting domains used in CAR constructs,, nanobodies, designed ankyrin repeats (DARPs), ligands, and receptors are used as novel targeting domains, providing more diverse and tailored options [26-29]. In addition, a new approach introduced adapter CARs, in which antigen recognition and T cell activation were spatially separated [30]. This novel strategy allowed for a more precise and temporally controlled therapeutic effect through the addition of separate adapter molecules (AMs), which were specific for tumor antigens and CAR immune cells [31]. This approach allowed to target multiple antigens simultaneously and ensured therapeutic success even if escape or downregulation of particular antigens occurred in tumors. Furthermore, it offered the potential for safer and more effective CAR-T cell therapy by modulating or stopping the immune response in the event of severe side effects [32]. These developments in CAR-T cell technology will finally improve cancer treatment and expand precision immunotherapies (Figure 3).

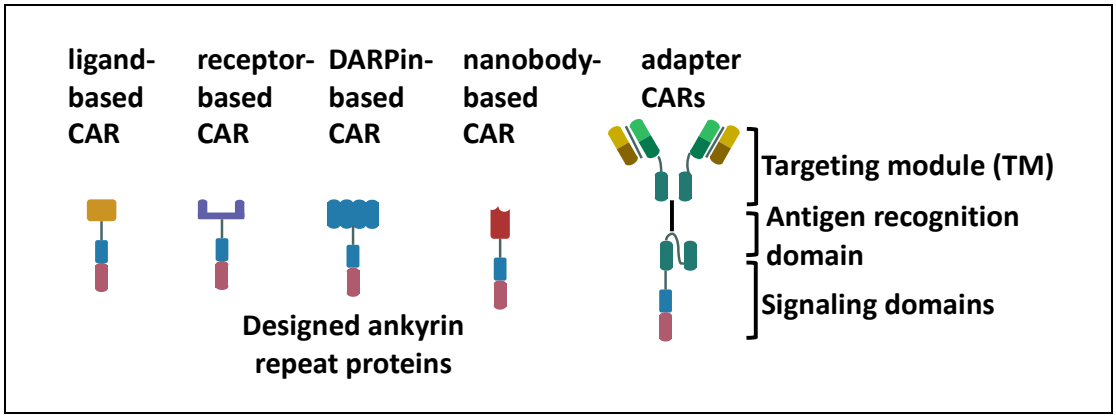

Figure 3: Novel chimeric antigen receptors (CARs). (Adapted from [33]).

1.1.3 Production chain of CAR-T cell therapy

CAR-T cell production is a multi-step process, which involves multiple sites and requires rigorous quality controls at every stage. Usually, CAR-T cells production starts with leukapheresis, a process in which a patient's blood is collected, and the leukocytes are separated. When a sufficient number of leukocytes was collected, the apheresis product is further processed to enrich and isolate T cells. Then, the T cells are stimulated and transduced with a viral vector encoding a CAR construct, followed by CAR-T cell expansion and cryopreservation. The whole process is performed under Good Manufacturing Practice (GMP) to ensure high product quality and patient safety. Finally, CAR-T cells are returned to the hospital and infused to patients [34] (Figure 4).

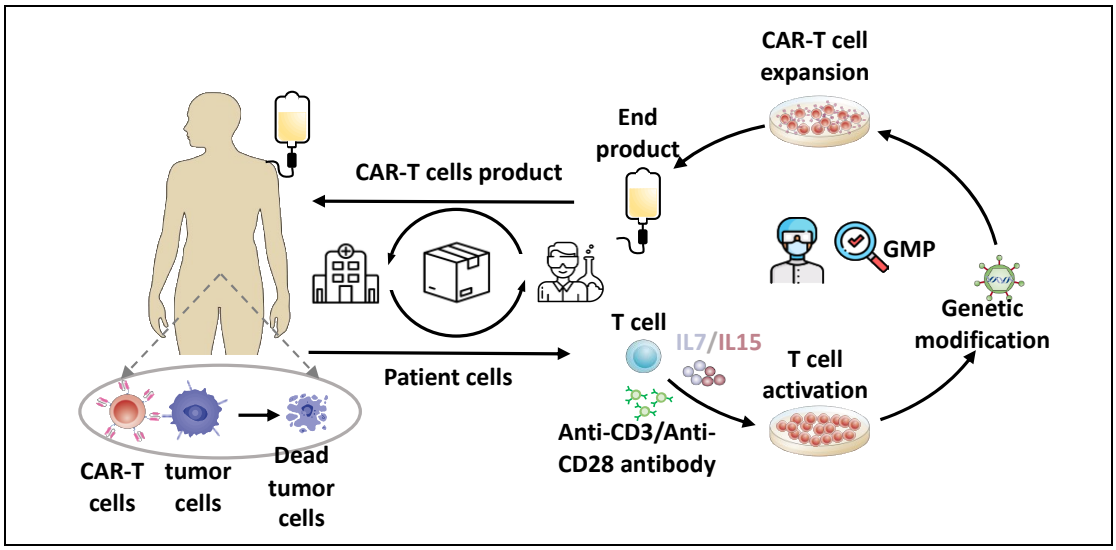

Figure 4: Production chain of CAR-T cell therapy. (Adapted from [35]).

1.1.4 Commercial CAR-T cell products and clinical response

Six CAR-T cell products were approved by the US Food and Drug Administration (FDA) and European Medicines Agency (EMA) for the treatment of relapsed/refractory (R/R) B cell malignancies, including tisagenlecleucel (Kymriah®, Novartis), axicabtagene ciloceucel (Yescarta®, Gilead), brexucabtagene autoleucel (Tecartus®, Gilead), lisocabtagene maraleucel (Breyanzi®, Brisol Myers Squibb), idecabtagene vicleucel (Abecma®, Bristol Myers Squibb and Bluebird Bio), and ciltacabtagene autoleucel (Carvykti®, Legend and Janssen), which target CD19 and B cell maturation antigen (BCMA) (**Table 1**).

The ELIANA study (Tisagenlecleucel) demonstrated an overall remission rate of 81%, including 60% complete remission (CR) and 21% CR with incomplete hematological recovery. Notably, 73% of pediatric ALL patients experienced grade 3 or 4 adverse events, which are product related. Cytokine release syndrome (CRS) was reported in 46% of patients and cytopenia was observed in 61% of patients [36]. Patients with refractory follicular lymphoma (FL) showed a CR of 69.1% (95% CI, 58.8-78.3) in the efficacy set (n=94), and within 8 weeks of infusion in the safety set (n=97), the rate of CRS (grade ≥ 3) was 48.5%, neurological events 37.1% (grade ≥ 3) and infections 5% (grade ≥ 3), with no treatment-related deaths [37].

In the JULIET study (Tisagenlecleucel), the best overall response rate was 52%, with 40% of adult DLBCL patients achieving a CR and 12% of patients achieving a partial response (PR). CRS occurred in 22% of patients, neurological events in 12%, infections in 20% and febrile neutropenia in 14% of patients among the grade 3 or 4 adverse events [16].

A total of 101 patients with refractory B cell lymphoma were enrolled in the ZUMA-1 study (Axicabtagene ciloleucel). Of these patients, 84 (83%) responded overall and 59

(58%) responded completely. Of note, CRS (grade ≥ 3) occurred in 12 (11%) patients and neurologic events (grade ≥ 3) were observed in 35 (32%) patients [15].

A total of 74 patients with mantle cell lymphoma were enrolled in the ZUMA-2 study (Brexucabtagene autoleucel) and the objective response rate was 85%, with 59% of patients achieving a CR. Of note, the estimated progression-free survival and overall survival rates at the 12-month time point were 61% and 83%, respectively. CRS and neurological events (grade ≥3) occurred in 15% and 31% of patients, respectively, among the most common adverse events of grade 3 or higher [38].

A total of 256 patients with refractory B cell lymphoma were included in the efficacy evaluation set in the TRANSCEND study (Lisocabtagene maraleucel). Of these patients, an objective response was achieved in 186 patients (73%, 95% CI 66.8% to 78.0%), while a CR was achieved in 136 patients (53%, 95% CI 46.8% to 59.4%). CRS (grade ≥3) was observed in 6 patients (2%) and neurological events (grade ≥3) in 27 patients (10%) [39].

In the KarMMa study (Idecabtagene vicleucel) for patients with multiple myeloma, the 12-month progression-free rate was 77% (95% CI 66.0-84.3) and the overall survival rate was 89% (95% CI 80.2-93.5) in 97 patients who received CAR-T cell therapy. CRS was observed in 92 patients (95%). Only 4% of patients experienced grade 3 or 4 CRS [40].

The CARTITUDE study (Ciltacabtagene autoleucel) showed that 94 of 128 patients (73%) had a response and 42 of 128 (33%) had a CR or better at a median follow-up of 13.3 months. CRS was reported in 107 patients (84%). Seven patients (5%) experienced grade 3 or higher events. Neurotoxic effects occurred in 23 patients (18%). Four patients (3%) experienced grade 3 neurotoxic effect [41].

Table 1: Landmark clinical trials of CAR-T cell products.

CAR-T Products	Target	Year	Indications	Clinical trial	Response	Toxicities (Grade 3/4)
Tisagenlecleucel	CD19	2017	R/R pediatric B-ALL	ELIANA	ORR 81%, CR 60%	CRS 46%, cytopenia 61%
		2018	R/R DLBCL	JULIET	ORR 52%, CR 40%, PR 12%	CRS 22%, infection 20%
		2021	R/R FL	ELARA	ORR 86.2%, CR 69.1%	CRS 49%, infection 5%
Axicabtagene ciloleucel	CD19	2017	R/R DLBCL	ZUMA-1	ORR 83%, CR 58%	CRS 11%, neurological events 32%
Brexucabtagene autoleucel	CD19	2020	FL, PMBCL, and HGBCL	ZUMA-2	ORR 85%, CR 59%	CRS 15%, neurological events 31%
Lisocabtagene maraleucel	CD19	2021	R/R DLBCL, HGBCL, PMBCL, and FL grade 3B	TRANSCEND	ORR 73%, CR 53%	CRS 2%, neurological events 10%
Idecabtagene vicleucel	BCMA	2021	R/R MM	KarMMa	ORR 97%, CR 65%	CRS 4%
Ciltacabtagene autoleucel	BCMA	2022	R/R MM	CARTITUDE	ORR 97%, CR 67%	CRS 4%, cytopenia 95%

Abbreviations: R/R B-ALL, Relapsed/Refractory B-cell Acute Lymphoblastic Leukemia; R/R DLBCL, Relapsed/Refractory Diffuse Large B-cell Lymphoma; R/R FL: Relapsed/Refractory Follicular Lymphoma; PMBCL: Primary Mediastinal B-Cell Lymphoma; HGBCL, High grade B cell lymphoma; R/R MM, Relapsed/Refractory multiple myeloma; ORR, Overall Response Rate; CR, Complete Response; CRS, Cytokine Release Syndrome. Adapted from [2]

1.2 Limitations of CAR-T cell therapy

Despite the promising results and prospects of CAR-T cell therapy in the treatment of hematological malignancies, there are substantial drawbacks which prevent its use to treat other types of cancer [2]. While CAR-T cell therapy relies on precise discrimination between cancerous and healthy tissues as well as specific targeting, conventional drug-based cancer therapies often follow broad targeting approaches [42]. Achieving this goal is still difficult, as CAR-T cell therapy is associated with poor persistence, off-target effects, and related toxicities [43]. In addition, achieving true tumor targeting can lead to excessive activation of CAR-T cells. This can result in markedly increased cytokine secretion and severe systemic toxicity [44]. Furthermore, tumor immune evasion has been observed in a significant number of CAR-T cell therapies, prompting numerous investigations into immune escape mechanisms and the development of various multi-target strategies [45].

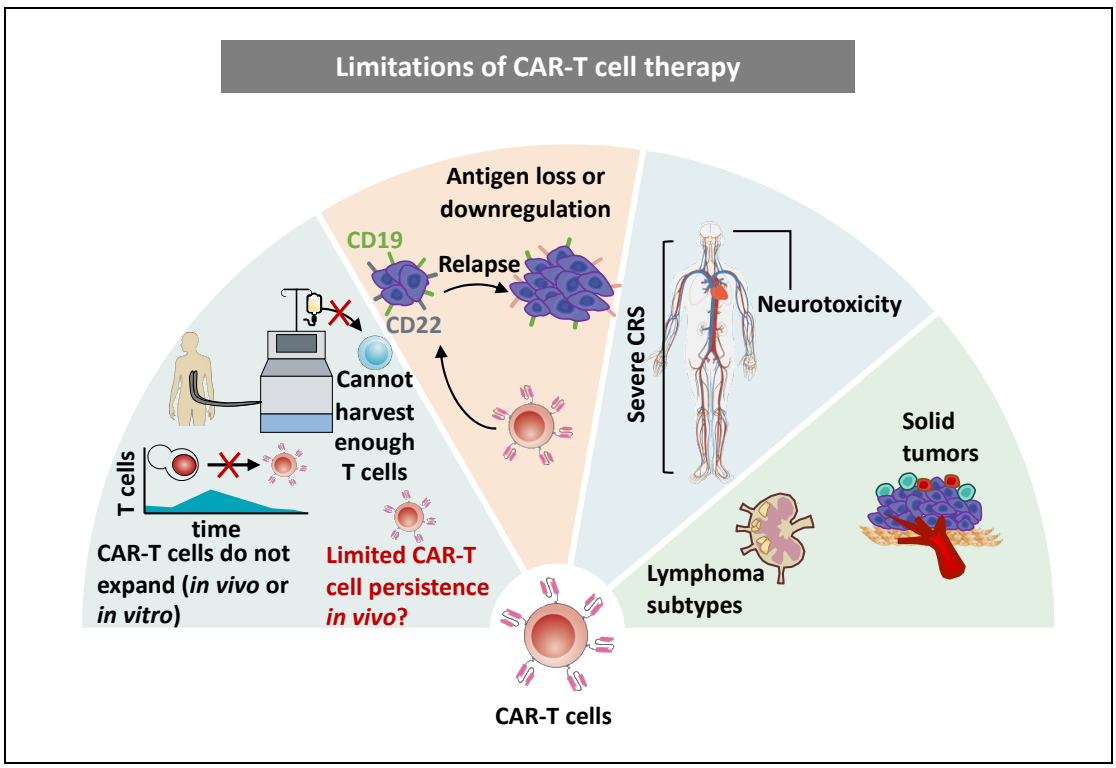

Figure 5: An overview of limitations of CAR-T cell therapy. (Adapted from [46]).

1.2.1 *Ex vivo* manipulation

The collection of sufficient numbers of T cells from patients is a challenge in the CAR-T cell manufacturing process due to the low numbers of T cells that are often isolated from apheresis products of patients with pre-existing lymphopenia resulting from previous cytotoxic therapies or exhaustion of bone marrow. Even when collection is successful, the effects of prior chemotherapy regimens may result in insufficient numbers or compromised quality of CAR-T cells [46]. These T cells can be selectively depleted by chemotherapeutic agents like cyclophosphamide and cytarabine and have worse expansion capability *in vivo* [47,48].

1.2.2 Disease relapse

1.2.2.1 Antigen-positive relapse

The occurrence of early relapses in ALL is often associated with limited persistence of CAR-T cells, primarily in the first few months after successful remission induction [49]. The intrinsic T cell quality varying between patients and the initial T cell phenotype including the proportion of $CD4^+$ and $CD8^+$ T cells, are key factors that influence CAR-T cell persistence [50]. Moreover, the choice of co-stimulatory domain incorporated into each CAR construct also matters [51]. A study by Wittibschlager et al. showed that patients had a reduced frequency of lymphoma relapse (29% vs. 60%) and progression-free survival PFS (Hazard Ratio HR: 2.79, 95% CI confidence interval: 1.09-7.11) when CAR-T cells were persistently present in the peripheral blood (PB) after 6 months. This study highlights the critical impact of CAR-T cell persistence on long-term outcomes, although the trend towards improved overall survival (OS) (HR: 1.99, 95% CI: 0.68-5.82) requires further investigation. The data also confirmed that CAR-T cells with a 4-1BB co-stimulatory domain have prolonged persistence compared with those with a CD28 domain [52]. To some extent, a reduced susceptibility to T cell exhaustion

induced by consistent CAR signaling may explain the increased durability of CAR-T cells containing the 4-1BB domain [53]. It is thought that the way in which the 4-1BB domain facilitates co-stimulation, as opposed to the CD28 domain, is responsible for this reduced susceptibility to exhaustion [54,55]. Comprehensive research has shown that CAR-T cell therapy provides promising results in hematological cancers, but not in solid tumors [56-58]. One explanation for this is that T cells infiltrating the microenvironment of solid tumors are more susceptible to exhaustion [59,60]. Naive T cells are activated and differentiate into effector T cells during acute phase [61]. However, continuous exposure to antigens can lead to T cell exhaustion in chronic infections or cancer [62]. Exhausted T cells have reduced production of cytokines and high levels of inhibitory markers such as programmed death 1 (PD-1), lymphocyte activation gene 3 protein (Lag3) and T cell immunoglobulin 3 (Tim3) [63]. The poor outcomes observed in CAR-T cell therapy for solid tumors may be due to the T cell exhaustion [64,65].

1.2.2.2 Antigen downregulation or modulation relapse

Patients diagnosed with ALL have been the primary focus of describing the phenomenon of antigen loss following successful CAR-T cell therapy [66,67]. This complexity is exacerbated by the fact that CAR-T cell therapy may interact with prior targeted immunotherapy. For example, FDA-approved therapies, anti-CD19 BiTE blinatumomab and anti-CD22 antibody-drug conjugate lintuzumab toyocamycin, have shown resistance in patients treated with these immunotherapies due to escape variants lacking CD19 or CD22 expression [68-70]. Inherent tumor heterogeneity also plays a role in predisposing to the emergence of an antigen-negative clone, independent of treatment-related antigen loss or modulation. It has been suggested that CD19 is ubiquitously expressed on all pre-B-cell ALL clones, with the development of antigen-negative sub-clones following treatment targeting CD19 [71]. Some studies have raised the possibility that malignant B-cell precursors may be $CD19^-$, particularly in patients with *BCR-ABL1* ALL [72]. Although CD22 was expressed in a high percentage of pre-B

ALL cells, there is still heterogeneity in surface expression [71]. This is particularly observed in children with *KMT2A (MLL)*-rearranged ALL, where $CD22^-$ ALL cell populations are more frequently detected [73,74].

1.2.3 Cytokine release syndrome and neurotoxicity

Following the activation of CAR-T cells, there is often a large release of cytokines, both from the CAR-T cells and from bystander cells [75]. High levels of inflammatory cytokines circulating in the body can trigger over-activation of the cytokine signaling network, potentially leading to cytokine toxicity or the development of CRS [76]. CRS is characterized by the secretion of a variety of cytokines, including IL-6, IL-10, interferon-gamma (IFN-γ), tumor necrosis factor-alpha (TNF-α) or granulocyte-colony stimulating factor (GM-CSF) by CAR-T cells and other immune cells [77].

Moreover, another severe side-effect of CAR-T therapy is neurotoxicity. However, it remains unclear exactly what mechanisms are responsible for CAR-T cell-associated neurotoxicity [78]. Several mechanisms may contribute to the development of neurotoxicity, including passive or active blood-brain barrier (BBB) permeation and localized cytokine and immune cell accumulation within the central nervous system [79]. Headache, seizures, delirium, anxiety, tremor, aphasia, decreased consciousness and even coma, often accompanied by cerebral oedema, are the most common syndromes of immune effector cell-associated neurotoxicity syndrome (ICANS) [80].

1.2.4 Immunosuppressive microenvironment

Unlike hematological malignancies, the efficacy of CAR-T in solid tumors is limited by the challenge of directing CAR-T cells to migrate and infiltrate solid tumor masses [81]. The immunosuppressive milieu within the solid tumor and the physical barriers posed by components such as the tumor stroma. In the tumor microenvironment, a variety of immunosuppressive cell types infiltrate solid tumors. These include myeloid-

derived suppressor cells (MDSCs), tumor-associated macrophages (TAMs) and regulatory T cells (Tregs) [82-84]. These infiltrated cells actively orchestrate the secretion of factors such as cytokines, chemokines, and growth factors that promote tumor progression, leading to a reduced clinical response to CAR T-cell therapy [85,86].

1.2.5 Lymphoma subtypes

Although CAR-T cell therapies have shown remarkable efficacy in the treatment of relapsed and/or refractory large B-cell lymphomas, certain challenges remain. These include lower remission rates and an incomplete understanding of relapse mechanisms. While loss of antigen may indeed be a trigger for relapse of lymphoma following CAR T-cell therapy, this phenomenon appears to be less common compared to patients with ALL [87,88]. In addition, although FDA approved the CAR-T cell therapy for adult with large B cell lymphoma, the use of CAR-T cell therapies in pediatric lymphomas remains limited and responses have been less substantial. This situation requires further investigation to gain a more complete understanding.

1.3 TCF-1 in T cell immunity

1.3.1 Overview of TCF-1

T cell factor 1 (TCF-1), encoded by Tcf-7, is a transcription factor and histone deacetylase (HDAC) essential for mammalian T cell and innate lymphoid cell (ILC) commitment [89]. The Tcf-7 gene is located on chromosome 5 (5q31.1) in the human genome. TCF-1 has been described as having several isoforms. The long isoform contains an N-terminal and beta-catenin interaction domain and a C-terminal high-mobility group (HMG) box DNA-binding domain, while the short isoforms lack the beta-catenin interaction domain [90]. The β-catenin interaction domain facilitates the expression of downstream targets of the WNT pathway, while the DNA binding domain

binds to gene enhancer and promoter regions to directly regulate gene transcription [91]. A study has shown that there is a 30 amino acid domain between the N-terminal and C-terminal regions, which contains HDAC activity [92]. The HDAC activity of TCF-1 appears to be essential for the stabilization of the fate of naive $CD8^+$ T cells through the silencing of CD4 and its associated lineage gene by means of increased histone deacetylation [93]. Another high mobility group transcription factor that shares significant homology with TCF-1 in its DNA-binding and HDAC domains is lymphoid enhancer binding factor 1 (LEF-1) [94]. TCF-1 and LEF-1 have been implicated in the control of T-cell development in numerous reports [95].

1.3.2 Role of TCF-1 in the thymus

T cell development begins during the early stages of thymocyte development, when multipotent common lymphoid progenitors (CLPs) migrate and colonize the thymus [96]. These precursors migrate from the bone marrow into the thymus where they initiate the differentiation process that leads to mature T cells. Notch signaling, which triggers the expression of TCF-1, is central to this process [97]. Binding to its specific binding site, TCF-1 promotes differentiation of early progenitor thymocytes (EPTs), commonly known as double-negative $CD4^-CD8^-$ (DN1) cells [98]. In addition, by interacting with its binding site, TCF-1 activates genes critical for T cell differentiation. These include GATA binding protein 3 (GATA3) and B-cell lymphoma/leukemia 11B (Bcl11b). As T precursors progress through the stages of DN2, DN3 and DN4 development, ultimately maturing into double positive (DP) $CD4^+CD8^+$ cells, the expression of TCF-1 is essential at different stages. TCF-1 drives the commitment of DN1 cells to differentiate into DN2 cells by inducing the expression of GATA3. After inducing Bcl11b in DN3 cells, TCF-1 promotes differentiation into DN4 cells by directly binding to the GATA3 and Bcl11b promoter and enhancer regions [93,99]. TCF-1 cooperates with the transcription factor HeLa E-box binding protein (HEB), which has similar binding sites in the genome, to facilitate the maturation of DP cells. This cooperation serves to

enhance maturation and prevent HEB from being proteasomal degraded and can prevent differentiation into T helper (Th)17 or IL-17 producing $CD8^+$ T cells (Tc17) [100-102]. During the differentiation of DP cells into single positive naïve $CD4^+$ T cells, TCF-1 plays a role in inducing the expression of Th-inducing POZ-Kruppel factor (Th-POK), thereby promoting commitment to the $CD4^+$ T cell lineage [103]. Despite TCF-1 is not critical for the commitment to $CD8^+$ T cell lineage, it still help to stabilize $CD8^+$ T cell by cooperating with Runt related transcription factor 3 (RUNX3) to limit the expression of CD4 [104] (Figure 6).

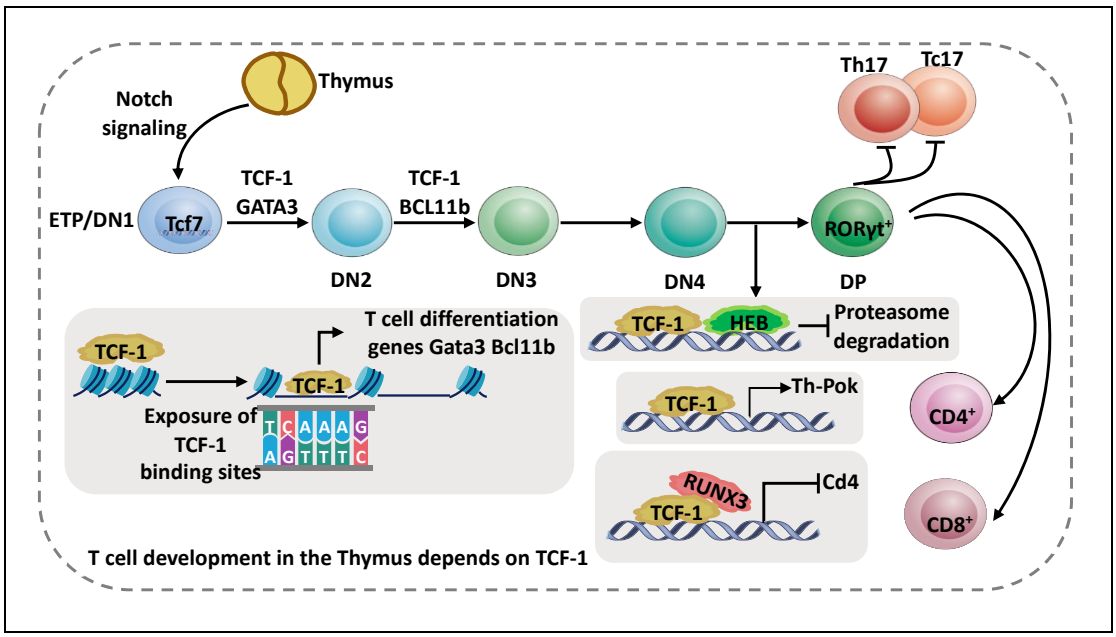

Figure 6: T cell development in thymus depends on T cell factor 1 (TCF-1). (Adapted from [90]).

ETP: Early thymic progenitor; TCF-1: T cell factor 1; DN1: Double negative CD4-CD8- cells; GATA3: Transcription factor GATA-binding protein 3; BCL11b: B cell lymphoma/leukemia 11B; Th17: CD4+RORγt+ T cells characterized by the secretion of IL-17; Tc17: IL17 producing CD8+ T cell; Th-Pok: Th-inducing POZ-Kruppel factor; RUNX3: Runt related transcription factor 3.

1.3.3 TCF-1 determines $CD4^+$ T helper cell differentiation.

Upon encounter with a pathogen, antigen presenting cells (APCs) promote the differentiation of naive $CD4^+$ cells into Th1, Th2, Th17 or Tfh cells [105]. In the differentiation of each T helper cell subset lineage, TCF-1 plays a critical role. Th1, a

subset of $CD4^+$ T cells, serves to promote cell-mediated immunity by enhancing macrophage function and aiding $CD8^+$ T cells [106], and Tfh, a subset of $CD4^+CXCR5^+$ cells, can prime B cells to mount antigen-specific antibody responses in germinal centers and is critical for long-term antibody-mediated immunity [107]. Both subsets share a common early differentiation pathway through the expression of the T-box transcription factor (T-bet) and B cell lymphoma 6 (BCL6) [108]. T-bet expression, which is essential for Th1 differentiation, can be suppressed by the persistence of BCL6 expression. TCF-1 is also known to complex with BCL6, thereby increasing Bcl6 transcription [109]. In addition, TCF-1 has a repressive effect on PR domain zinc finger protein 1 (Prdm1), which encodes B lymphocyte induced maturation protein-1 (BLIMP1) [110]. This dual mechanism results in the promotion of the differentiation of T follicular helper cells (Tfh cells) and the inhibition of the differentiation of T helper 1 cells (Th1 cells).

Under the influence of TCF-1, naive $CD4^+$ T cells differentiate into Th2 cells upon exposure to helminth infections or allergic responses. This occurs through the binding of TCF-1 to the promoter regions of GATA3 binding protein 3 (GATA3) which facilitates the upregulation of Gata3 expression [111]. TCF-1 plays a critical role in promoting Th17 differentiation in the periphery, despite its role in suppressing Th17 and Tc17 cell differentiation in developing thymocytes [112]. Several studies have shown that TCF-1 marks $CD27^+$ Th17 cells. These cells have stem cell-like properties and are in a metabolically inactive state [91]. This means that changing metabolic conditions may affect its expression and thus differentiate metabolic Th17 cells.

Natural regulatory T cells (nTregs) are a special group of immune cells that play a key role in the maintenance of the immune balance and the prevention of inappropriate immune responses [113]. Their characteristic feature is the presence of forkhead box protein P3 (FOXP3) [114]. The importance of GATA3 in the maintenance of FOXP3 expression provides a link to TCF-1, suggesting that TCF-1 could potentially control nTregs by modulating GATA3 through the regulation of FOXP3 expression [115]. In

addition, induced regulatory T cells (iTregs), which are generated from mature $CD4^+$ T cells in response to peripheral stimulation, play a role in the modulation of immune responses within the germinal centers [116]. It can inhibit the activity of T cells, preventing excessive immune responses. TCF-1 plays a role in directing the fate of iTreg cells in the direction of Tfr cells by forming a complex with BCL6, thereby promoting the differentiation of Tfr cells [117] (Figure 7).

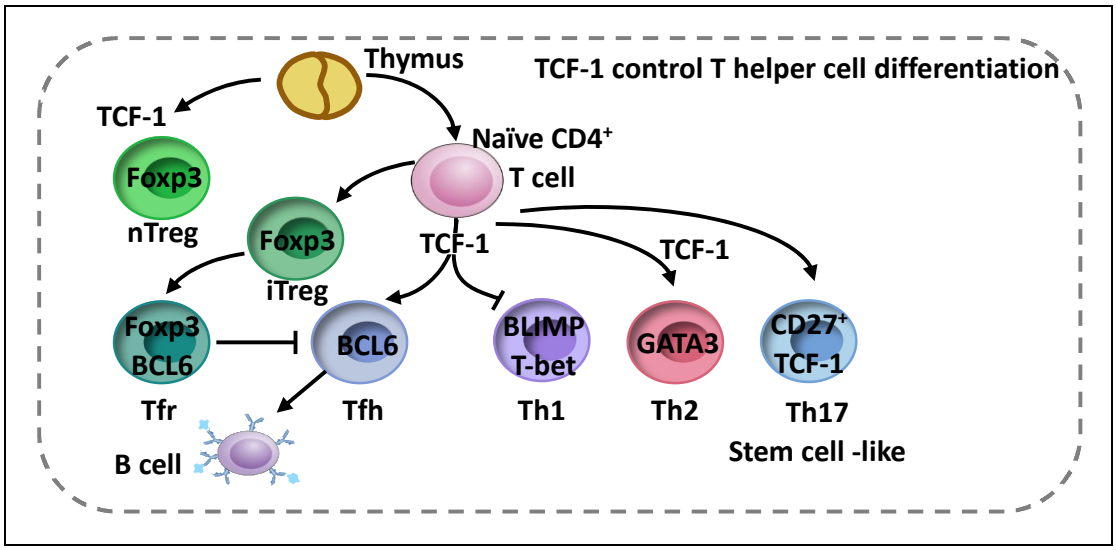

Figure 7: T cell factor 1 controls T helper cell differentiation. (Adapted from[90]).

TCF-1: T cell factor 1; FoxP3: Forkhead Box Protein P3; nTreg: Natural regulatory T cells; iTregs: Induced regulatory T cells; Tfr: $CD4^+CXCR5^+FOXP3^+$ T cells; Tfh: $CD4^+CXCR5^+$ cells; Th1: subset of $CD4^+T\text{-}bet^+$ T cells; Th2: subset of $CD4^+GATA3^+$ T cells; Th17: $CD4^+ROR\gamma t^+$ T cells characterized by the secretion of IL-17; BCL6: B cell lymphoma 6; BLIMP: B lymphocyte-induced maturation protein-1; T-bet: T box transcription factor; GATA3: GATA3 binding protein 3.

1.3.4 TCF-1 as a master regulator of $CD8^+$ T cell fate.

$CD8^+$ T cells play a central role in the defense against both acute and chronic viral infections, as well as in the fight against cancer [118]. During acute viral infection, TCF-1 emerges as a key player by binding to the promoter region of Eomesodermin (Eomes), enhancing its expression and thereby driving the development of $KLRG1^{low}IL\text{-}7R^{hi}$ memory precursor (Tmp) cells and central memory $CD8^+$ T cells (T_{CM}) [119,120]. T-bet, B lymphocyte-induced maturation protein-1 (BLIMP1), inhibitor of DNA binding protein

2 (ID2) and zinc finger E-box binding homeobox 2 (ZEB2) are key regulators of T_{eff} ($TCF\text{-}1^{-}CCR7^{-}KLRG1^{hi}IL\text{-}7R^{low}CD8^{+}$) cell differentiation [121]. The central role of TCF-1 downregulation in T_{eff} and $T_{ex\text{-}term}$ ($CD8^{+}TCF\text{-}1^{+}PD1^{+}Tim3^{-}$) cell differentiation is highlighted in acute and chronic LCMV (lymphocytic choriomeningitis virus) infections [104]. Binding of signal transducer and activator of transcription factor 4 (STAT4) to Tcf-7 promoter regions mediates this modulation in acute infections. Conversely, interferon regulatory factor 4 (IRF4) binds to Tcf-7 promoter regions and effectively represses its expression during chronic viral infection with LCMV (clone 13) [122].

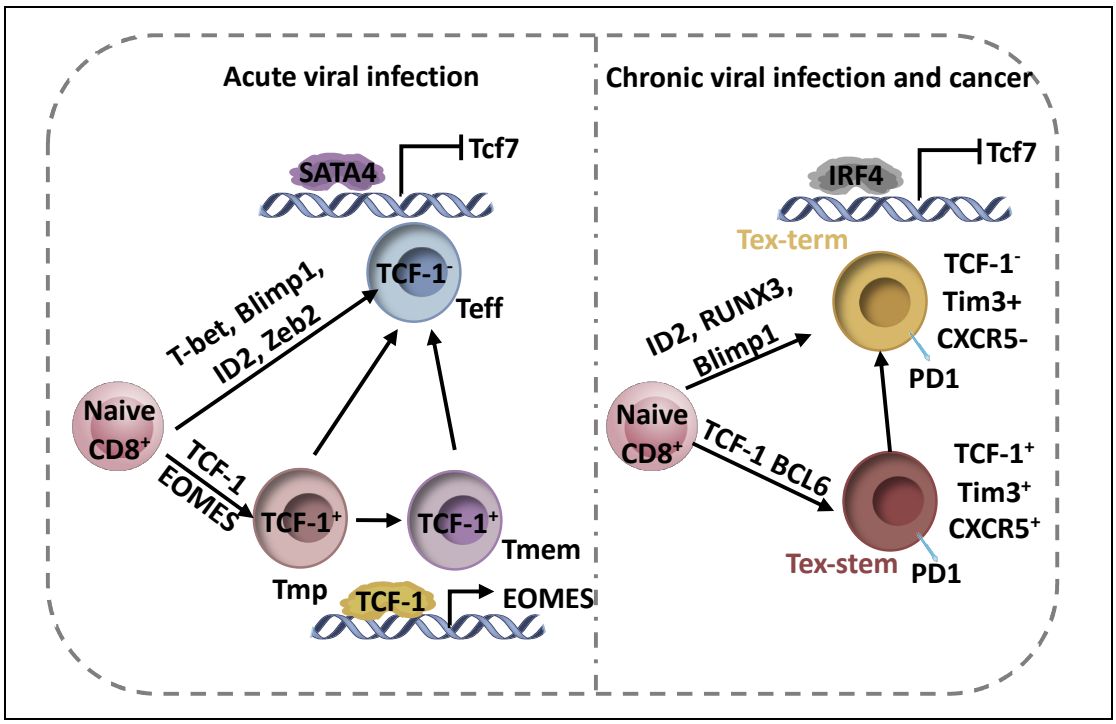

Figure 8: $CD8^{+}$ T cell development depends on T cell factor 1. (Adapted from [90]).

TCF-1: T cell factor 1; SATA4: signal transducer and activator of transcription factor 4; T-bet: T cell-specific T box transcription factor; Blimp1: B lymphocyte-induced maturation protein-1; ID2: inhibitor of DNA binding protein 2; Zeb: zinc finger E-box binding homeobox 2; EOMES: Eomesodermin; Teff: $TCF\text{-}1^{-}CCR7^{-}KLRG1^{hi}IL\text{-}7R^{low}CD8^{+}$ T cells; Tmp: $KLRG1^{low}IL\text{-}7R^{hi}$ memory precursor T cells; Tmem: central memory $CD8^{+}$ T cells; RUNX3: Runt related transcription factor 3; CXCR5: C-X-C motif chemokine receptor 5; PD1: programmed cell death protein 1; Tim3: Mucin-domain containing-3; BCL6: B cell lymphoma 6; IRF4: Interferon regulatory factor 4; Tex-stem: $TCF\text{-}1^{+}Tim3^{-}CXCR5^{+}PD1^{+}$ T cells; Tex-term: $TCF\text{-}1^{-}Tim3^{+}CXCR5^{-}PD1^{+}$ T cells.

The dynamic interaction between TCF-1 and BCL6 is emerging as a driving force behind the differentiation and maintenance of T_{ex} stem cells in chronic viral infections and melanoma. These specific cells express PD-1 and C-X-C motif chemokine receptor 5 (CXCR5), whilst showing reduced expression of other inhibitory receptors and markers of exhaustion, including Tim3 [123] (Figure 8).

1.3.5 The application of TCF-1 in immunotherapy.

Strong correlations were observed between levels of TCF-1 expressing $T_{ex\text{-}stem}$ cells in melanoma and improved tumor clearance in response to immune checkpoint blockade (ICB) [119,124,125]. Inhibition of PD-1 has been shown to induce the transformation of $T_{ex\text{-}stem}$ cells into TCF-1-negative $T_{ex\text{-}term}$ cells in both mouse cancer models and human melanoma patients [126]. In this context, $T_{ex\text{-}term}$ cells retain certain effector functions and begin to secrete cytotoxic molecules and cytokines with the potential for tumor cell targeting and elimination. $T_{ex\text{-}stem}$ cells have the unique ability to self-renew and replenish the reservoir of $T_{ex\text{-}stem}$ and $T_{ex\text{-}term}$ cells within the tumor, despite their reduced effector functions [126] (Figure 9). In addition to ICB, other immunomodulatory treatments such as CAR-T cell therapy have been successful in the treatment of certain types of cancer. CAR-T cell therapy has been remarkably effective in the treatment of lymphoblastic leukemia, with benefit in around 90% of patients. However, its effectiveness in CLL has been more limited. Only 26% of patients benefit from this approach [127]. Increased gene expression associated with $CD8^+$ memory T cells, including increased expression of TCF-1, was observed in CAR-T cells from CLL patients who achieved CR compared to non-responders [127]. These findings highlight the need to further understand how CAR-T cells and specific T cell subsets can be manipulated to enhance the ability to target and destroy tumor cells in specific malignancies.

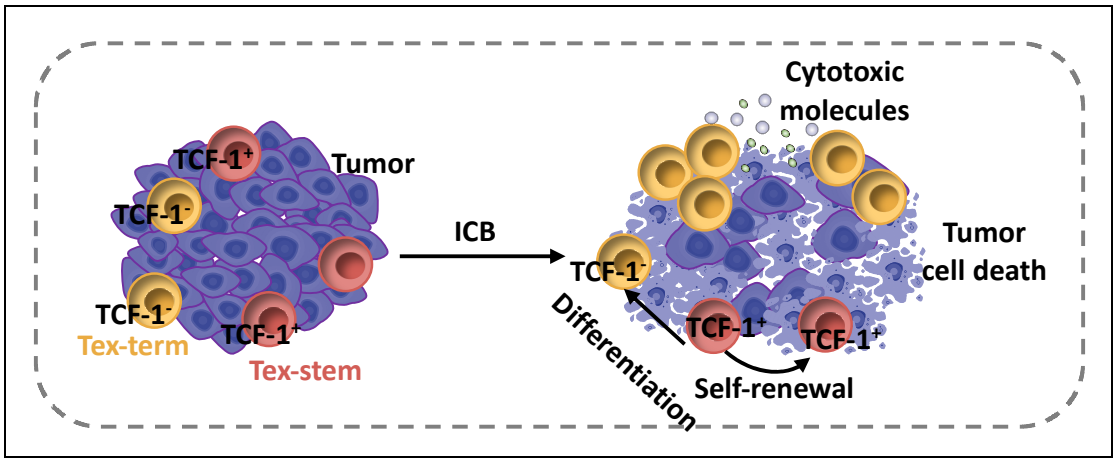

Figure 9: Tex-stem cells response to immune checkpoint blockade (ICB). (Adapted from [90])

Tex-stem: TCF-1$^+$ Tim3$^-$CXCR5$^+$PD1$^+$ T cells; Tex-term: TCF-1$^-$Tim3$^+$CXCR5$^-$PD1$^+$ T cells; ICB: immune checkpoint blockade.

1.4 Aim of the study

In recent years, CAR-T cell therapy has marked a transformative advancement in cellular immunotherapy, particularly in treating certain B-cell-driven hematological malignancies. Despite its impressive efficacy, the extension of CAR-T therapy to a broader spectrum of cancers remains limited, and a significant number of patients experience treatment failures. This is often due to the immunosuppressive tumor microenvironment and reduced *in vivo* persistence of CAR-T cells, which facilitate immune evasion. Research indicated that TCF-1 modulation could enhance the persistence and efficacy of T cells [128] and TCF-1 has been identified as a protective agent against activation-induced cell death in TCR-engineered $CD8^+$ T cells and is under expressed in tumor infiltrating Treg cells in colorectal cancer [129]. These insights suggest TCF-1 as a promising target for augmenting CAR-T cell therapy's effectiveness. Thus, this study aims to explore whether overexpressing TCF-1 could enhance the efficacy and reduce the side effect of CAR-T cell therapy.

The aims of this study were:

1. Establishment of a double transduced system for a novel CAR-T cell product;
2. Investigation of the effect of overexpression of TCF-1 on CAR-T cell generation;
3. Investigation of the effect of overexpression of TCF-1 on the functionality of CAR-T cells;
4. Elucidation of the mechanism of overexpression of TCF-1 in CAR-T cells.

2. METHODS AND MATERIALS

2.1 Materials

2.1.1 Consumables

Axygen® Filter-Pipette tip, 10 µl	Cat. NO.: 302-05-151 Axygen (Corning), Union City, CA, USA
Axygen® Filter-Pipette tip, 20 µl	Cat. NO.: 302-03-151 Axygen (Corning), Union City, CA, USA
Axygen® Filter-Pipette tip, 100 µl	Cat. NO.: 302-08-151 Axygen (Corning), Union City, CA, USA
Axygen® Filter-Pipette tip, 200 µl	Cat. NO.: 302-04-151 Axygen (Corning), Union City, CA, USA
Axygen® Filter-Pipette tip, 1000 µl	Cat. NO.: 302-01-151 Axygen (Corning), Union City, CA, USA
Bad Stabil	Cat. NO.: 1-6095 neoLab, Heidelberg, Germany
C-Chip Counting Chamber	Cat. NO.: 2N13202 NanoEnTek, Seoul, South Korea
Cellstar® 96 well Cell culture plate, U-bottom	Cat. NO.: 650180 Greiner Bio-One, Frickenhausen, Germany
Cellstar® 96 well Cell culture plate, flat-bottom	Cat. NO.: 655101 Greiner Bio-One, Frickenhausen, Germany
Cryo.s™ Freezing Tube, 2 ml	Cat. NO.: 126263, Greiner Bio-One, Frickenhausen, Germany
Falcon® 24-Well-Plate	Cat. NO.: 15705-060 Corning, Corning, NY, USA
Falcon® round bottom polystyrene tube, 5 ml	Cat. NO.: 10186400 Corning, Corning, NY, USA
Feather® Disposable Scalpel	Cat. NO.: 02.001.30.011 Feather Safety Razor, Osaka, Japan
Multiwell 6-Well-Plate	Cat. NO.: 83.3920 Sarstedt, Nümbrecht, Germany

Multiwell 12-Well-Plate	Cat. NO.: 83.3921 Sarstedt, Nümbrecht, Germany
Multiwell 24-Well-Plate	Cat. NO.: 83.3922 Sarstedt, Nümbrecht, Germany
Multiwell 48-Well-Plate	Cat. NO.: 83.3923 Sarstedt, Nümbrecht, Germany
Parafilm M® Laboratory Film	Cat. NO.: PM-996 Bemis, Neenah, WI, USA
PP Tube, 15 ml	Cat. NO.: 188271 Greiner Bio-One, Frickenhausen, Germany
PP Tube, 50 ml	Cat. NO.: 227261 Greiner Bio-One, Frickenhausen, Germany
Reagent low binding, 1.5 ml	Cat. NO.: 20010113 Sarstedt, Nümbrecht, Germany
Reagent SafeSeal, 0.5 ml	Cat. NO.: 20010143 Sarstedt, Nümbrecht, Germany
Reagent SafeSeal, 1.5 ml	Cat. NO.: 50-809-150 Sarstedt, Nümbrecht, Germany
Rotilabo® Aluminum foil	Cat. NO.: 2596.1 Carl Roth, Karlsruhe, Germany
Serological pipette, 2 ml	Cat. NO.: 4486 Corning Incorporated, NY, USA
Serological pipette, 5 ml	Cat. NO.: 4487 Corning Incorporated, NY, USA
Serological pipette, 10 ml	Cat. NO.: 4488 Corning Incorporated, NY, USA
Serological pipette, 25 ml	Cat. NO.: 4489 Corning Incorporated, NY, USA
Serological pipette, 50 ml	Cat. NO.: 4490 Corning Incorporated, NY, USA
Sterile Pasteur Pipette	Cat. NO.: S0957A LP Italiana Spa, Mailand, Italy

T25 TC-flask with vented cap	Cat. NO.: 83.3910.002 Sarstedt, Nümbrecht, Germany
T75 TC-flask with vented cap	Cat. NO.: 83.3911.002 Sarstedt, Nümbrecht, Germany
T175 TC-flask with vented cap	Cat. NO.: 83.3912.002 Sarstedt, Nümbrecht, Germany
TC Dish 100, Standard	Cat.: SAR-833902, Hoelzel-biotech, Germany
Pre-Separation Filters (30 µm)	Cat.: 130-041-407 MACS Miltenyi Biotec, Germany
LS column	Cat.: 130-042-401 MACS Miltenyi Biotec, Germany
MS column	Cat.: 130-042-201 MACS Miltenyi Biotec, Germany
TouchNTuff® Nitrile glove	Cat. NO.: 112-0997 Ansell, Brüssel, Belgien

2.1.2 Media, Solutions and Buffers

BD Horizon brilliant™ stain buffer	Cat. NO.: 563794 BD Biosciences, Heidelberg, Germany
Bovine serum albumin (BSA)	Cat. NO.: 130-091-376 Miltenyi Biotec, Germany
RPMI 1640	Cat. NO.: 21875-034 Thermo Fisher Scientific, Waltham, MA, USA
Trypsin-EDTA (0.05%)	Cat. NO.: 25300054 Gibco Thermo Fisher Scientific, USA
Fetal Bovine Serum, heat inactivated (h.i. FBS)	Cat. NO.: 10082147 Thermo Fisher Scientific, Waltham, USA
Clicks (EHAA) Medium	Cat. NO.: 9195 Irvine Scientific, Santa Ana, CA, USA
Complete Medium	45% RPMI 1640 (+ 2 mM L-Gln) + 45% EHAA + 2 mM L-Gln + 10% h.i. FBS

Dulbecco's phosphate buffered saline (PBS)	Cat. NO.: D8537-500 ml Sigma-Aldrich, St. Louis, MO, USA
FACS Buffer	PBS + 1% BSA + 2 mM EDTA, Miltenyi
MACS Buffer	5% MACS BSA Stock Solution (Cat. NO.: 130-091-376) + 95% autoMACS Rinsing Solution (Cat. NO.: 130-091-222), Miltenyi
Ficoll-H	Cat. NO.: GTF1511KYA Linaris, Dossenheim, Germany
FoxP3 Staining Buffer Set	Cat. NO.: 130-093-142 Miltenyi Biotec, Bergisch-Gladbach, Germany
Freezing Medium (FM)	90% h.i. FBS + 10% DMSO
Aqua ad iniect Ampuwa	Cat. No.: PZN-00041476 Fresenius, Bad Homburg, Germany
Nuclease-Free Water	Cat. No.: 129114 Qiagen, Hilden, Germany
Gibco™ Penicillin-Streptomycin	Cat. No.: 15140122 Gibco, USA

2.1.3 Reagents and chemicals

Brefeldin A Solution	Cat. No.: 420601 Biolegend, USA
Monensin Solution	Cat. No.: 420701 Biolegend, USA
Dimethylsulfoxid (DMSO)	Cat. No.: 51779 Honeywell, Morristown, NJ, USA
Ethanol absolute	Cat. No.: 32205-1L Sigma Aldrich,Steinheim, Germany
Interleukin-7 (IL-7)	Cat. No.: 207-1L-025 R&D System, USA
Interleukin-15 (IL-15)	Cat. No.: 247-ILB-025 R&D System, USA
Interleukin-2 (IL-2)	Cat. No.: 202-IL-050 R&D System, USA
L-Glutamine (200 mM)	Cat. No.: 25030081 ThermoFisher, USA

LIVE/DEAD™ fixable Near-IRDead Cell Stain Kit (633 or 635 nm excitation)	Cat. No.: L34976 ThermoFisher, USA
RetroNectin®, 1 mg/ml	Cat. No.: T100B Takara, Japan
RNeasy® Plus Mini Kit	Cat. No.: 74134 QIAGEN, Germany
Trypan Blue Solution, 0.4%	Cat. No.: 15250061 ThermoFisher, USA
CD19 Microbeads, human	Cat. No.: 130-050-301 Miltenyi Biotec, Germany
CFSE Cell Division Tracker Kit	Cat. No.: 423801 Biolegend, USA
Count Bright Absolute Counting Beads	Cat. No.: C36950 Invitrogen, USA
GeneJuice® Transfection Reagent	Cat. No.: 70967-3 Merck Millipore, German
Antifect® N liquid	Cat.: 1558446 Schülke, Germany

2.1.4 Antibodies

anti-human CD3	Alexa Fluor 700	BioLegend	Cat. No.: 300424
anti-human CD3	APC	BioLegend	Cat. No.: 300412
anti-human CD3	APC-Cy7	BioLegend	Cat. No.: 344818
anti-human CD3	BV 510®	BioLegend	Cat. No.: 300448
anti-human CD3	PE/Dazzle™ 594	BioLegend	Cat. No.: 300335
anti-human CD3	FITC	BioLegend	Cat. No.: 300406
anti-human CD3	BV 421®	BioLegend	Cat. No.: 300434
anti-human CD3	PE	BioLegend	Cat. No.: 300308
anti-human CD3	PE-Cy7	BioLegend	Cat. No.: 300420
anti-human CD3	PerCP	BioLegend	Cat. No.: 300326
anti-human CD4	APC-Cy7	BioLegend	Cat. No.: 317418
anti-human CD4	BV 510®	BioLegend	Cat. No.: 317444
anti-human CD4	Alexa Fluor 700	BioLegend	Cat.No.:357418

anti-human CD8	Pacific Blue	BioLegend	Cat. No.: 344718
anti-human CD8	PerCP	BioLegend	Cat. No.: 344708
anti-human CD8	BV 510®	BioLegend	Cat. No.: 344732
anti-human CD8	APC-Cy7	BioLegend	Cat. No.: 344714
anti-human CD8	FITC	BioLegend	Cat. No.: 344704
anti-human CD8	PE-Cy7	BioLegend	Cat. No.: 344712
anti-human CD10	FITC	BioLegend	Cat. No.: 982210
anti-human CD20	FITC	BioLegend	Cat. No.: 375508
anti-human CD27	PE-Cy7	BioLegend	Cat. No.: 356412
anti-human CD57	Pacific Blue	BioLegend	Cat. No.: 322316
anti-human CD62L	Pacific Blue	BioLegend	Cat. No.: 304826
anti-human CD69	PE/Dazzle™ 594	BioLegend	Cat. No.: 310942
anti-human CD95	BV 510®	BioLegend	Cat. No.: 305640
anti-human CD154	FITC	BioLegend	Cat. No.: 310804
anti-human CD253	PE-Cy7	BioLegend	Cat. No.: 308216
anti-human CD271	Pacific Blue	BioLegend	Cat. No.: 345132
anti-human CD271	APC	BioLegend	Cat. No.: 345108
anti-human CD371	FITC	BioLegend	Cat. No.: 353608
gt F(ab')2 anti-hum IgG	PE	Jackson ImmunoResearch	Cat. No.: 109-116-088
7AAD		BD Biosciences	Cat. No.: 559925
anti-human CD45RA	PE/Dazzle™ 594	BioLegend	Cat. No.: 304146
anti-human CCR7	PE-Cy7	BioLegend	Cat. No.: 353418
anti-human LAG-3	BV 510®	BioLegend	Cat. No.: 369318
anti-human Tim-3	BV 421®	BioLegend	Cat. No.: 345008
anti-human TNF	BV 421®	BioLegend	Cat. No.: 562783
anti-human PD-1	APC	BioLegend	Cat. No.: 329908
anti-human ICOS	Pacific Blue	BioLegend	Cat. No.: 313522
anti-human CTLA-4	PE-Cy7	BioLegend	Cat. No.: 369614
anti-human IFN-γ	APC	BD Biosciences	Cat. No.: 554702
Apotracker™ Green	FITC	BioLegend	Cat. No.: 427402

2.1.5 Equipment

4 °C fridge	Liebherr, Bulle, Swtizerland
-20 °C freezer	Liebherr, Bulle, Swtizerland
-80 °C freezer	Sanyo Electric Biomedial Co. Ltd, Osaka,
Aqualine AL 12 Water bath	Lauda, Lauda-Königshofen, Germany
Autoklav	Tuttnauer, Breda, Nederland
Cell incubator Heracell 240i	Thermo Fisher Scientific, Waltham, MA, USA
Cell incubator INCO	Memmert, Schwabach, Germany
Centrifuge Heraeus® Megafuge® 16R	Thermo Fisher Scientific, Waltham, MA, USA
Centrifuge Hermle Z300	Hermle Labortechnik, Wehingen, Germany
FACS BD LSRII	Becton Dickinson, Franklin Lakes, NJ, USA
Hemocytometer Chamber	Optik Labor, Berlin, Germany
Heraeus Pico17 Centrifuge	Thermo Fisher Scientific, Waltham, MA, USA
Ice maschine AF20	Scotsman International, Mailand, Italy
Leica DM 3000 Lab microscope	Leica, Wetzlar, Germany
Leica Labovert FS inverse Microscope	Leica, Wetzlar, Germany
Liquid nitrogen tank	Messer Griesheim, Mudersbach, Germany
M-20 microplate swing bucket rotor	Thermo Fisher Scientific, Waltham, MA, USA
FACS CantoII flow cytometer	BD Biosciences San Jose, CA, USA
Microcentrifuge, MiniStar	VWR International, Radnor, PE, USA
Minicentrifuge	Labnet International Inc., Edison, NJ, USA
Mr. Frosty Freezing Container	Thermo Fisher Scientific, Waltham, MA, USA
Pipetman Classic® Pipette, 100 µl	Gilson, Middleton, WI, USA
Pipetman Classic® Pipette, 1000 µl	Gilson, Middleton, WI, USA

Pipetman Classic® Pipette, 20 µl	Gilson, Middleton, WI, USA
Pipetman Classic® Pipette, 200 µl	Gilson, Middleton, WI, USA
Pipette Eppendorf Reference®, 10 µl	Eppendorf, Hamburg, Germany
Pipette Eppendorf Research®, 2.5 µl	Eppendorf, Hamburg, Germany
Pipetus® Pipette boy	Hirschmann Laborgeräte, Eberstadt Germany
Multipette® stream	Eppendorf, Hamburg, Germany
Sterile Workbench Hera Safe	Heraeus, Hanau, Germany
Tube Rack, 20 mm, 6x6 Row	neoLab, Heidelberg, Germany
Tube Rack, 30 mm, 4x4 Row	neoLab, Heidelberg, Germany
VF2 Vortexer	IKA Labortechnik, Staufen, Germany
Vortexer	Heidolph Instruments, Schwabach, Germany
BD FACSAria	BD Biosciences, New Jersey, USA
NanoDrop™ One/OneC Microvolume UV-Vis Spectrophotometer	Thermo Scientific™ ND-ONE-W
MACS MultiStand	MACS Miltenyi Biotec
QuadroMACS™ Separator	MACS Miltenyi Biotec
OctoMACS™ Separator	MACS Miltenyi Biotec
UV cross-linker (Bio-Link)	Labortechnik, Germany
Cabinet X-ray Irradiator (X-RAD-320)	Precision X-ray, North Branford, CT, USA
Thermomixer comfort	Eppendorf, Hamburg, Germany

2.1.6 Software

FACSDiva software	BD Biosciences, San Diego, CA, USA
FlowJo software	BD Biosciences, USA
Microsoft Excel	Microsoft, Redmond, WA, USA
Microsoft PowerPoint	Microsoft, Redmond, WA, USA
Microsoft Word	Microsoft, Redmond, WA, USA
GraphPad PrismTM 9.0 software	San Diego, CA, USA
Endnote 20™	Clarivate Analytics, USA

RStudio	Boston, MA, USA
LEGENDplex™ Data Analysis Software	Biolegend, San Diego, CA, USA

2.1.7 Cell lines

All cell lines used in the current study, including the $CD19^+$ Burkitt lymphoma cell lines Raji, $CD19^+$ B cell precursor leukemia cell line Nalm6, and $CD33^+$ biphenotypic B-myelomonocytic leukemia cell line MV4-11, were obtained from the German Collection of Microorganisms and Cell Cultures (DSMZ, Braunschweig, Germany) and cultured in medium including 90% RPMI 1640 supplemented with 2 mM L-glutamine and 10% h.i. FBS at 37 °C and 5% CO_2. The medium was changed every three days to passage cells. Moreover, mycoplasma was checked by polymerase chain reaction (PCR) before use of the above cells in following experimental assays.

2.1.8 Healthy donors' samples

Buffy coats from voluntary healthy donors (HDs) were provided by the German Red Cross Blood Donor Service Baden-Württemberg, Mannheim Germany. All donors signed the consent forms.

2.2 Methods

2.2.1 Tcf-7 plasmid DNA production

2.2.1.1 Transformation

Stellar competent cells were thawed in an ice bath, followed by being mixed gently to ensure even distribution. 50 µl of competent cells was transferred into reaction tube for the further steps. RV-SFG.CD70_1F6.CH3-IgG4h-CH2-IgG4h.CD28z.I. NGFR was chosen as DNA template. 3 ng of DNA template was added into the reaction tube, then the tube was placed on the ice for 30 minutes. After incubation, competent cells were heat shocked for exactly 45 seconds at 42 ℃, following incubation on ice for 2 minutes. SOC medium was added into the reaction tube to bring the final volume to 500 µl. The mixture was incubated by shaking 160 rpm for 1 hour at 37 ℃. 10 µl of mixture was added drop wisely onto the LB agar plate followed by the incubation overnight at 37 ℃.

2.2.1.2 Growth of bacterial cultures

A single colony was picked from LB agar plate and inoculated a culture of 5 mL LB medium containing the Ampicillin in a round bottom tube. The mixture was incubated for 14 hours at 37 ℃ with vigorously shaking.

2.2.1.3 Purification of plasmid DNA

After incubation, the competent cells were harvested by centrifugation at 8000 rpm in a conventional table-top microcentrifuge for 3 minutes at room temperature. QIAprep Miniprep kit™ was used in the following steps. The cell pellet was resuspended in 250 µl Resuspension solution™ (Buffer P1) and transferred to a microcentrifuge tube. 250 µl Alkaline lysis solution™ (Buffer P2) was added and mixed thoroughly by inverting tube 4-6 times. 350 µl Neutralization solution™ (Buffer N3) was added to the mixture,

and then the microcentrifuge tubes were inverted 4-6 times again. Centrifuge was followed for 10 minutes at 13000 rpm in the table-top microcentrifuge. 800 µl of the supernatant was applied to the QIAprep Spin Column™ (containing filter) by pipetting and centrifuged for 60 seconds. The flow through was discarded after the centrifugation. 0.75 ml of Washing Buffer™ (Buffer PE) was added to wash QIAprep Spin Column™ and centrifuged for 60 seconds. The flow through was discarded again and the QIAprep Spin Column™ was centrifuged at full speed for an additional 1 minute to remove residual washing buffer. The QIAprep Spin Column™ was placed in a clean 1.5 ml microcentrifuge tube. To elute DNA, 50 µl of UltraPure® water was added to the center of each QIAprep Spin Coulmn™, followed by centrifugation for 1 minute. The eluted plasmid DNA was stored in -20 ℃ fridge for further experiments.

2.2.1.4 Restriction cloning

2 µg of eluted plasmid DNA, 3 µl of CutSmart™ 10x reaction buffer, 1 µl of *Ncol* restriction enzyme, 1 µl of *Xhol* restriction enzyme and 10 µl of nuclease water were added to a 1.5 ml microcentrifuge tube. The mixture was incubated for 2 hours at 37 ℃ in a ThermoBlock™.

2.2.1.5 Gel extraction

After incubation, 5 µl of loading buffer was added into the 30 µl of eluted plasmid DNA mixture. A molecular weight ladder was loaded into the first lane of the gel and eluted plasmid DNA mixture was loaded into the additional wells of the gel. The gel was runed at 90 V for 1 hour until the dye line was approximately 75-80% of the way down the gel. An UV light device was used to visualize the DNA fragments. The fragments of DNA were usually referred to as “bands” due to their appearance on the gel. The gel was cut by using the DNA ladder in the first lane as a guide.

2.2.1.6 DNA fragment extraction from polyacrylamide gels

To extract the DNA fragment from polyacrylamide gels, the QIA quick Gel Extraction Kit™ was used. The gel should be excised as small as possible by removing excess polyacrylamide, then the gel slice was transferred into a 15 ml reaction tube. One or two volumes of diffusion buffer from the QIA quick Gel Extraction Kit™ were added to 1 volume of gel following by incubation at 50 ℃ for 30 minutes. Afterwards, the sample was centrifuged for 1 minutes. The supernatant was firstly taken out carefully using a pipette or a draw-out pasteur pipette, then passed through a disposable plastic column to remove the residual polyacrylamide. The volume of the recovered supernatant was determined following last step. Three volumes of Buffer QG™ were added to 1 volume of supernatant and then mixed until the color of mixture becomes yellow. Thereafter, the sample was applied to a QIAquick Spin Column™, which was placed in a provided 2 ml collection tube and centrifuged for 60 seconds. The flow-through was discarded and the QIAquick Spin Column™ was placed back in the same tube following a 1 minute centrifugation with the maximum speed. After the centrifugation, the QIAquick Spin Column™ was transferred into a clean 1.5 ml microcentrifuge tube and 50 µl buffer EB™ was added to the center of the QIAquick Spin Column™, then centrifuged for 1 minute. The eluted DNA fragment was stored in -20 ℃ fridge for further experiments.

2.2.1.7 Infusion cloning

The concentration of eluted DNA fragment was measured, then the reagents were added into a reaction tube as follows to set up a reaction of infusion cloning, The mixture was incubated at 50 ℃ for 15 minutes and then at 4 ℃ for 5 minutes. The new synthesized plasmid DNA (RV-SFG.Tcf -7. NGFR) was transformed by Stellar Competent Cells™ (**Table 2**).

Component	Volume (µl)
Vector	2.5
Insert fragment	0.34
5X Infusion HD Enzyme Premix	2
Nuclease-free water	5.16

Table 2. Infusion cloning reaction.

2.2.2 Generation of CAR-T cells and DT.CAR-T cells

2.2.2.1 Preparation of plasmid DNA

100 ng of CD19 specific retroviral vector plasmid (RV-SFG.CD19.CD28.4-1BB.CD3zeta), CD33 specific retroviral vector plasmid (RV-SFG.CD33.CD28.4-1BB.CD3zeta), and Tcf-7 specific retroviral vector plasmid (RV-SFG.Tcf-7.NGFR) was mixed with 50 µl of competent cells (DH5α) in a microcentrifuge tube respectively and incubated on ice for 20-30 min. 25 µl of the competent cell/DNA mixture was plated onto a 10 cm LB agar plate containing 25 µg/ml ampicillin antibiotic and incubated at 37 °C overnight. The individual colonies of the transformed DH5α were picked and inoculated into 3 ml of LB media supplemented with ampicillin in 13 ml sterile polypropylene snap-cap tubes. The bacterial cultures were incubated overnight (18-20 h) at 37 °C in a shaker for uniform growth. The bacteria containing plasmid DNA were harvested by centrifugation at 5000 rpm for 10 min at RT. Plasmid DNA from bacteria was isolated and purified by the Miniprep Kit™ according to the instructions. DNA concentration was measured using a Nanodrop™.

2.2.2.2 Production of retrovirus

Cryopreserved 293T cells were thawed and resuspended in Iscove's modified dulbecco's medium (IMDM) containing L-glutamine, supplied with 10% FBS, 0.1 mM Na-Pyruvate and 500 µg/ml antibiotic geneticin (termed as complete IMDM). 2 x 10^6 of 293T cells was seeded in a 10 cm tissue culture-treated dish and incubated at 37 °C,

5% CO_2. The medium was replaced by fresh complete IMDM after an overnight culture. One day later, 293T cells were detached by 0.05% trypsin and 0.02 % EDTA, and then resuspended in 10 ml of complete IMDM, followed by seeding into a new dish at 1:10 dilution. 3 days later, 293T cells were detached again by Trypsin-EDTA™ and seeded into new dishes at a density of 2.0 x 10^6 per dish.

One day later, Gene Juice®/IMDM solution was firstly prepared as the following table, and incubated at RT for 5 minutes, followed by adding into the plasmid DNA mixture. After incubation of Gene Juice®/IMDM with plasmid DNA mixture for 15 min, 510 µl of the complete mixture solution was added dropwise into the 293T cell dish. Post 48 h and 72 h of transfection, the supernatant from the retrovirus culture was harvested and aliquoted, then stored at -80 °C until being used (**Table 3**).

Component	Volume
CD19/CD33/TCF-1 vector plasmide	3.75 µg
Packing plasmide PegPam3	3.75 µg
Envelope plasmide RDF	2.5 µg
GeneJuice® transfection reagent	30 µl
IMDM	470 µl
Total	510 µl

Table 3. Retrovirus production reaction.

2.2.2.3 Isolation of peripheral blood mononuclear cells

Buffy coat from health donor was 1:1 diluted with PBS containing 2% FBS. 20 ml of diluted buffy coat was carefully placed on the top of 15 ml of lymphoprep density gradient medium in a 50 ml reaction tube. Peripheral blood mononuclear cells (PBMCs) were isolated by centrifugation at 500 g for 30 min at room temperature (RT) without breaking. Following aspiration of the upper layer plasma and platelets, the mononuclear cell layer was transferred into a new 50 ml reaction tube using a sterile pipette. Thereafter, PBMCs were washed twice with 20 ml PBS plus 2% FBS (500 g, 10 min). Cell viability and cell number were determined by a trypan blue staining. Then PBMCs were cryopreserved as described below.

2.2.2.4 Cryopreservation of peripheral blood mononuclear cells

PBMCs were resuspended at 1×10^7 cells/ml in cold freezing media that contain 90% FBS and 10% DMSO, and then aliquoted into 1 ml cryovials. Samples were kept in cryogenic safety coolers at -80 °C overnight, followed by a long-term storage in liquid nitrogen till use.

2.2.2.5 Thawing of peripheral blood mononuclear cells

Cryovials were removed from the liquid nitrogen tank and kept on dry ice till thawing. Samples were thawed in a water bath at 37 °C for 2 min. Afterwards, the thawed PBMCs were transferred dropwise into a 50 ml reaction tube containing 9 ml warm complete medium (dilution ≥ 1:9), followed by centrifugation (500 g, 5 min). The supernatant was discarded, and the cell pellet was resuspended with 10 ml complete media. After cell counting, cell concentration was adjusted at 1×10^6 cells/ml for the following experiments.

2.2.2.6 Activation of T cells

The anti-CD3 (1 µg/ml) and anti-CD28 (1 µg/ml) antibodies were precoated in the non-tissue 24-well plates (day -1), and then the plates were incubated at 4 °C overnight. Next day (day 0), PBMCs from healthy donors were thawed and resuspended in the complete medium containing 45% (vol/vol) clicks medium (EHAA), 45% (vol/vol) RPMI 1640 medium, 10% (vol/vol) FBS, and 2 mmol/l L-glutamine. 1 x 10^6 of PBMCs per well were seeded in the pre-coated plates. After two-day cultivation (day 2), half of cultured medium was replaced by fresh complete medium containing 10 ng/ml IL-7 and 5 ng/ml IL-15, which led to an expansion of T cells. In the same day, a new non-tissue 24 well plate was precoated with 1 ml of 7 µg/ml retronectin and then incubated at 4 °C overnight.

2.2.2.7 Retroviral transduction of T cells

On day 3, supernatant was discarded, and 1 ml of thawed retroviral supernatant was seeded in the precoated wells. The plate was centrifuged for 90 minutes, at 2000 xg and at room temperature. Thereafter, the retroviral supernatant was discarded. Activated T cells (ATCs) were harvested and resuspended in complete medium at a density of 1 x 10^5 cells/ml. Besides adding 1 ml of complete medium with 10 ng/ml IL-7 and 5 ng/ml IL-15, 1 ml of cell suspension was added into the wells.

2.2.2.8 Expansion of CAR-T cells and DT.CAR-T cells

Post transduced T cells were expanded in either 6-well plates or T75 flasks in the presence of IL-7 (10 ng/ml) and IL-15 (5 ng/ml) and the complete medium with cytokines was half changed in every 3-4 days. The transduction efficacy was analyzed on indicated time by flow cytometry.

2.2.3 Western blot

2.2.3.1 Cell lysis and protein extraction

Protein was extracted from non-transduced T cells, CAR-T cells and double-transduced T cells at day 13 of generation. Briefly, cells were harvested in 1.5 ml microfuge tubes and washed with cold PBS by centrifuging at 2000 g for 5 min at 4 °C. Ice-cold lysis buffer (RIPA buffer with adequate protease and phosphatase inhibitors) was added to the cell pellet and incubated for 30 min in the ice or at 4 °C. Afterwards, the tubes were centrifuged at 16000 g for 20 min at 4 °C, and then the supernatant was collected in fresh tubes. Protein estimation was performed by bicinchoninic acid assay (BCA) with 10 µl of lysate. The protein concentration of interested cells was determined by comparison with the standards. Adequate volume of loading buffer was added to cell

lysate and incubated at 95 °C for 5 min to digest genomic DNA. These samples were stored at -20 °C or used to proceed with gel electrophoresis.

2.2.3.2 Western blot

30 µg of protein samples and 5 µl of prestained molecular weight markers were loaded onto SDS-PAGE gel. The proteins and markers were separated under the indicated voltage for 1-2 hours. The proteins were electrotransferred on nitrocellulose membrane at 300 mA for 2 hours in the cold room. After transfer, nitrocellulose membrane was washed with 25 ml tris-buffered saline with tween 20 (TBS-T) buffer for 5 min at RT, followed by incubating in 25 ml of blocking buffer (5% milk in TBS-T) for 1 hour at RT. After washing with TBS-T, membrane was incubated with primary antibody at the recommended dilution (1:1000) with gentle agitation overnight at 4 °C. After washing 3 times with TBS-T for 5 min each, membrane was incubated with anti-rabbit/-mouse IgG HRP-linked antibody in blocking buffer at recommended dilution and gently agitated for 1 hour at RT. Then the membrane was washed and incubated with appropriate enzyme substrate solution for 2 min. Proteins were visualized in an Amersham Imager 600^{TM}. Quantification of the intensity of protein bands was performed by using software ImageJ^{TM}.

2.2.4 Killing assay

To investigate the repetitively killing capacity of CAR-T cells and DT.CAR-T cells, effector cells were co-cultured with tumor cells at an E/T ratio of 1 to 1 and 1 to 2. Subsequently, effector cells were re-challenged with the identical number of fresh tumor cells until no or only a few effector cells were left in the co-culture system. The numbers of residual tumor cells and CAR-T cells were quantified every three days using a flow cytometry.

2.2.4.1 Short-term killing assay

To assess the short-term killing capacity of CAR-T cells, CAR-T cells were co-cultured with tumor cells at an E/T ratio of 1:1 and 1: 2 for 24 hours. The absolute numbers of CAR-T cells and tumor cells were quantified by a flow cytometry.

2.2.4.2 Long-term co-culture assay

0.25 x 10^5 of CAR-T cells were co-cultured with tumor cells at an E/T ratio of 1:1 or 1:2 on day 0, followed by adding identical number of tumor cells every day to challenge CAR-T cells until the CAR-T cells cannot control the growth of tumor cells anymore. The cells and the supernatant were harvested every 2 days for quantifying and immunophenotyping the cells as well as assessing the cytokine profiling.

2.2.5 Flow cytometry

The fluorochrome-conjugated antibodies: CD3 (clone UCHT1), CD4 (clone SK3), CD8 (clone SK1), CD45RA (clone HI100), CCR7 (clone G043H7), CD62L (clone DREG-56), CD27 (clone O323), CD57 (clone QA17A04), CD69 (clone FN50), CD95 (clone DX2), CD253 (clone RIK-2), CD40L (clone 24-31), CTLA-4 (clone BNI3), ICOS (clone C398.4A), PD1 (clone EH12.2H7), Tim3 (clone F38-2E2), Lag3 (clone 11C3C65), Ki67 and apotracker from BioLegend™ were used for cell surface marker staining. Dead cells were excluded with the LIVE/DEAD™ fixable near-infrared (IR) dead cell stain kit™ (Thermo Fisher Scientific) or 7AAD (BD Biosciences). The anti-human goat F(ab)2 IgG (H+L) PE reagent (Dianova, Hamburg, Germany) was used to identify CAR expression. The anti-human CD271 (NGFR) antibody as a reporter gene marker was used to identify TCF-1 expression. To ensure the accuracy of measurement, fluorescence compensation was applied before acquisition. Appropriate fluorescence minus one (FMO) control and non-transduced control were included to properly place

the gates. All flow cytometric data were acquired using a BD LSRII™ flow cytometer (BD Biosciences) and analyzed using FlowJo™ v.10 software.

2.2.5.1 Cell surface staining

5-10 x 10^5 cells per tube were introduced into 12 x 75 mm FACS tubes and washed once with 500 cold FACS Buffer™. After washing and centrifugation, the supernatant was discarded, and the cells were resuspended in 100 µl of FACS Buffer™. The antibody cocktail was added into the cell suspension at an optimum concentration, and then incubated with the cells for 30 minutes in the dark at room temperature. After staining, the cells were washed twice with 1 ml of FACS Buffer™ by centrifugation at 500 g for 4 minutes. The supernatant was discarded after the centrifugation, and the cell pellets were resuspended in 0.5 ml of FACS Buffer™. 5 µl of 7AAD Viability Staining Solution™ was added into the reaction tubes before flow cytometric analysis.

2.2.5.2 Intracellular cytokine staining

For cytokine release analysis, effector cells (CAR-T cells or DT.CAR-T cells) were stimulated with target cells (CD19 positive tumor cells: Raji cells and Nalm-6 cells; CD33 positive tumor cells: MV4-11 cells) for 5 hours in the presence of a protein transport inhibitor monensin, an ATPase inhibitor brefeldin A and CD107a antibody as a marker of degranulation. For the negative control, CAR-T cells and DT.CAR-T cells were cultured without tumor cells in the presence of secretion inhibitors and CD107a antibody. After incubation, cells were harvested and washed twice by the centrifugation at 500 g for 4 minutes. The supernatant was discarded, and the cells were stained with antibodies against surface markers for 30 minutes. Following the surface marker staining, the cells were fixed and permeabilized with the FoxP3 staining buffer set™. After fixation and permeabilization, cells were stained with interferon (IFN)-γ and tumor necrosis factor (TNF)-α for 30 minutes. In the end, cells were washed and resuspended in 500 µl of FACS Buffer™ for flow cytometric analysis.

2.2.5.3 Cytokine detection

For quantification of cytokines in the supernatant, beads based multiplex LEGENDPlex™ analysis (Biolegend) was performed following the manufacturer's instructions. Thirteen bead populations with distinct fluorescence intensities have been coated with capture antibodies specific for IL-2, IL-4, IL-6, IL-10, IL-17A, TNF-α, IFN-γ, sFas, sFasL, granzyme A, granzyme B, perforin and granulysin proteins. The acquisition was performed on a BD FACSCantoII™ flow cytometer (BD Biosciences San Jose, CA, USA). Data were analyzed with the LEGENDPlex™ V8.0 software (Biolegend)

2.2.5.4 Sorting of CAR-T cells and DT.CAR-T cells

During the long-term co-culture assay, CAR-T cells and DT.CAR-T cells were harvest at Day1, Day5, and Day9. After washing by FACS Buffer™, the cells were stained with CD3 and gt F(ab')2 anti-humna IgG antibodies at 4 ℃ for 30 minutes in the dark. After labelling, cells were washed once with 500 µl of FACS Buffer™ and resuspended in 1.5 ml of FACS Buffer™ in a 15 ml PP tube for sorting by BD FACSAria™. Gates were placed based in an un-transduced control. The sorted CAR-T cells and DT.CAR-T cells were collected in 15 ml PP tubes with 2 ml of PBS containing 2% h.i. FBS.

2.2.6 Elimination of dead cells

Dead Cell Removal MicroBeads® recognize a moiety in the plasma membrane of apoptotic as well as dead cells. For the dead cell depletion, cells were resuspended in 1 x Binding Buffer® and stained with 100 µl of Dead Cell Removal MicroBeads® for 15 minutes at RT, subsequently passed through a LS column™. The magnetically labeled dead cells were retained within the column. The untouched living cells were further processed.

2.2.7 RNA isolation

The sorted CAR-T cells and DT.CAR-T cells were harvested by centrifuging at 13000 rpm for 5 minutes at RT. Then 350 µl of Buffer RLT Plus™ was added into the tube with cell pellet and vortexed for 30 seconds to lyse the cells. RNA isolation was performed following the standard protocol of RNeasy Plus Mini Kit®. RNA concentration was determined by measuring the absorption at 260/280 nm using a Nanodrop™.

2.2.8 FACS data mining

To comprehensively investigate the overexpression of TCF-1 on the immunophenotype of CAR-T cells and DT.CAR-T cells, two different strategies for data mining have been developed in our current study.

2.2.8.1 Cell cluster-based algorithm

To deep in the immunological data, a pipeline based on the advanced FACS analysis strategies and machine learning methods was developed in our study. A down-sample method was applied to normalize the population size of each sample. The dimensionality of serial cell populations was reduced by using t-distributed stochastic neighborhood embedding (t-SNE). Afterwards, cell clusters based on marker expression density were identified by PhenoGraph. To determine the discriminative power of defined cell clusters, unsupervised methods, principal component analysis (PCA) and hierarchical clustering were performed. All identified cell clusters were checked for significance by a p-value below 0.05 compared to the control group and then validated by manual gating. The final cell cluster were selected when the shape of the cell population was clear.

2.2.8.2 Antigen-based algorithm

To explore the overexpression of TCF-1 on antigen expression of CAR-T cells, A semi-automated FACS analysis strategy was established. t-SNE dimensionality reduction was performed first, and then the expression density of each antigen was projected onto the t-SNE plot. In addition, the frequency of antigen expression on lineage cell populations was analyzed and further filtered by significance analysis.

2.2.9 Machine learning-based advanced analysis

2.2.9.1 Unsupervised dimensional reduction

t-distributed stochastic neighbor embedding (t-SNE). The Barnes-Hut implementation of t-SNE is a non-linear dimensionality reduction tool used to reduce the dimensionality of immunophenotyping data to visualize the expression patterns of all stained markers in two dimensions simultaneously. t-SNE can preferentially preserve local structures in high-dimensional data. The number of iterations is an iterative adjustment process, to best reflect the similarity of cells, it is set to 8000. A perplexity of 30 was applied to reveal differences in the immune landscape between different groups.

Principal component analysis (PCA). PCA is a linear transformation algorithm that summarizes the characteristics of data through dimensionality reduction, thereby assessing the similarity and difference between groups and identifying key variables. After normalization, the frequencies of the subset of cells that are variables are scaled to have a standard deviation of 1 and centered to have a mean of zero. PCA extracts eigenvalues from the dataset that measure the amount of variation retained by each principal component and variable contribution. They are further analyzed when principal components (PCs) account for at least 70% of the total variance. The contribution of variables explaining variability in these PCs was examined. Variables

with contributions greater than the expected average contribution were identified as key factors.

2.2.9.2 Unsupervised clustering

PhenoGraph analysis. Due to dimensionality reduction, distinct subsets of cells in multidimensional space may visually overlap in low dimensions. Computational clustering algorithms allow users to independently and unbiasedly identify subpopulations of cells defined by their multidimensional phenotypes. Most importantly, strategies for identifying cell populations automatically partition cells based on the natural structure of cellular data, without regard to prior knowledge. PhenoGraph is a clustering algorithm that robustly and automatically divides cells into phenotypically distinct subpopulations by creating a graph representing phenotypic similarities between cells and then identifying communities in this graph. PhenoGraph was applied to our dataset to generate cell clusters using input of k-nearest neighbors30 and Euclidean distance metric.

Hierarchical clustering. Cell clusters defined by PhenoGraph are further clustered using full linkage, which is based on the similarity of cell cluster proportions. A dendrogram was constructed between the different samples, which naturally defined cell clusters through branches in a hierarchical tree.

LOESS regression. LOESS regression is also called Locally Weighted Scatterplot Smoothing. It is a non-parametric statistical technique used for estimating the underlying trend or relationship in a scatterplot and particularly useful when the data points exhibit complex patterns that cannot be easily captured by a simple linear or polynomial regression model. The first step of LOESS regression is Local Neighborhood Selection. For each data point, a subset of nearby data points is selected based on a specified bandwidth or smoothing parameter. Then a weight is assigned to each nearby data point based on its proximity to the central data point. Points closer to the central point receive higher weights, while those farther away receive lower weights.

Following the weighting, polynomial fitting is applied. A low-degree polynomial is fit to the weighted data points within the local neighborhood. This polynomial captures the local trend or relationship among the data points. In the end, the fitted polynomials from different local neighborhoods are combined to form the overall smoothed curve. This combination is done by using a weighted average of the local polynomial fits, where the weights are determined by the kernel function and the distance from the central point.

2.2.9.3 Correlation analysis

Correlation analysis was conducted to discover whether there is a relationship among different cytokines, and how strong it is. Spearman correlation coefficient was calculated to assess the degree and direction of correlation by using R function corrplot. Correlation coefficient was indicated by circle size and significance was indicated by *p* value shown by color code.

2.2.10 Statistical analysis

The statistical analysis for FACS data mining, machine learning based advanced analysis were described previously. Unless indicated otherwise, all statistical tests comparing two groups were performed using paired t test. $P < 0.05$ were regarded as significant difference. Results are shown as mean ± standard deviation (SD) if not specifically labelled. Plots and statistical tests were mainly performed with GraphPad Prism 9 (San Diego, CA, USA). Figures were carried out with GraphPad Prism 9 (San Diego, CA, USA) and software R (R Foundation for Statistical Computing, Vienna, Austria).

3. RESULTS

3.1 Successful generation of TCF-1^{+}CAR^{+} T cells

In order to generate CAR-T cells which overexpress TCF-1, T cells were simultaneously co-transduced with viral vectors. In particular, a third-generation retroviral CD19.CAR vector (RV-SFG.CD19.CD28/4-1BB/ζ) was co-transduced together with an additional TCF-1 retroviral vector (RV-SFG.Tcf-7. NGFR) into T cells. Flow cytometry was used to measure the transduction efficiency and the expression levels of CAR and NGFR were used as reporters to monitor TCF-1 expression.

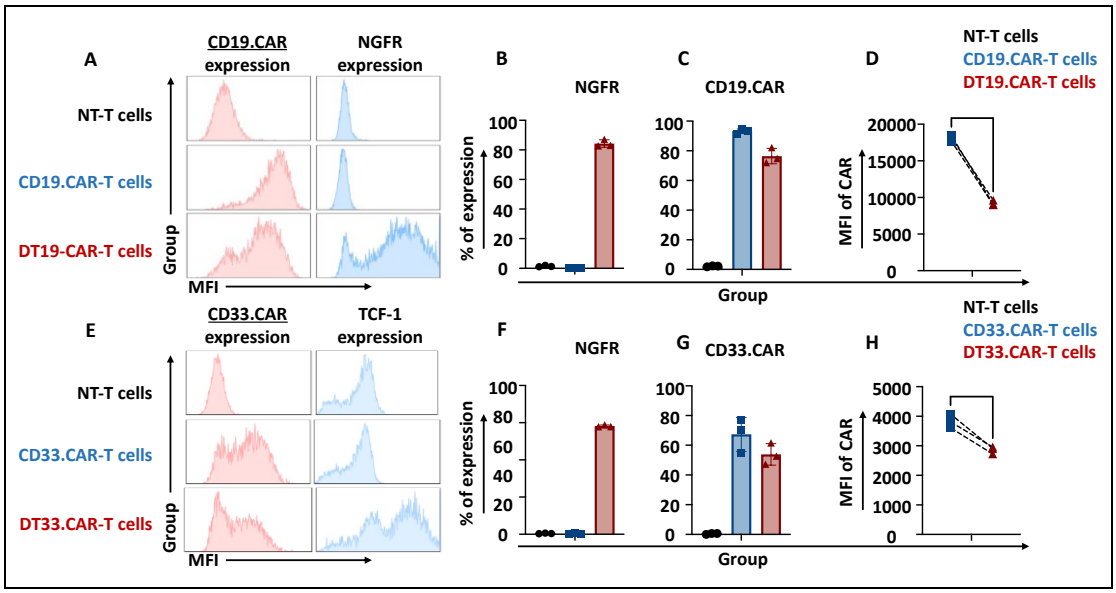

Figure 10: The expression of CAR and TCF-1 on CAR-T cells and DT.CAR-T cells.

Representative histogram of CAR and TCF-1 expression in non-transduced T cells, CAR-T cells, and DT.CAR-T cells (A, E). Statistical analysis of the percentage of TCF-1 expression in non-transduced T cells, CAR-T cells and DT.CAR-T cells (B, F). Statistical analysis of percentage of CAR expression in non-transduced T cells, CAR-T cells, and DT.CAR-T cells (C, G). Statistical analysis of MFI (Median Fluorescence Intensity) of CAR expression in CAR-T cells and DT.CAR-T cells (D, H). Three individual donors were tested. A paired t-test was used for statistical analysis. (*P<0.05, **P<0.01, ***P<0.001, ****P<0.0001, *ns= no significant difference*).

Both CD19.CAR-T cells and DT.CAR-T cells were successfully generated, demonstrating a consistent and stable CAR transduction efficiency (CD19.CAR-T cells:

93.20%±1.54, DT19.CAR-T cells: 76.30%±5.21, as shown in Figure 10A). Of note, not only the frequency of CD19.CAR-T cells (Figure 10C and 10G) but also the mean fluorescence intensity (MFI) of CD19.CAR (Figure 10D and 10H, $P<0.001$ and $P<0.05$, respectively) was decreased in DT.CAR-T cells, which was particularly mirrored by the MFI of CAR expression levels. Moreover, our data show that after the double transduction, the majority of T cells express both CD19.CAR and NGFR (73.3% out of $CD3^+$ T cells), as shown in Figure 11A.

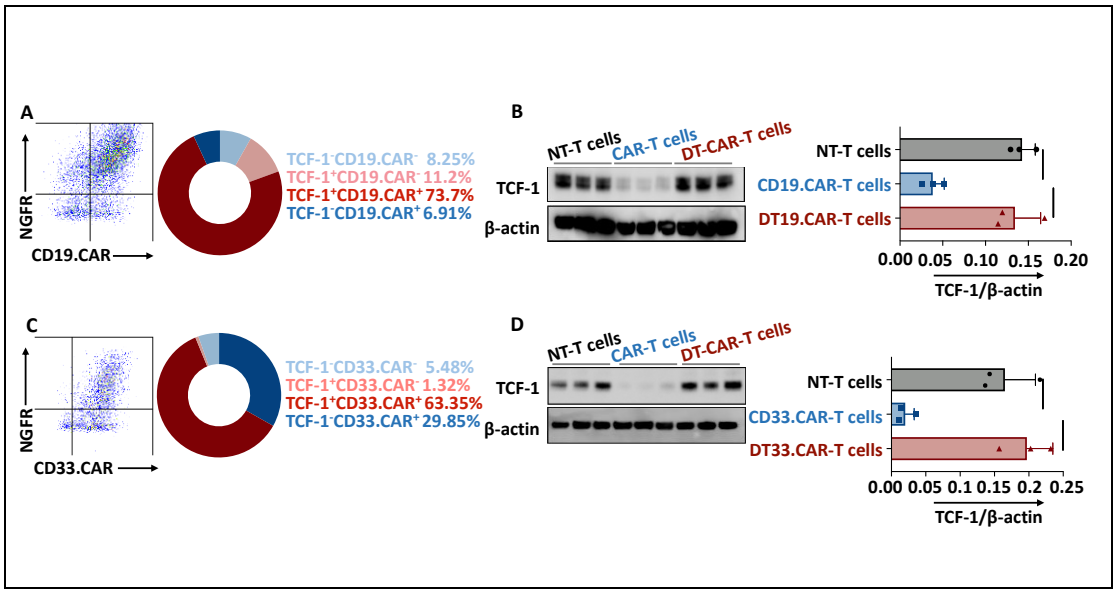

Figure 11: The composition of DT.CAR-T cells and protein level of TCF-1 on non-T cells, CAR-T cells, and DT.CAR-T cells.

Representative dot plots obtained from flowcytometry to evaluate the composition of DT. CAR-T cells (A, C). Statistical analysis protein level of TCF-1 on non-T T cells, CAR-T cells, and DT.CAR-T cells, as detected by Western Blot (B, D), three individual donors were tested. A paired t-test was used for statistical analysis. (*$P<0.05$, **$P<0.01$, ***$P<0.001$, ****$P<0.0001$, *ns= no significant difference*).

Since NGFR was utilized solely as a reporter gene, the protein level of TCF-1 was further examined by western blot. Notably, the expression of TCF-1 in DT.CAR-T cells exhibited a remarkable upregulation when compared to CD19.CAR-T cells. Intriguingly, it was observed that the protein level of TCF-1 in DT.CAR-T cells was similar to non-transduced T cells (Figure 11B, $P<0.001$). This finding suggests a loss of TCF-1 expression during the generation of CAR-T cells, but it could be restored by the double transduction (Figure 11B).

To strengthen our findings, we conducted additional experiments using a third-generation retroviral CD33.CAR vector. The results demonstrated a similar pattern, which confirms and validates our findings (Figure 11C and 11D).

3.2 No alteration of the CD4/CD8 component in the final products

Since the importance of the CD4/CD8 component in CAR-T cell products, we have evaluated it by a flow cytometry-based method conducted on day 14 after transduction. Our data indicated that there were no significant differences in both the percentage and the MFI of the CD4/CD8 component between CD19.CAR-T cells and DT.CAR-T cells (Figure 12A-C). Consistent results were observed in the CD33.CAR-T cells and DT.CAR-T cells as well (Figure 12 D-F).

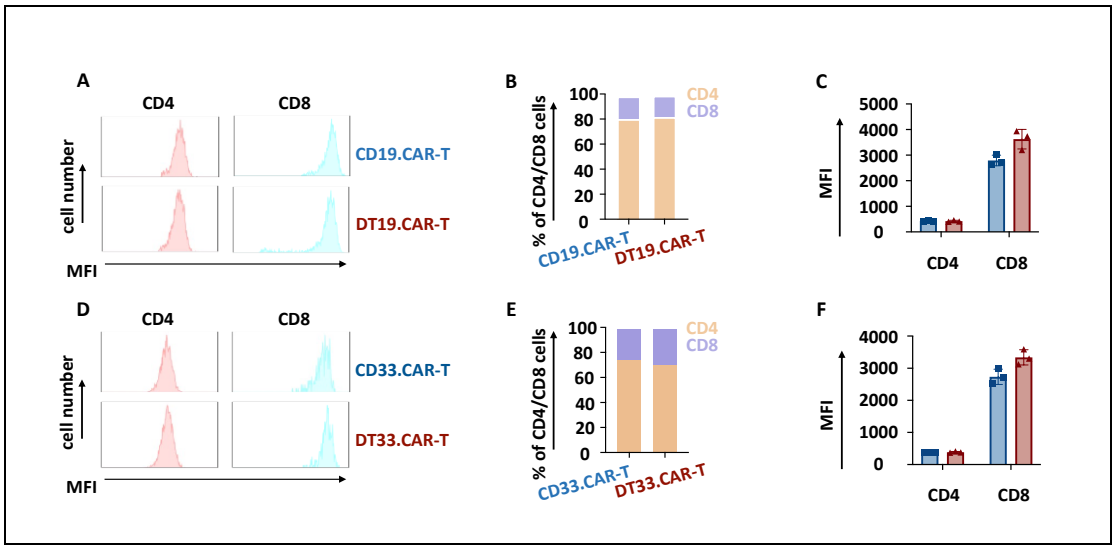

Figure 12: CD4/CD8 composition in CAR-T cells and DT.CAR-T cells

Representative histogram obtained from flowcytometry to evaluate the correlation between CAR-T cell number, DT-T cell number and MFI of CD4/CD8 component (A, D). Statistical analysis of percentage of CD4/CD8 in CAR-T cells and DT.CAR-T cells at Day14 (B, E). Statistical analysis of MFI of CD4/CD8 in CAR-T cells and DT.CAR-T cells at Day14 (C, F), six individual donors were tested. A paired t-test was used for statistical analysis. (*P<0.05, **P<0.01, ***P<0.001, ****P<0.0001, *ns= no significant difference*).

3.3 Apoptosis resistance contributed to the higher number of DT.CAR-T cells

The dynamic of T cell expansion was monitored during the generation phase. Interestingly, CAR-T cells with TCF-1 transduction consistently exhibited a higher cell number starting from day 7 (Figure 13A, 7.27±1.49 x 10^6 vs. 9.87±1.15 x 10^6, $^{**}P<0.01$) to day 11 (Figure 13A, 28.53±9.62 x 10^6 vs. 47.28 ±10.45 x 10^6, $^{*}P<0.05$) in both CD19.CAR-T (Figure 13A) and CD33.CAR-T cells (Figure 13B).

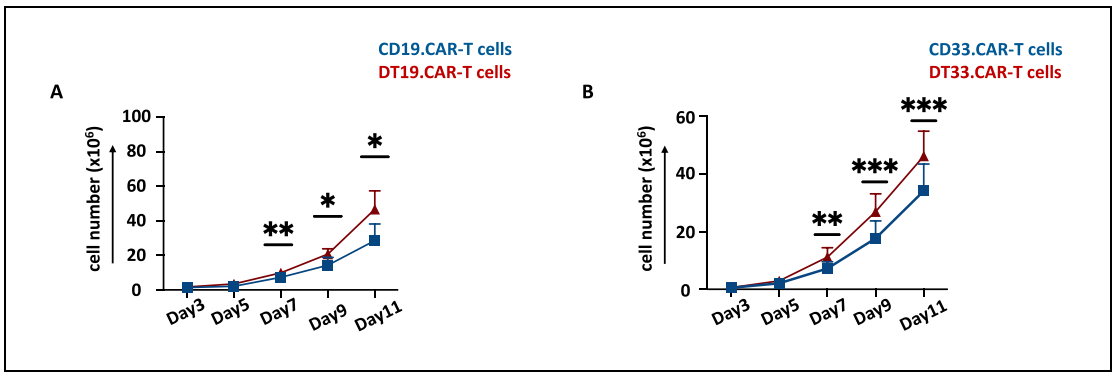

Figure 13: Proliferation dynamics of CAR-T cells and DT.CAR-T cells from Day 3 to Day 11.

Statistical analysis of cell numbers from Day 3 to Day 11 in CAR-T cells and DT.CAR-T cells, three individual donors were tested. A paired t-test was used for statistical analysis. ($^{*}P<0.05$, $^{**}P<0.01$, $^{***}P<0.001$, $^{****}P<0.0001$, *ns=no significant difference*)

To explain the phenomenon of higher cell number in DT.CAR-T cells, the cell proliferative and apoptotic capacities have been investigated in the current study. Proteins related to cell apoptosis have been examined by western blot assay. Specifically, caspase 3 and activated caspase 3 (cleaved caspase 3) that play crucial roles in the process of apoptosis, as well as Poly-(ADP-ribose)-polymerase (PARP), a protein whose activation can result in the cleavage of PARP itself by caspases leading to enzymatic inactivation and the release of a c-terminal fragment, were analyzed.

A downregulation of cleaved caspase 3 and cleaved PARP in DT19.CAR-T cells and non-transduced T cells were observed when compared to CD19.CAR-T cells (Figure 14A, $^{***}P<0.0001$). These findings suggest an increase of active apoptosis in CD19.CAR-T cells, but the upregulation of TCF-1 could reduce the level of active

apoptosis. The results were further proved in the case of CD33.CAR-T cells and DT33.CAR-T cells (Figure 14B, ***P<0.0001).

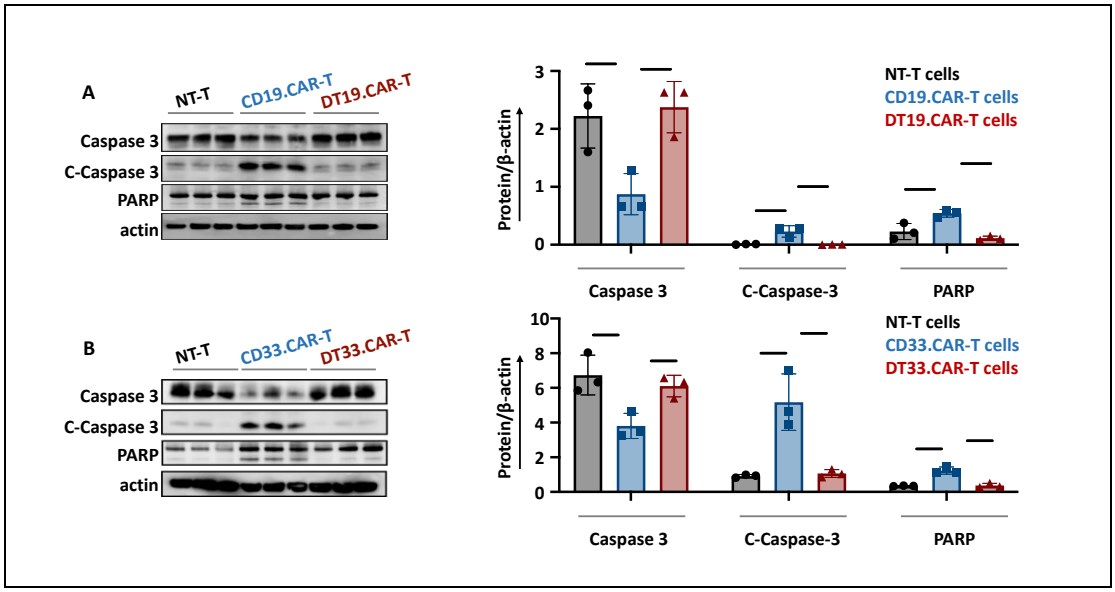

Figure 14: The expression of apoptotic proteins in non-transduced T cells, CAR-T cells and DT.CAR-T cells.

Statistical analysis of the protein level of caspase 3, cleaved caspase3, and PARP in non-transduced T cells, CAR-T cells and DT.CAR-T cells were assessed by western blot, three individual donors were tested. A paired t-test was used for statistical analysis. (*P<0.05, **P<0.01, ***P<0.001, ****P<0.0001, *ns=no significant difference*)

In the study, the proliferative potential of the cells was assessed by determining Ki67 expression using a flow cytometer-based assay. Interestingly, DT19.CAR-T cells exhibited a lower frequency of Ki67-positive cells compared to CD19.CAR-T cells (Figure 15A, 75.02%±2.93 vs. 60.000±2.756, n=6, ****P<0.0001). Moreover, a significant lower expression of MFI of Ki67 in DT.CAR-T cells was observed than that in CD19.CAR-T cells (Figure 15B, 20266±1266.162 vs. 16866.333±682.749, n=6, ***P<0.001). Of note, transduced cells, both CD19.CAR-T and DT19.CAR-T cells, have a higher proliferative capacity when compared to the non-transduced T cells, evidenced by the lowest percentage and MFI of Ki67 (Figure 15C-D, percentage: 39.367%±5.384, MFI: 14331.5±371.071, n=6, ****P<0.0001). To validate these findings, we performed additional experiments using the CD33.CAR vector, and the

results demonstrated a similar pattern of decreased Ki67 expression in DT33.CAR-T cells (Figure 15E-H).

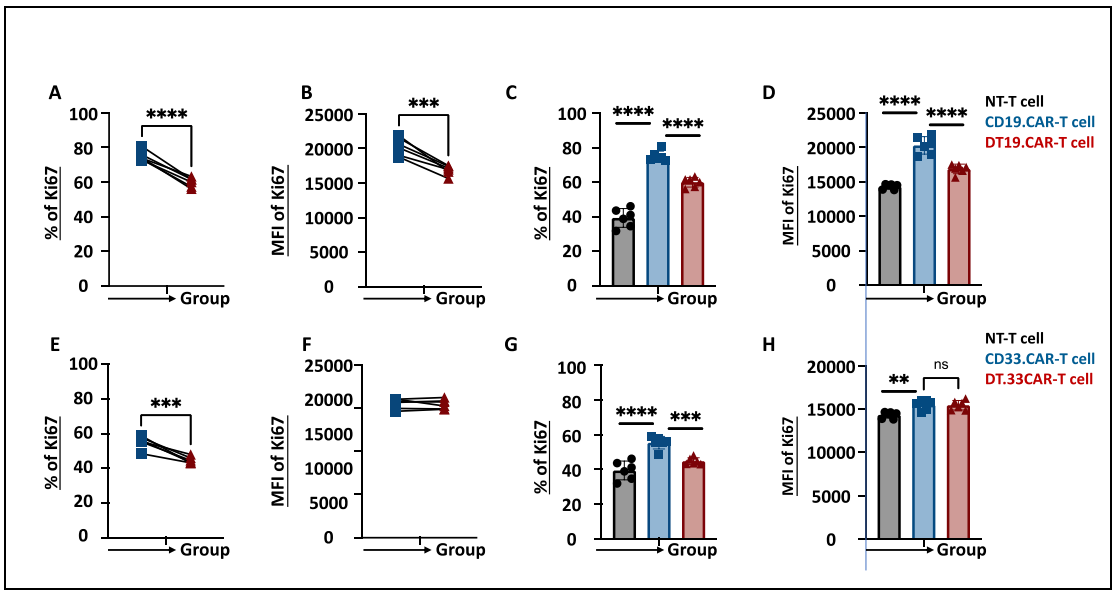

Figure 15: The expression of Ki67 in non-transduced T cells, CAR-T cells and DT.CAR-T cells.

Statistical analysis of the percentage and expression intensity of Ki67 in non-transduced T cells, six individual donors were tested. A paired t-test was used for statistical analysis. (*P<0.05, **P<0.01, ***P<0.001, ****P<0.0001, *ns=no significant difference*).

3.4 Modulation of CAR-T cell surface protein expression by overexpression of TCF-1

To comprehensively investigate the influence of TCF-1 on CAR-T cells, the dynamics of surface protein profile of CAR-T cells were monitored during the generation phase by flow cytometry. The apoptosis (apotracker, CD95 and CD253), differentiation (CD45RA, CCR7, CD62L and CXCR3), activation (CD27, CD57 and CD69) and co-stimulation (CD40L, CTLA-4 and ICOS) related proteins as well as the CAR expression have been examined on day 5, day 8, day 11 and day 14.

Besides an expert-driven flow cytometric analysis (a manual gating strategy), an advanced analytical strategy based on machine learning was established and applied to our immunophenotyping data (Figure 16), which allowed us to detect previously unknown cell populations in an unbased, data-driven manner without information loss.

As shown in Figure 16, the advanced analytical strategy comprises an advanced flow cytometric analysis, identification of cell population using several machine learn-based methods, significant analysis, and validation by visualization.

Dimensionality reduction and clustering methods were applied for the advanced flow cytometric analysis. t-distributed stochastic neighbor embedding (t-SNE) is employed to reduce the high-dimensional data into a lower-dimensional space, facilitating visualization and exploration of cell populations' intrinsic structure. Subsequently, phenograph clustering is utilized to identify distinct cell populations based on their expression profiles.

To further refine the analysis and enable predictive modeling, principal component analysis (PCA) was employed to find the key cell populations retaining the most significant variance. Hierarchical clustering was then implemented to cell populations based on their proximity, allowing to merge the cell populations with a similar marker expression. Finally, the cell populations with statistical significance were reviewed and validated through the manual gating. This iterative process allows us to easily identify discrepancies, refine the analysis, and improve the reliability of the findings.

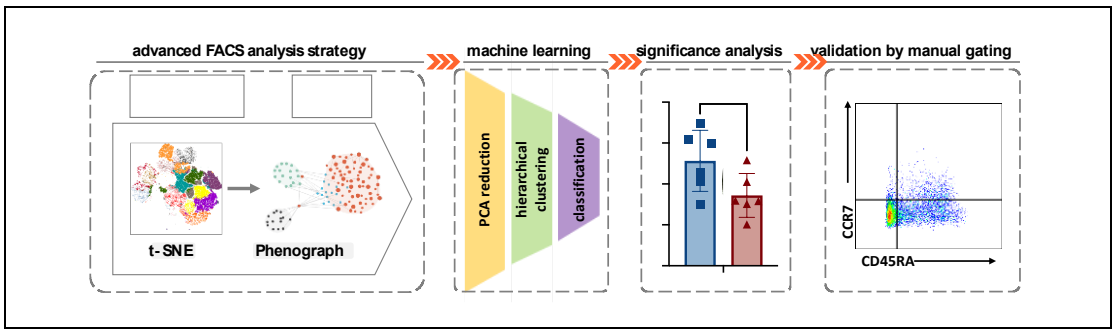

Figure 16: Workflow of data mining algorithm.

t-SNE: t-distributed stochastic neighbor embedding; PCA: principal component analysis.

It is of note that overexpression of TCF-1 obviously affected CD19.CAR-T cells with a change of the density of apoptotic proteins (Figure 17), differentiation related surface markers (Figure 18), activation markers (Figure 19), and co-stimulatory markers (Figure 20). A similar pattern has been observed in the CD33.CAR-T cell model (Appendix Figure 1 – Figure 4).

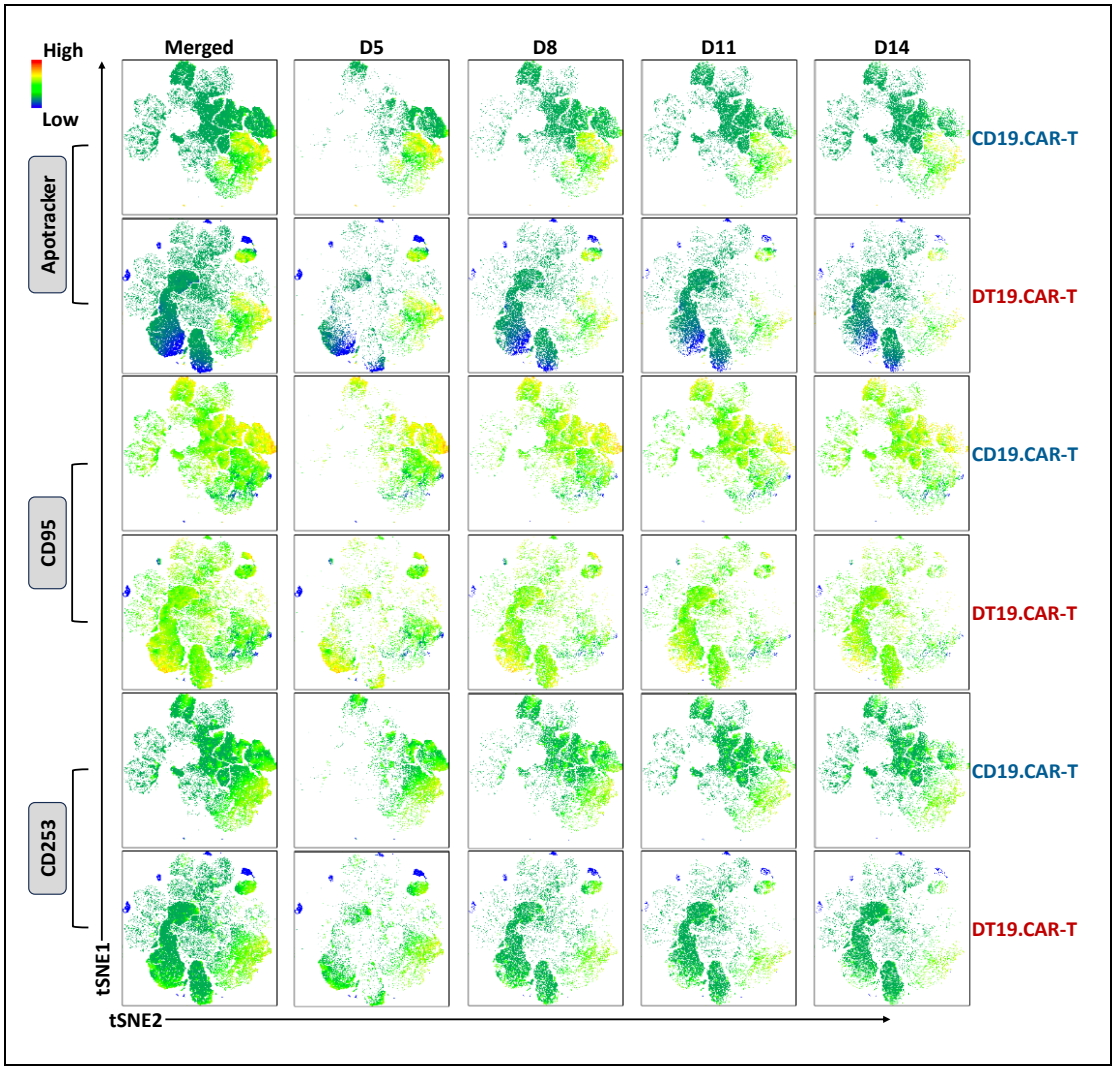

Figure 17: The intensity of apoptosis related proteins on CD19.CAR-T cells and DT19.CAR-T cells in t-SNE plot.

Merged: t-SNE figures from day 5 to day 14 were combined; D5: marker expression on t-SNE from generation day 5; D8: marker expression on t-SNE from generation day 8; D11: marker expression on t-SNE from generation day 11; D14; marker expression on t-SNE from generation day 14.

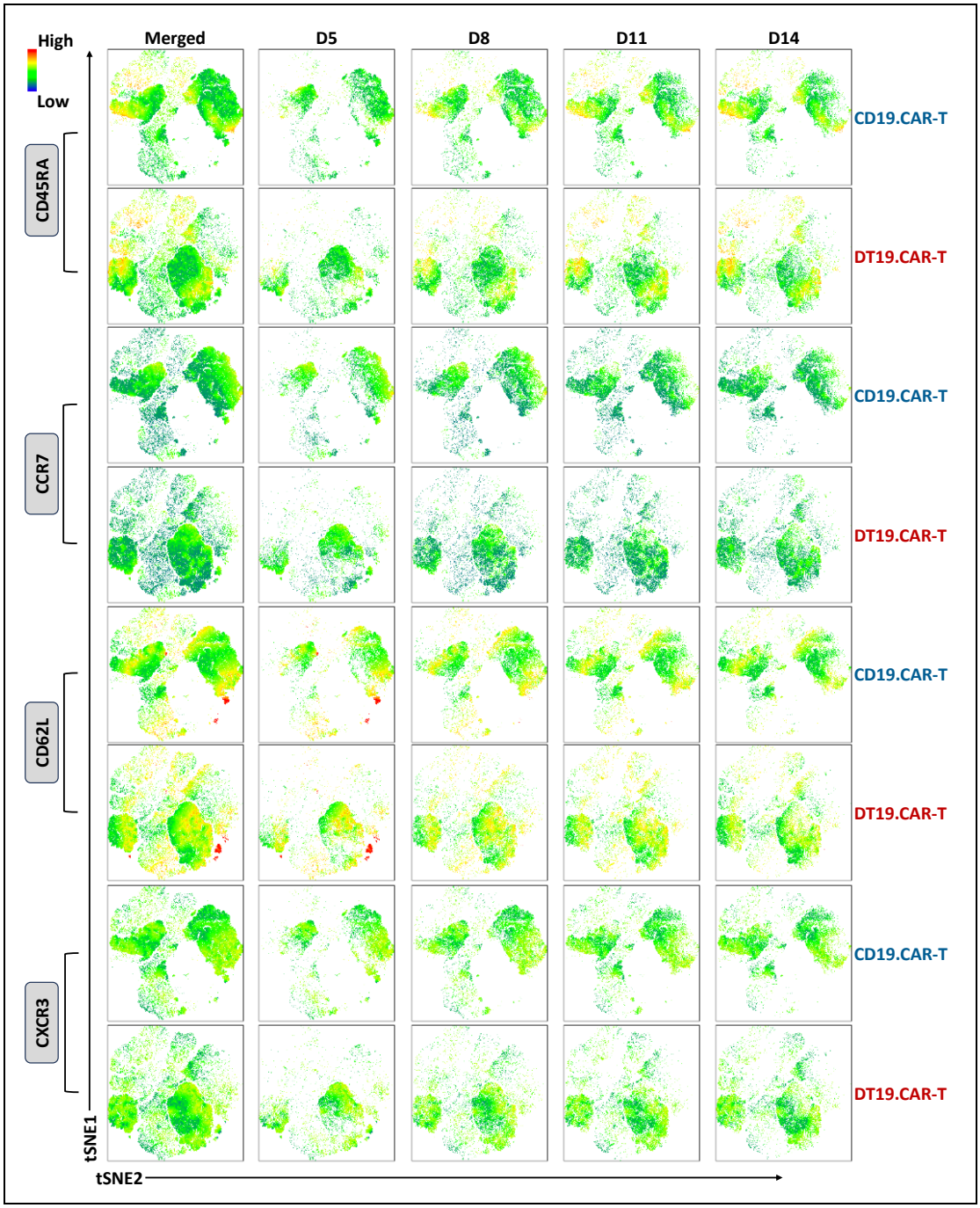

Figure 18: The intensity of differentiation markers on CD19.CAR-T cells and DT19.CAR-T cells in t-SNE plot.

Merged: t-SNE figures from day 5 to day 14 were combined; D5: marker expression on t-SNE from generation day 5; D8: marker expression on t-SNE from generation day 8; D11: marker expression on t-SNE from generation day 11; D14; marker expression on t-SNE from generation day 14.

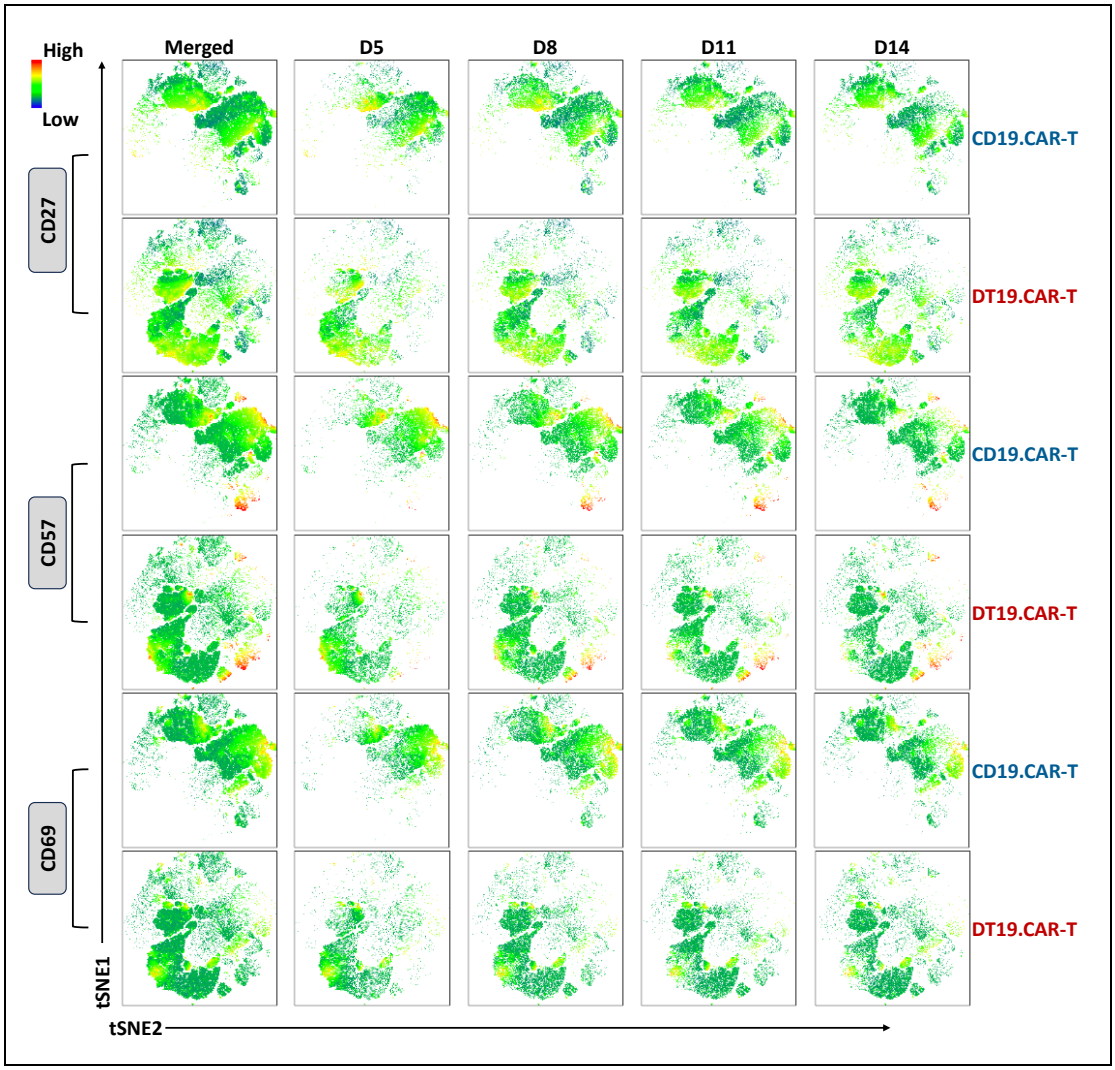

Figure 19: The intensity of activation markers on CD19.CAR-T cells and DT19.CAR-T cells in t-SNE plot.

Merged: t-SNE figures from day 5 to day 14 were combined; D5: marker expression on t-SNE from generation day 5; D8: marker expression on t-SNE from generation day 8; D11: marker expression on t-SNE from generation day 11; D14; marker expression on t-SNE from generation day 14.

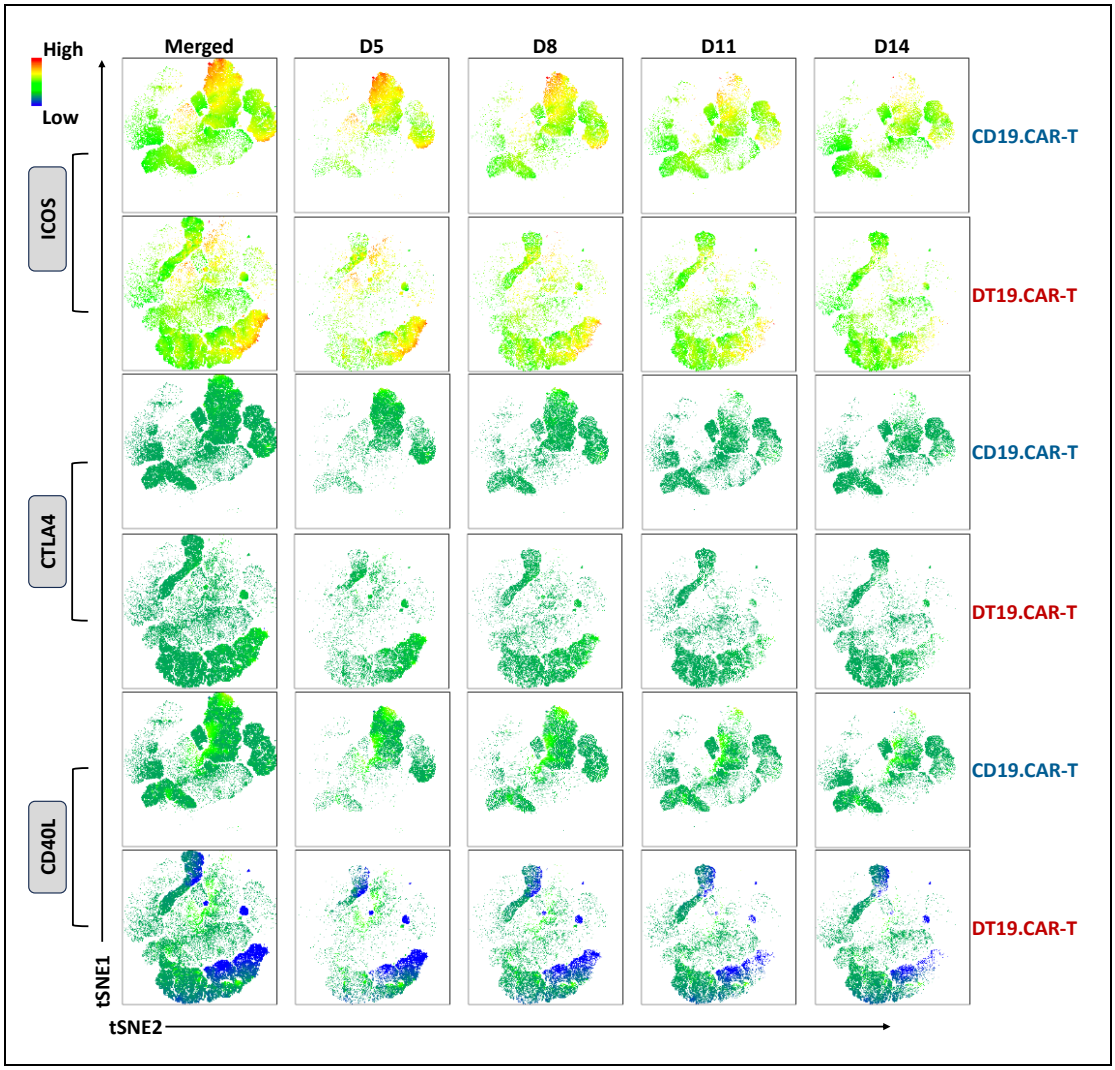

Figure 20: The intensity of co-stimulatory markers on CD19.CAR-T cells and DT19.CAR-T cells in t-SNE plot.

Merged: t-SNE figures from day 5 to day 14 were combined; D5: marker expression on t-SNE from generation day 5; D8: marker expression on t-SNE from generation day 8; D11: marker expression on t-SNE from generation day 11; D14; marker expression on t-SNE from generation day 14.

3.4.1 Reduction of apoptosis by overexpression of TCF-1

In order to deeply explore the apoptosis of CAR-T cells during the generation phase, a dynamic of multiple apoptotic proteins including phosphatidylserine residues detected by apotracker, CD95, and CD253 was examined on CAR-T cells at day 5, 8, 11, and 14. As depicted in Figure 21, the apoptotic marker positive cells were decreasing over time. Importantly, the percentages of apotracker, CD95, and CD253 positive cells were

consistently lower in DT19.CAR-T cells than CD19.CAR-T cells (Figure 21A-C), which was in line with our western blot data. Furthermore, CD33.CAR vector used to validate these results demonstrated a similar pattern as shown in Figure 21D-G.

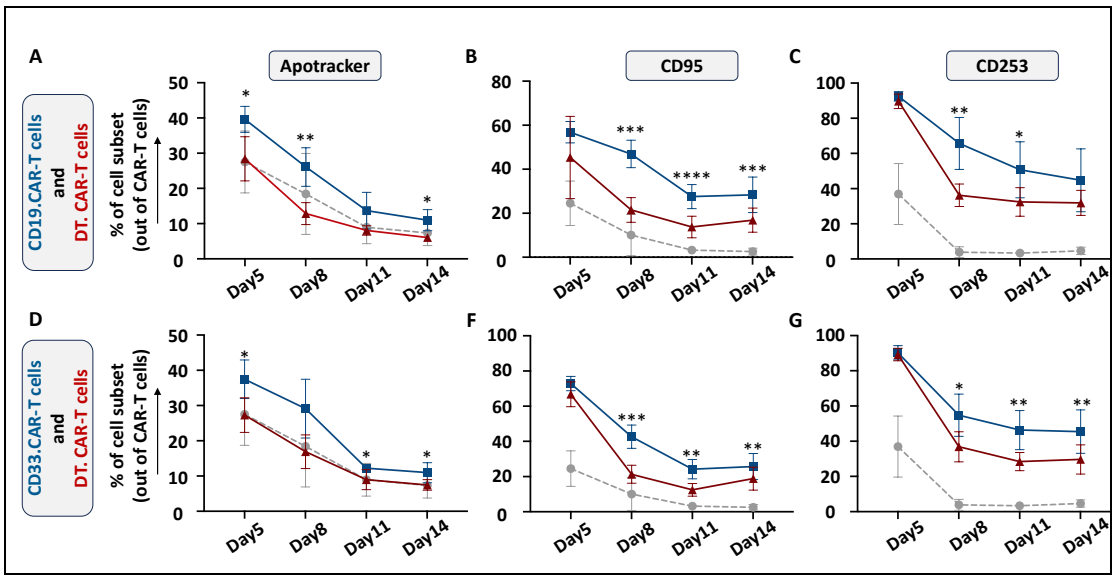

Figure 21: The dynamics of apoptotic marker expression on CAR-T cells and DT.CAR-T cells.

Statistical analysis of expression percentage of apotracker on CAR-T cells and DT.CAR-T cells, six individual donors were tested. A paired t-test was used for statistical analysis. (negative control: non-transduced T cell, n=6, **P*<0.05, ***P*<0.01, ****P*<0.001, *****P*<0.0001)

By using the advanced flow cytometric analysis, a total of 23 different cell clusters were identified and projected in the t-SNE space (Figure 22A), providing a comprehensive view of the cellular heterogeneity within the samples. Notably, CD19.CAR-T cells and DT19.CAR-T cells exhibited distinct patterns in a principal component analysis (PCA) plot (Figure 22B), indicating TCF-1 overexpression has a strong impact on CD19.CAR-T cells.

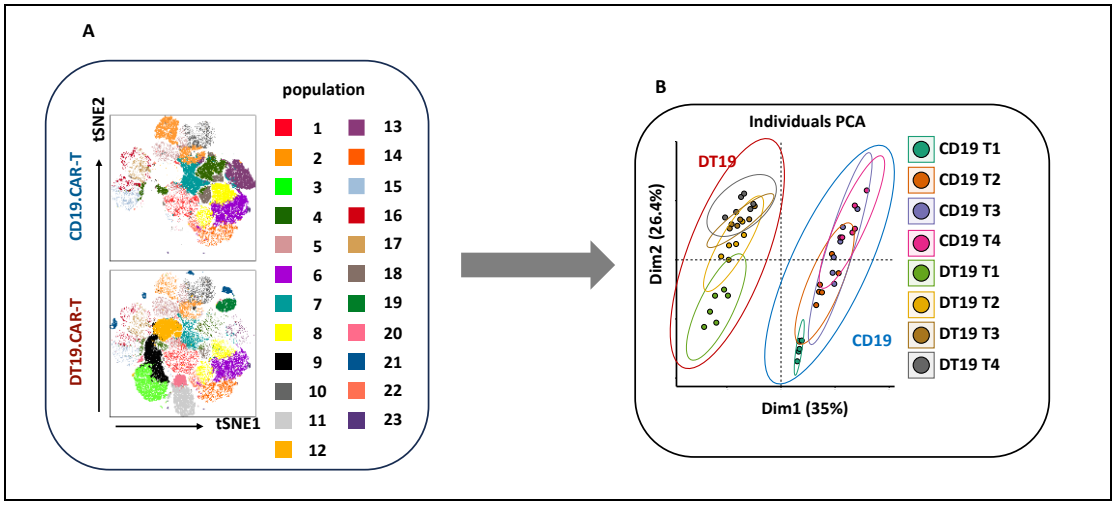

Figure 22: Cell clustering and PCA.

A: t-SNE plot pf phonograph identified cell clusters. B: Evaluation of distinguishing capability of cell clusters by PCA.

Considering that the clinical utilization of CAR-T product is normally after 10 days *ex vivo* expansion, our subsequent downstream analyses only focused on day 11 and 14. PCA was performed to identify the major principal components (PCs) that contributed at least 70% of the total variance for day 11 (Figure 23A, left panel) and day 14 (Figure 23B, left panel). The contribution of each variable (cell subset frequency) in accounting for the variability in these principal components was further analyzed. Through PCA analysis, 13 and 15 cell populations were identified for day 11 (Figure 23A, right panel) and day 14 (Figure 23B, right panel), respectively.

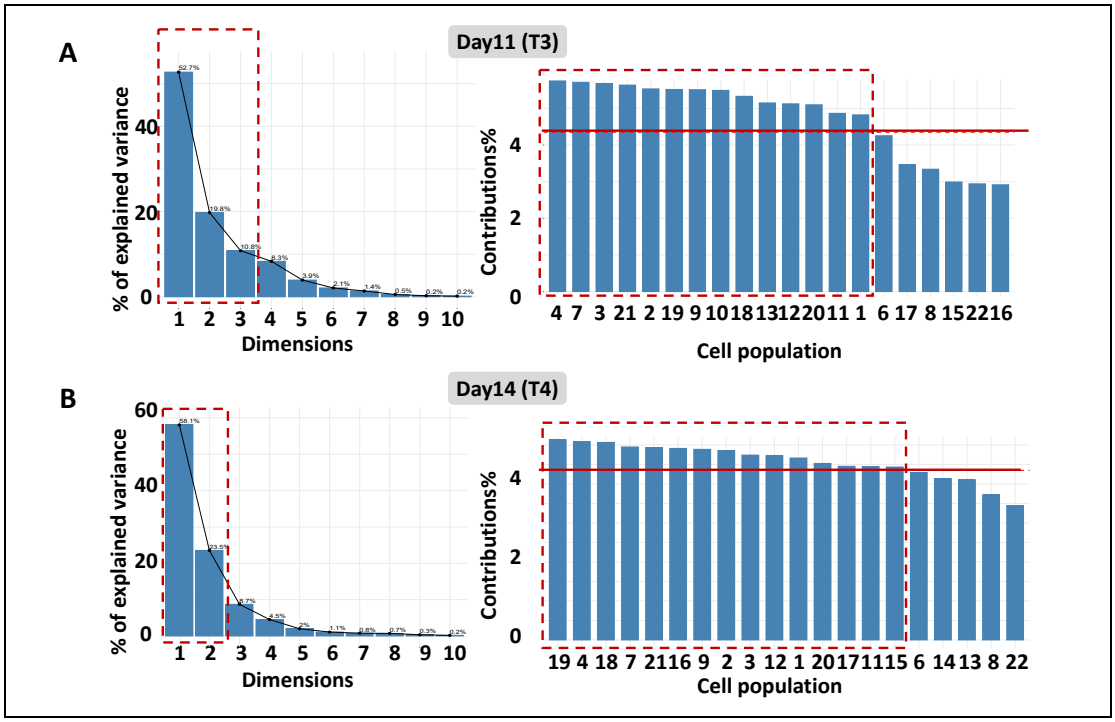

Figure 23: Dimension reduction by PCA.

Elbow-shaped scree plot to determine the number of factors to retain in an exploratory principal component (left panel). Contribution of rows to the dimensions (right panel), Rows that contribute the most to dimension 1 and dimension 2 or/and dimension 3, in total >70%, are the most important in explaining the variability in the data set. Rows that do not contribute much to any dimension or that contribute to the last dimensions are less important.

The commonality of cell populations between day 11 and day 14 was shown in a Venn diagram in Figure 24A. These 11 common cell populations were further combined into four distinct cell clusters by a manual classification based on the FACS dot plots (Figure 24B).

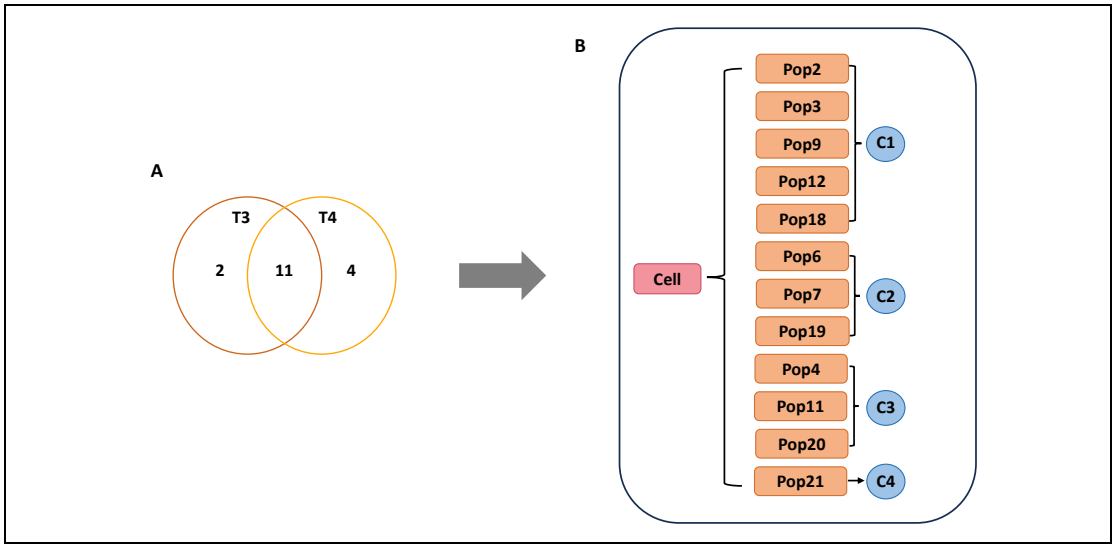

Figure 24: Workflow of Venn diagram and clustering of common cell populations

Figure A: The relationships between most important cell populations at day 11 and day 14 by Venn diagram. Figure B: Manual classification of common cell populations by flowcytometry dot plots (Pop: cell population, C: cell cluster).

The retained cell populations were further validated by a manual gating approach and a robustness check. Cell clusters with a cell count of less than 300 were excluded from the analysis. Consequently, two cell populations were found to be significantly correlated with the effect of TCF-1 overexpression (Figure 25A-B).

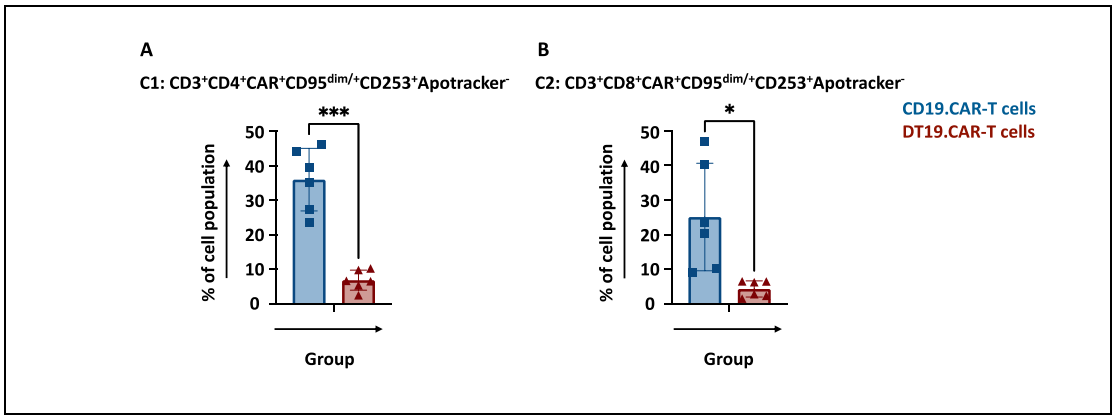

Figure 25: Statistical analysis of key cell clusters in CD19.CAR-T cells and DT19.CAR-T cells.

Statistical analysis of the percentage of $CD3^+CD4^+CAR^+CD95^{dim/+}CD253^+$ $Apotracker^-$ and $CD3^+CD8^+CAR^+CD95^{dim/+}CD253^+Apotracker^-$ in CD19. CAR-T cells and DT19.CAR-T cells. Six individual donors were tested. A paired t-test was used for statistical analysis. (*P<0.05, **P<0.01, ***P<0.001, ****P<0.0001)

Same analysis was applied to CD33.CAR-T cell model and similar observation was seen that DT33.CAR-T cells consistently exhibited lower expression levels of Apotracker, CD95, and CD253 when compared to CD33.CAR-T cells (Appendix Figure 5). $CD3^+CD4^+CAR^+CD95^{dim/+}CD253^+Apotracker^-$ cells as the key cell cluster were identified, as shown in Figure 26.

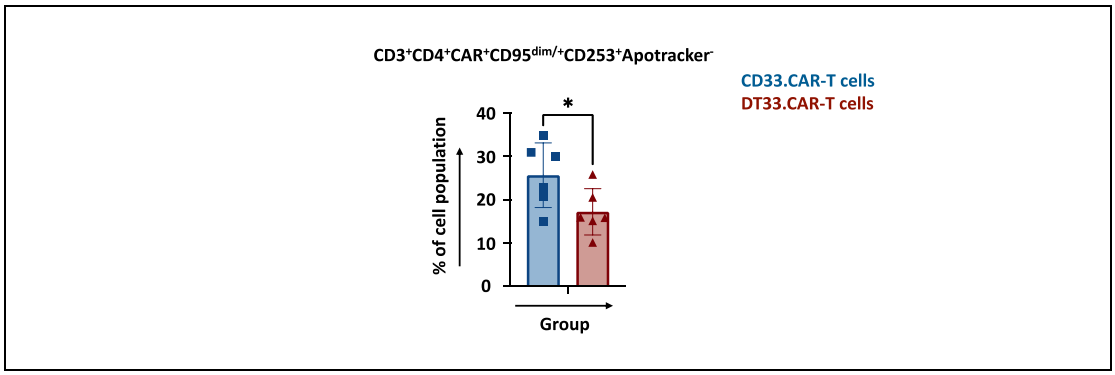

Figure 26: Statistical analysis of key cell clusters in CD33.CAR-T cells and DT33.CAR-T cells.

Statistical analysis of the percentage of $CD3^+CD4^+CAR^+CD95^{dim/+}$ $CD253^+Apotracker^-$ in CD33.CAR-T cells and DT33.CAR-T cells. Six individual donors were tested. A paired t-test was used for statistical analysis. (*P<0.05, **P<0.01, ***P<0.001, ****P<0.0001)

3.4.2 Maintaining of naïve status by overexpression of TCF-1

The impact of TCF-1 overexpression on the differentiation status of CAR-T cells was investigated. Of note, TCF-1 transduction could significantly increase the naïve T cells (T_N, $CCR7^+CD45RA^+$) at the formulation day in both CD19.CAR (Figure 27A) and CD33.CAR (Figure 27B) models, while no significant difference was observed in other cell components like effector T cells (T_E, $CCD7^-CD45RA^-$) and central memory T cells (T_{CM}, $CCR7^+CD45RA^-$) (Figure 27). Moreover, the frequency of effector memory T cells (T_{EM}, $CCR7^-CD45RA^+$) in DT19.CAR-T cells was significantly higher than CD19.CAR-T cells (Figure 27A), but not in CD33.CAR model (Figure 27B). Over the generation phase, we have also observed an increase of T_E cells along with a decrease of CD62L expression in both CD19.CAR (Figure 27A) and CD33.CAR (Figure 27B) models.

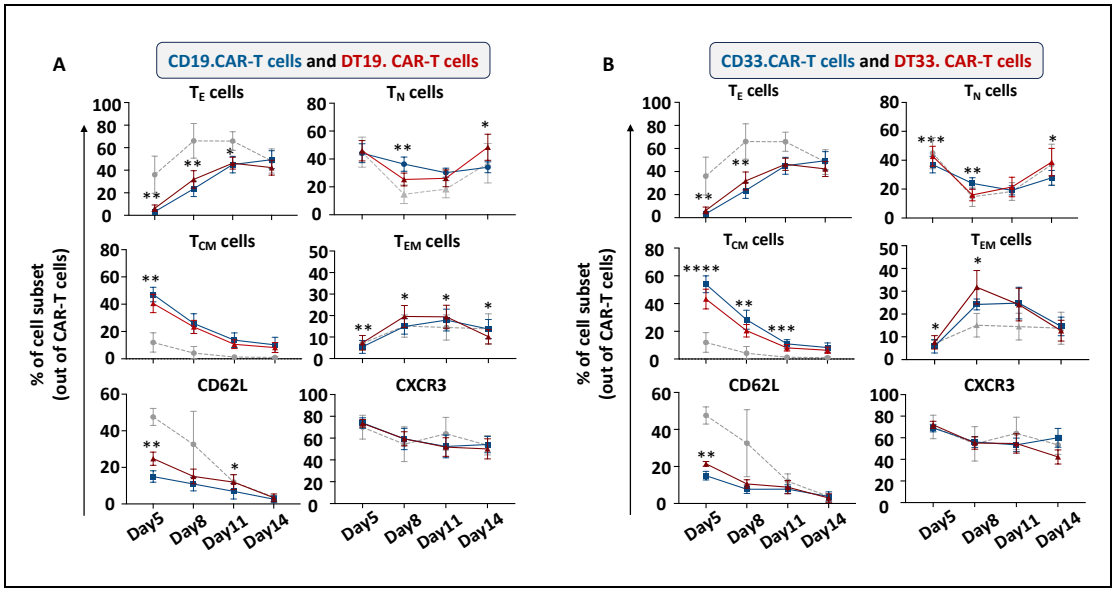

Figure 27: Effect of overexpression of TCF-1 on CAR-T cell differentiation over the generation period.

A: Statistical analysis of expression of differentiation markers (CD45RA, CCR7, CD62L, CXCR3) on CD19.CAR-T cells and DT.CAR-T cells. B: Statistical analysis of expression of differentiation markers (CD45RA, CCR7, CD62L, CXCR3) on CD33.CAR-T cells and DT.CAR-T cells. non-transduced T cells were used as control group. Six individual donors were use in this experiment. A paired t-test was used for statistical analysis. **P*<0.05, ***P*<0.01, ****P*<0.001, *****P*<0.0001.

To identify the key cell populations affected by TCF-1 transduction, our data mining algorithm was employed on the differentiation panel (Figure 28). Six cell clusters were automatically identified (Figure 28E) and further reduced to two cell clusters through a manual gating validation (Figure 29).

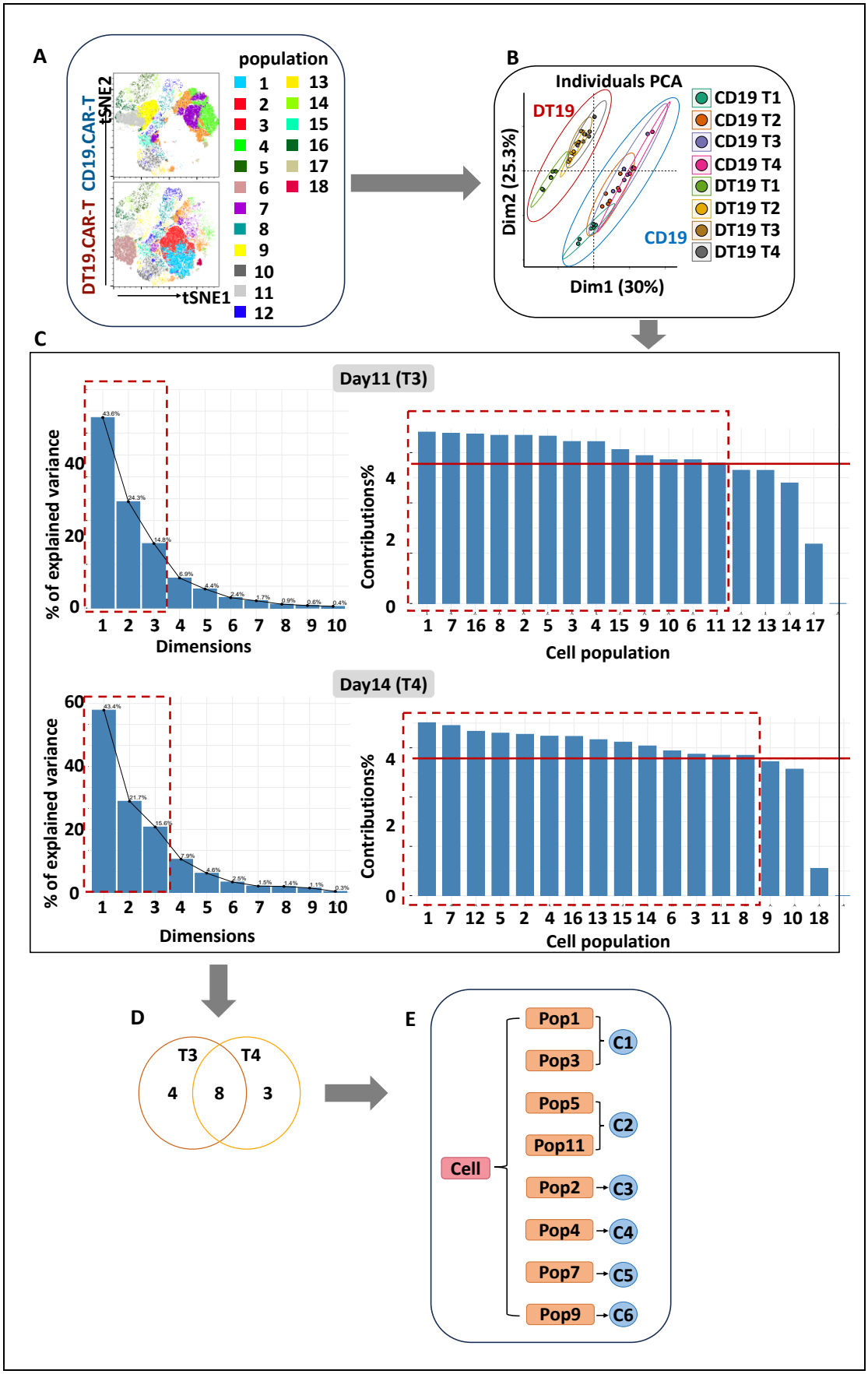

Figure 28: Workflow of data mining algorithm.

A: Cell clustering and PCA: t-SNE plot pf phonograph identified cell clusters. B: Evaluation of distinguishing capability of cell clusters by PCA. C : Dimension reduction by PCA: Elbow-shaped scree plot to determine the number of factors to retain in an exploratory principal component (left panel). Contribution of rows to the dimensions (right panel), Rows that contribute the most to dimension 1 and dimension 2 and dimension 3, in total >70%, are the most important in explaining the variability in the data set. Rows that do not contribute much to any dimension or that contribute to the last dimensions are less important. D: The relationships between most important cell populations at day 11 and day 14 by Venn diagram. Figure B: Manual classification of common cell populations by flowcytometry dot plots (Pop: cell population, C: cell cluster).

A lower frequency of $CD62L^+CXCR3^+CD4^+CAR\text{-}T_N$ cells (Figure 29A) but a higher frequency of $CD62L^+CXCR3^-CD4^+CAR\text{-}T_{CM}$ cells (Figure 29B) were found in DT19.CAR-T cells than CD19.CAR-T cells, which further supported by the consistent results obtained from CD33.CAR model (Figure 29C-D and Appendix Figure 6).

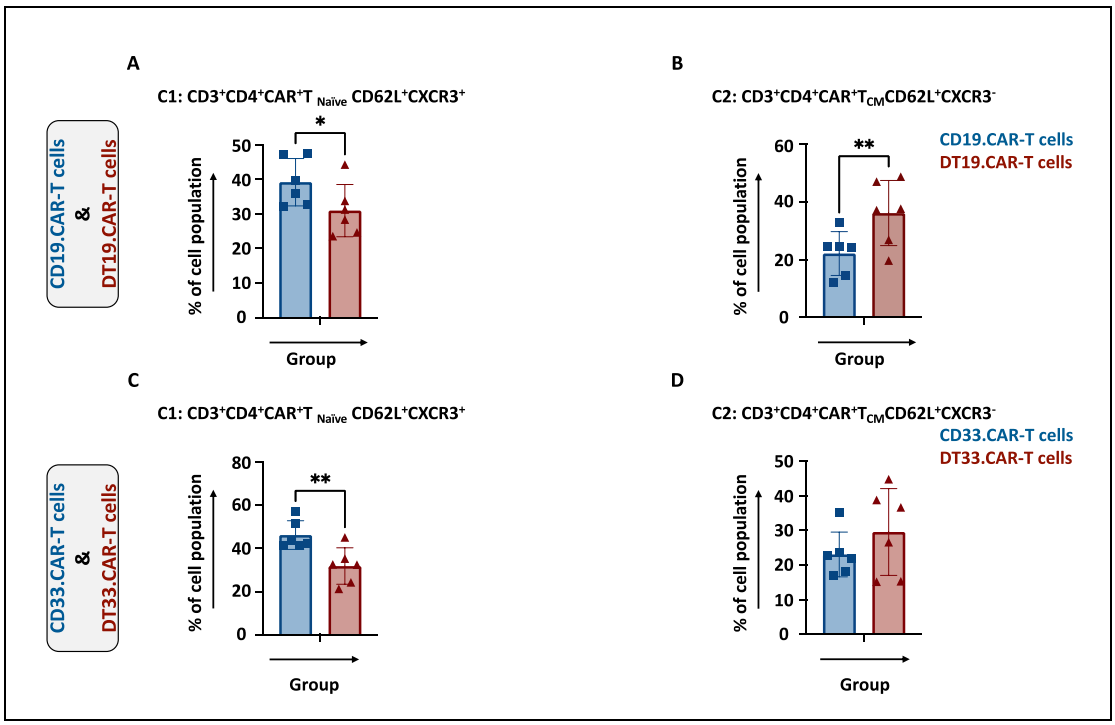

Figure 29: Statistical analysis of key cell clusters.

Statistical analysis of the percentage of $CD3^+CD4^+CAR^+T_N$ $CD62L^+CXCR3^+$ cells in CD19.CAR-T cells and CD33.CAR-T cells (Figure A and C). Statistical analysis of the percentage of $CD3^+CD4^+CAR^+T_{CM}$ $CD62L^+CXCR3^+$ cells in DT19.CAR-T cells and DT33.CAR-T cells. Six individual donors were tested. A paired t-test was used for statistical analysis. (*P<0.05, **P<0.01, ***P<0.001, ****P<0.0001)

3.4.3 Modulation of CAR-T cell activation by overexpression of TCF-1

Despite CD19.CAR-T cells and DT19.CAR-T cells showed a decreased tendency of activation markers over time, DT19.CAR-T cells exhibited a higher expression of CD27 (Figure 30A) and a lower expression of CD57 (Figure 30B) and CD69 (Figure 30C) throughout the generation phase. To validate and confirm the observed findings, similar experiments were conducted using the CD33.CAR vector. Remarkably, the results obtained with CD33.CAR-T cells (Figure 30D-F) were consistent and comparable to those obtained with CD19.CAR-T cells.

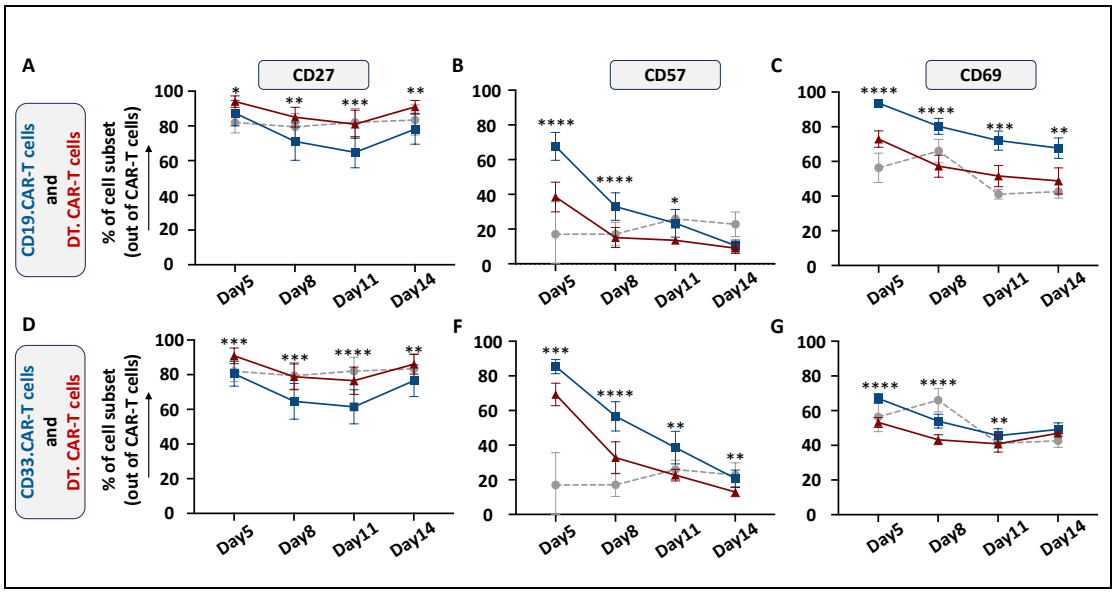

Figure 30: Effect of overexpression of TCF-1 on activation markers (CD27, CD57, CD69) expression on CAR-T cells and DT.CAR-T cells from Day 5 to Day 14.

Statistical analysis of expression percentage of apotracker on CAR-T cells and DT.CAR-T cells, six individual donors were tested. A paired t-test was used for statistical analysis. (negative control: non-transduced T cell, n=6, **P*<0.05, ***P*<0.01, ****P*<0.001, *****P*<0.0001)

The unbiased machine learning-based data mining strategy was applied to find specific cell populations influenced by overexpression of TCF-1 in CAR-T cells. Through this approach (Figure 31A-D), seven distinct cell populations of interest were identified (Figure 31E).

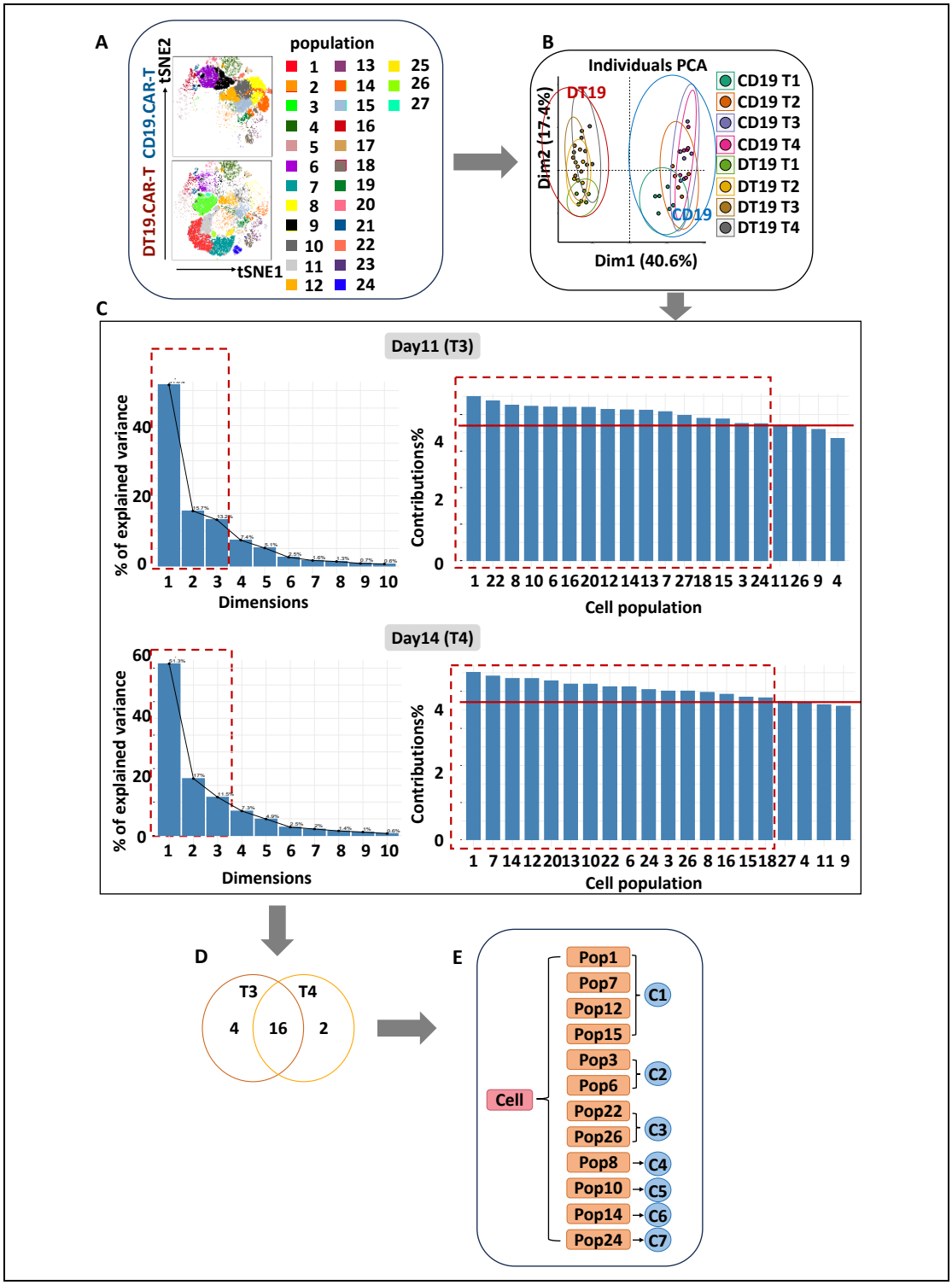

Figure 31: Workflow of data mining algorithm.

A: Cell clustering and PCA: t-SNE plot pf phonograph identified cell clusters. B: Evaluation of distinguishing capability of cell clusters by PCA. C : Dimension reduction by PCA: Elbow-shaped scree plot to determine the number of factors to retain in an exploratory principal component (left panel). Contribution of rows to the dimensions (right panel), Rows that contribute the most to dimension 1 and dimension 2 and dimension 3, in total >70%, are the most important in explaining the variability in the

data set. Rows that do not contribute much to any dimension or that contribute to the last dimensions are less important. D: The relationships between most important cell populations at day 11 and day 14 by Venn diagram. Figure B: Manual classification of common cell populations by flowcytometry dot plots (Pop: cell population, C: cell cluster).

Subsequently, a validation by manual gating was performed and three key cell populations were remained.

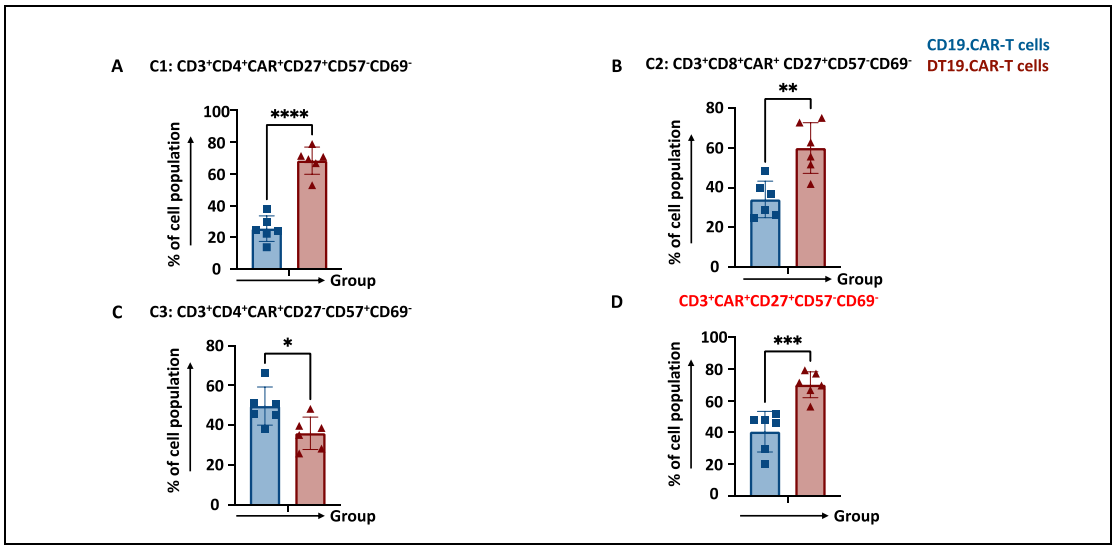

Figure 32: Statistical analysis of key cell clusters in CD19.CAR-T cells and DT19.CAR-T cells.

Statistical analysis of the percentage of different key cells clusters in CD19.CAR-T cells and DT19.CAR-T cells. Six individual donors were tested. A paired t-test was sued for statistical analysis. (*P<0.05, **P<0.01, ***P<0.001, ****P<0.0001)

DT19.CAR-T cells exhibited a higher proportion of the $CD27^+CD57^-CD69^-$ population in both $CD4^+$ (Figure 32A, 25.517±8.046 vs 68.283±8.553, ****P<0.0001;) and $CD8^+$ T cells (Figure 32B, 34.017±9.197 vs 59.900±12.765, **P<0.01), leading to a significance in the overall $CD3^+$ T cell as well (Figure 32D, 40.517±12.757 vs 70.000±8.156, ***P<0.001). Moreover, DT19.CAR-T cells contained a lower proportion of $CD27^-CD57^+CD69^-CD4^+$ T cells compared to CD19.CAR-T cells (Figure 32C, 49.617±9.589 vs 35.933±8.185, *P<0.05).

A similar pattern (Appendix Figure 7) was observed in CD33.CAR-T cells model, showing higher frequencies of $CD27^+CD57^-CD69^-CD4^+$ T cells (Figure 33A) and $CD27^-CD57^+CD69^-CD4^+$ T cells (Figure 33C) in DT33.CAR-T cells when compared

to CD33.CAR-T cells. Although there was no significant difference of $CD27^{+}CD57^{-}CD69^{-}CD8^{+}$ T cells between DT33.CAR-T cells and CD33.CAR-T cells (Figure 33B) like in CD19.CAR model, a significant difference of $CD27^{+}CD57^{-}CD69^{-}$ cells in CD3 T cells was still observed (Figure 33D).

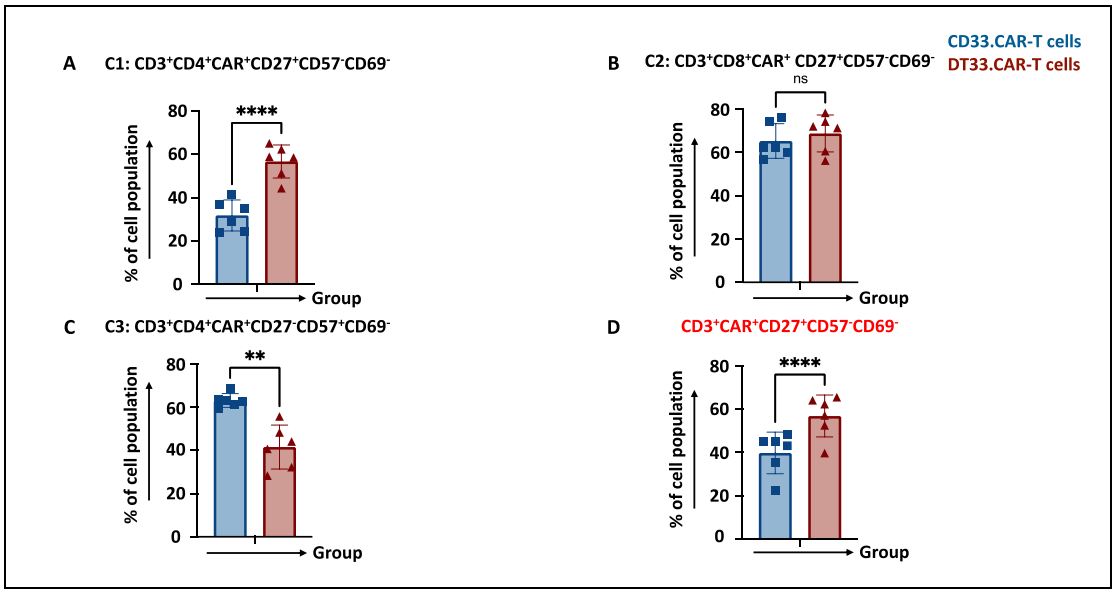

Figure 33: Statistical analysis of key cell clusters in CD33.CAR-T cells and DT33.CAR-T cells.

Statistical analysis of the percentage of different key cells clusters in CD33.CAR-T cells and DT33.CAR-T cells. Six individual donors were tested. A paired t-test was sued for statistical analysis. (*P<0.05, **P<0.01, ***P<0.001, ****P<0.0001, *ns= no significant difference*)

3.4.4 Modulation of co-stimulatory signal with a trend to inhibition by TCF-1 overexpression

Three different co-stimulatory markers have been monitored during the CAR-T generation. Our data showed that DT19.CAR-T cells had a consistently lower expression of CD40L since day 5 (Figure 34A, 46.467%±7.537 vs 13.207%±3.512, ****P<0.0001) till day 14 (Figure 34A, 23.050%±9.314 vs 6.043%±3.701, ***P<0.001). On the contrary, a higher expression of CTLA4 with a decreasing trend over time was observed in DT19.CAR-T cells (Figure 34B, day 14: 64.883%±5.735 vs 73.550%±2.414, **P<0.01). The expression of ICOS showed a significant difference

between DT19.CAR-T cells and CD19.CAR-T cells at the early stage (Figure 34C, day 5: 48.850%±7.739 vs 36.583%±7.678, ****P<0.0001, day 8: 15.610%±4.121 vs 9.533%±2.408, **P<0.01), but not at day 11 and day 14.

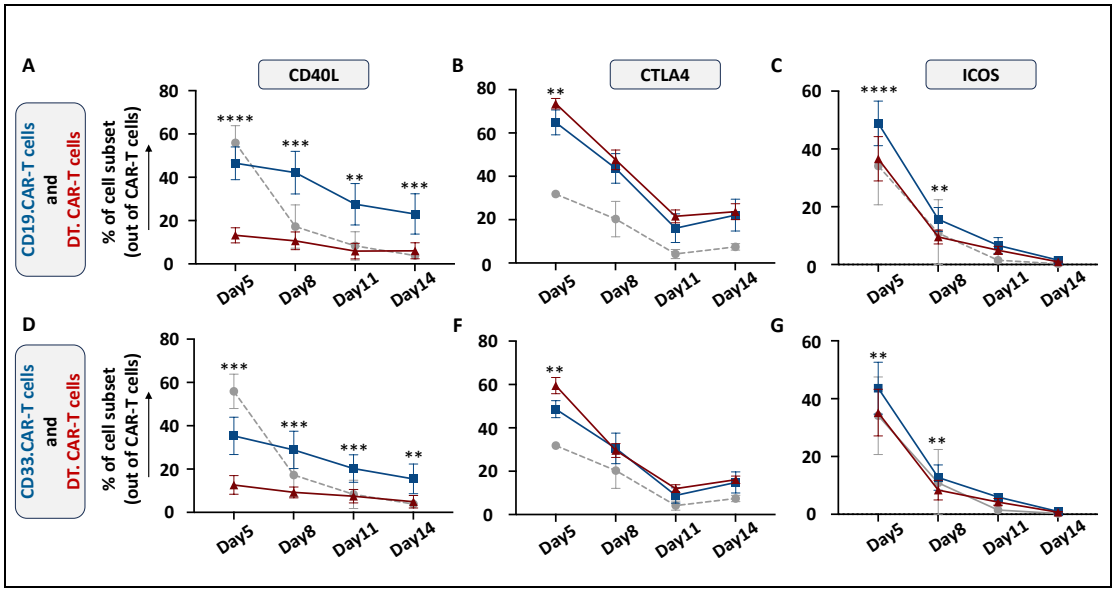

Figure 34: Effect of overexpression of TCF-1 on co-stimulatory markers expression on CAR-T cells and DT.CAR-T cells from Day 5 to Day 14.

ICOS (Inducible T-cell Co-Stimulator); CTLA4 (Cytotoxic T-lymphocyte antigen 4). Six individual donors were tested. A paired t-test was used for statistical analysis. (*P<0.05, **P<0.01, ***P<0.001, ****P<0.0001)

The consistent results were obtained with the CD33 vector validation, suggesting that the impact of TCF-1 overexpression on CAR-T cells in terms of co-stimulatory markers is independent from vectors (Figure 34D-F).

To identify the specific cell populations influenced by TCF-1, the advanced data mining strategy based-on machine learning was applied to the co-stimulatory marker panel (Figure 35), resulting in eight cell clusters (Figure 35E).

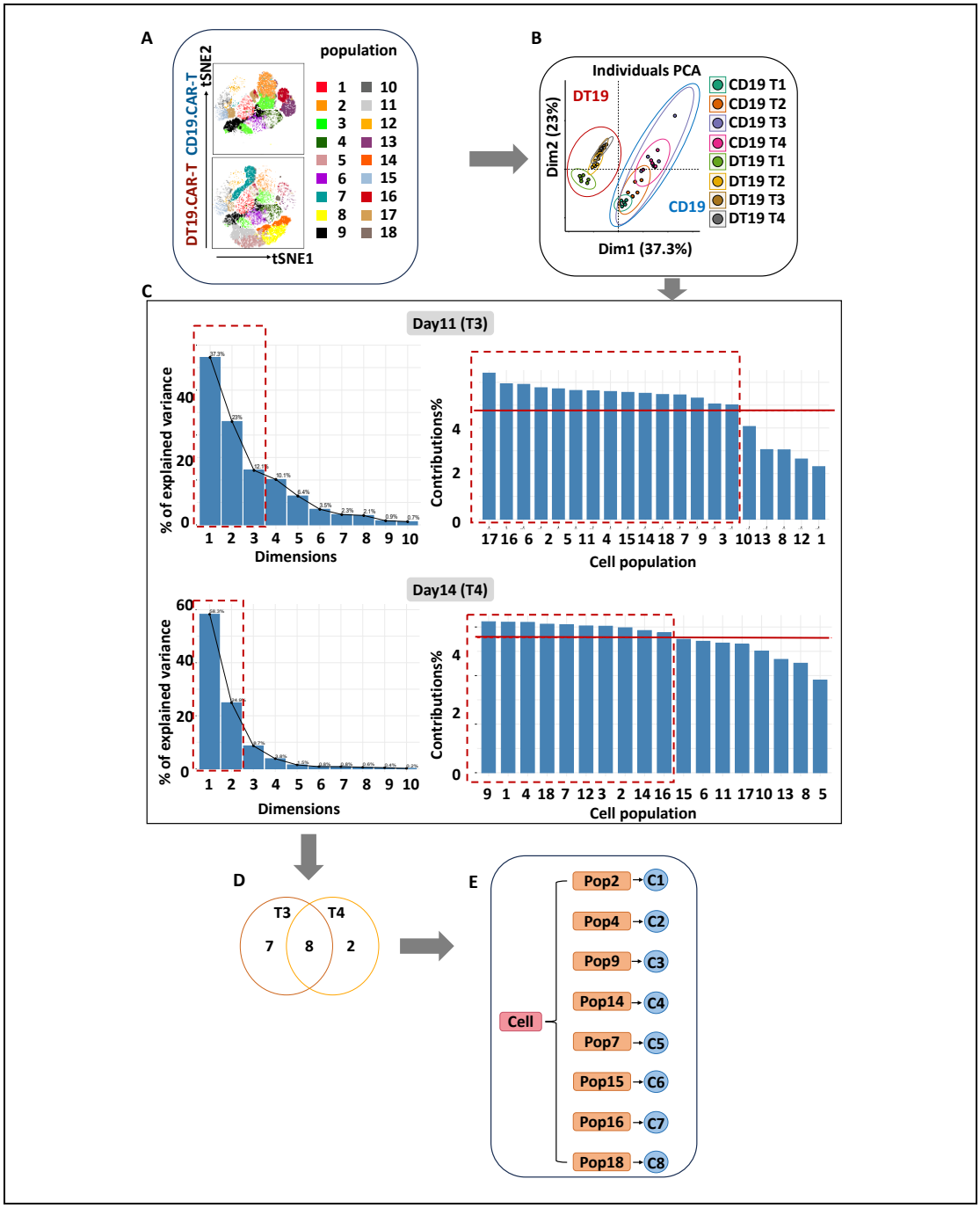

Figure 35: Workflow of data mining algorithm.

A: Cell clustering and PCA: t-SNE plot pf phonograph identified cell clusters. B: Evaluation of distinguishing capability of cell clusters by PCA. C : Dimension reduction by PCA: Elbow-shaped scree plot to determine the number of factors to retain in an exploratory principal component (left panel). Contribution of rows to the dimensions (right panel), Rows that contribute the most to dimension 1 and dimension 2, or/and dimension 3, in total >70%, are the most important in explaining the variability in the data set. Rows that do not contribute much to any dimension or that contribute to the last dimensions are less important. D: The relationships between most important cell populations at day 11 and day 14 by Venn diagram. Figure B: Manual classification of

common cell populations by flowcytometry dot plots (Pop: cell population, C: cell cluster).

Following the advanced analysis, a manual gating strategy was employed to further validate these eight cell populations. Only three cell clusters were remained with sufficient cell numbers. Compared to CD19.CAR-T cells, DT19.CAR-T cells exhibited distinct patterns of co-stimulatory marker expression as demonstrated in Figure 36.

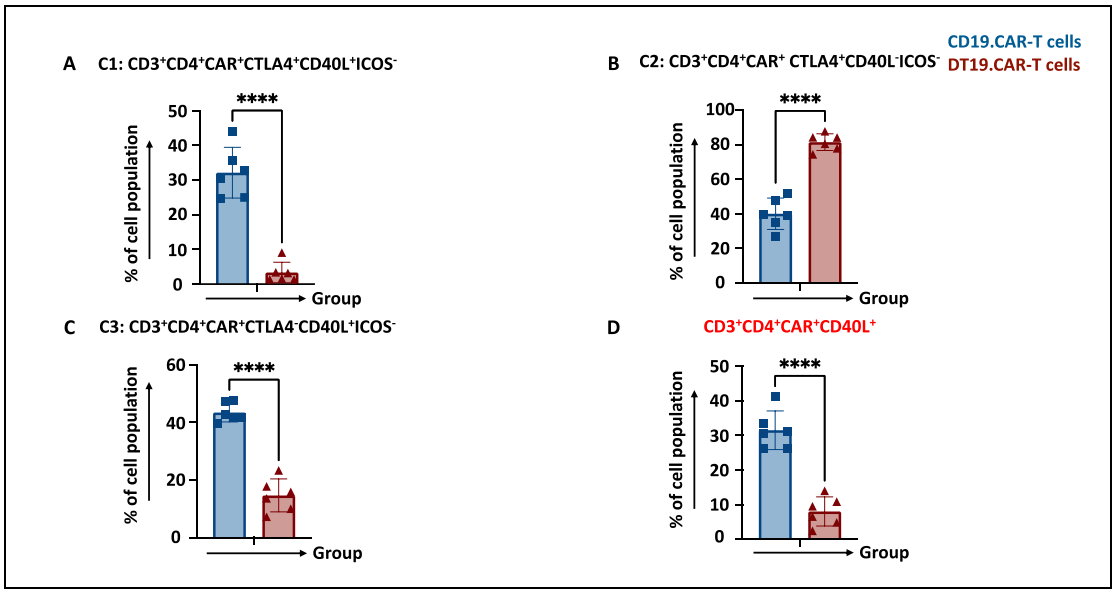

Figure 36: Statistical analysis of key cell clusters in CD19.CAR-T cells and DT19.CAR-T cells.

Statistical analysis of the percentage of different key cells clusters in CD33.CAR-T cells and DT19.CAR-T cells. Six individual donors were tested. A paired t-test was sued for statistical analysis. (*P<0.05, **P<0.01, ***P<0.001, ****P<0.0001, *ns= no significant difference*)

Specifically, DT19.CAR-T cells displayed a lower expression of multiple activating co-stimulatory markers $CD3^+CD4^+CAR^+CTLA4^+CD40L^+ICOS^-$ (Figure 36A: 32.167±7.303 vs 3.357±2.960, ****P<0.0001 ; Figure 36C: 43.467±3.267 vs 14.693±5.732, ****P<0.0001) and a higher expression of inhibitory co-stimulatory marker, $CD3^+CD4^+CAR^+CTLA4^+CD40L^-ICOS^-$ (Figure 36B, 40.017±9.070 vs 81.467±4.834, ****P<0.0001). Of note, CD40L potentially contribute to these differences, showing a significantly different expression on $CD4^+$ T cells between DT19.CAR-T cells and CD19.CAR-T cells (Figure 36D: 31.517±5.598 vs 8.080±4.211, ****P<0.0001). Further validation was conducted on CD33.CAR-T cells and

DT33.CAR-T cells (Appendix Figure 8). Notably, the results were found to be highly consistent with the findings observed in the CD19.CAR-T cells and DT19.CAR-T cells group (Figure 37).

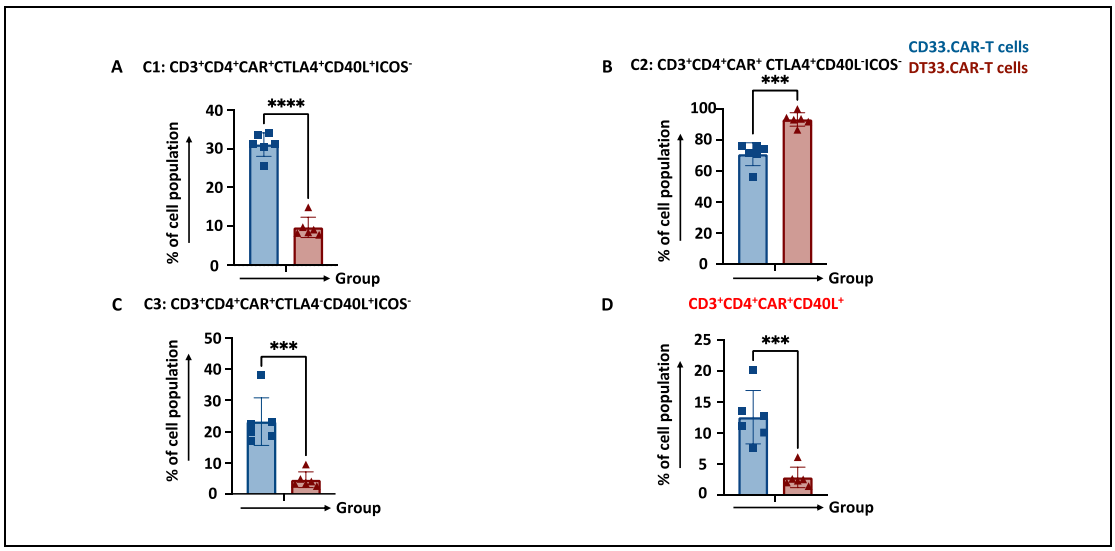

Figure 37: Statistical analysis of key cell clusters in CD33.CAR-T cells and DT33.CAR-T cells.

Statistical analysis of the percentage of different key cells clusters in CD33.CAR-T cells and DT33.CAR-T cells. Six individual donors were tested. A paired t-test was used for statistical analysis. (*P<0.05, **P<0.01, ***P<0.001, ****P<0.0001, *ns= no significant difference*)

3.5 Moderate cytokine release capacity of DT.CAR-T cells correlated with a low CAR density

To determine the effect of overexpression of TCF-1 on the cytokine profile of CAR-T cells, a broad array of cytokines in the supernatant was monitored at four different time points during the generation phase. A distinct cytokine secretion pattern between CD19.CAR-T cells and DT19.CAR-T cells was observed, showing a less capacity to release cytokines by DT19.CAR-T cells with a donor variation (Figure 38). Interestingly, IL-6 was apparently increasing released by DT19.CAR-T cells at the later phases (day 11 and day 14, Figure 38 C-D).

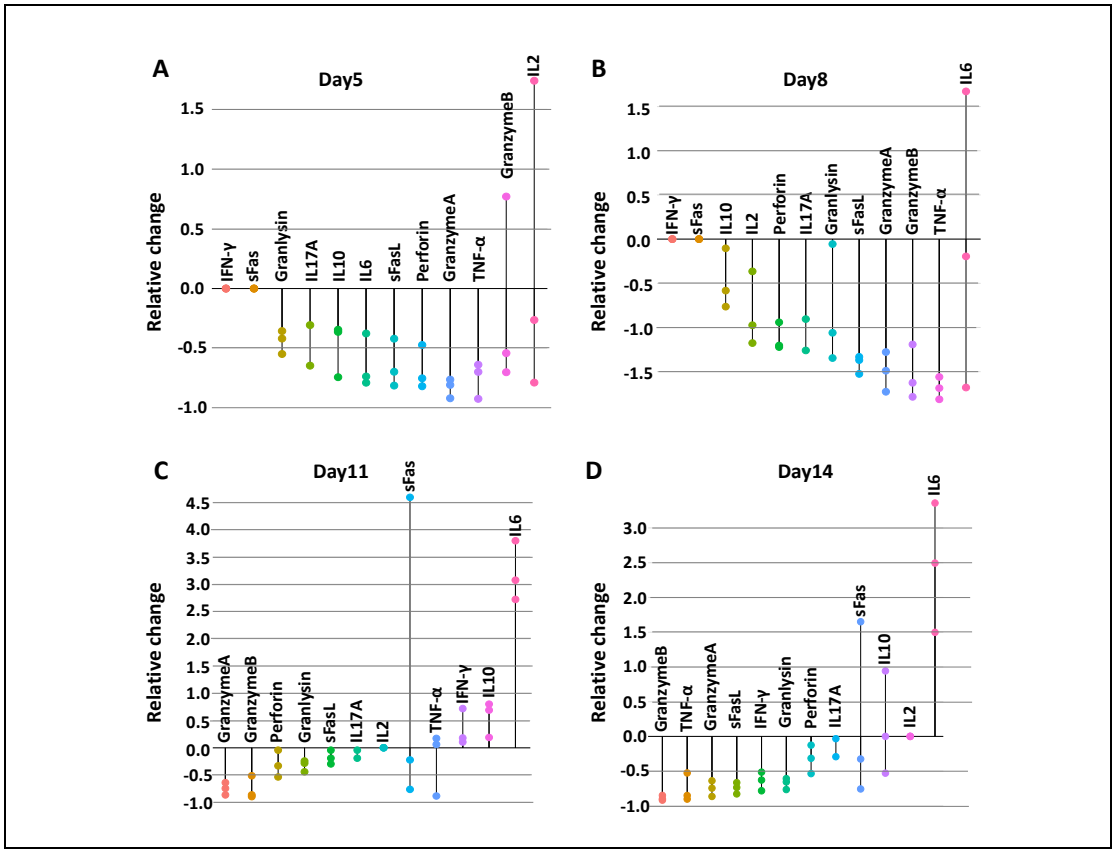

Figure 38: The relative change of cytokine secretion at different timepoint.

Three individual donors were tested. Relative change = (cytokine concentration of DT19.CAR-T cells-cytokine concentration of CD19.CAR-T cells) / (cytokine concentration of CD19.CAR-T cells).

To further confirm the reduced cytokine release capability of DT.19 CAR-T cells, an intracellular cytokine staining of CAR-T cells upon two different $CD19^{+}$ tumor cell stimulation was performed. In both conditions, Raji (Figure 39A-F) and Nalm6 (Figure 39G-M) tumor cell stimulations, the percentages of cytokine releasing CAR-T cells in terms of CD107a, TNF-α and IFN-γ were statistically significant decrease in DT19.CAR-T cells (CD107a in Raji stimulation: Figure 39A, 82.483%±4.266 vs 61.850%±8.118, ****P<0.0001; CD107a in Nalm6 stimulation: Figure 39G; TNF-α in Raji stimulation: Figure 39B, 67.683%±4.576 vs 52.267±3.926, ****P<0.0001; TNF-α in Nalm6 stimulation: Figure 39H; IFN-γ in Raji stimulation: Figure 39C, 42.633%±10.097 vs 29.667%±8.116, ***P<0.001; IFN-γ in Nalm6 stimulation: Figure 39I).

Moreover, the cytokine release capacity by per cells indicated by MFI was also reduced in DT19.CAR-T cells not only upon Raji stimulation (Figure 39D-F, CD107a: 1545±289.624 vs 974.667±97.635, ***P<0.001; TNF-α: 4654.167±2144.498 vs 3470±1362.109, *P<0.05; TNF-α: 6388±4452.528 vs 3483.833±1806.193, *P<0.05) but also upon Nalm6 stimulation (Figure 39J-M).

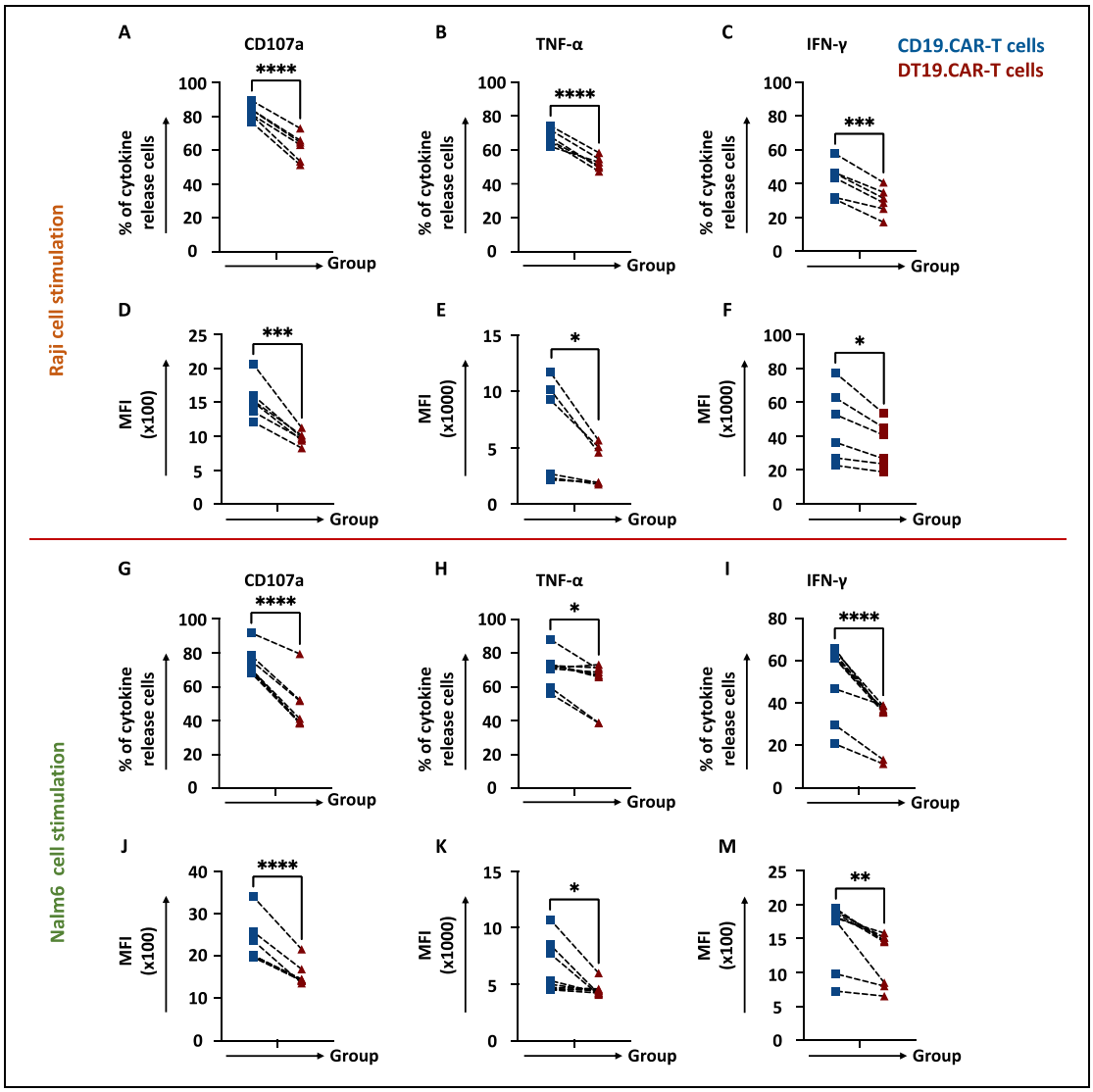

Figure 39: Statistical analysis of cytokine release of CAR-T cells and DT.CAR-T cells.

Statistical analysis of percentage of cytokine release of CAR-T cells and DT.CAR-T cells (Figure 39A-C, Raji cells stimulation, and Figure 40G-I, Nalm6 stimulation). Statistical analysis of MFI of cytokine release of CAR-T cells and DT.CAR-T cells (Figure 39D-F, Raji cells stimulation, and Figure 39J-M, Nalm6 stimulation). TNF-α: Tumor Necrosis Factor-alpha; INF-γ: Interferon-gamma. Six individual donors were tested. A paired t-test was used for statistical analysis. (*P<0.05, **P<0.01, ***P<0.001, ****P<0.0001, *ns= no significant difference*)

Additionally, multi-functional cytokine releasing cell populations were assessed in our study, since it provides valuable insights into the functional status and efficacy of CAR-T cells.

The results obtained from DT19.CAR-T cells revealed a distinct pattern of multi-functional cytokine release subpopulations compared to CD19.CAR-T cells (Figure 40A). DT19.CAR-T cells exhibited a reduced percentage of triple-positive (TNF-α^+IFN-γ^+CD107a$^+$) CAR-T cells (33.411%±7.484 vs 16.814%±6.241, $^{**}P<0.01$). On the other hand, DT19.CAR-T cells displayed a higher proportion of triple-negative (TNF-α^-IFN-γ^-CD107a$^-$) CAR-T cells (11.584%±2.141 vs 24.456%±3.913, $^{**}P<0.01$). Moreover, DT19.CAR-T cells showed a reduction in TNF-α^-IFN-γ^+CD107a$^+$ (double positive) cell population (5.003%±2.609 vs 2.688%±0.849, $^{**}P<0.01$) and TNF-α^+IFN-γ^-CD107a$^+$ (double positive) cell population (24.278%±5.453 vs 17.100%±4.133, $^{**}P<0.01$) compared to CD19.CAR-T cells. Conversely, DT19.CAR-T cells exhibited a higher percentage of TNF-α^+IFN-γ^+CD107a$^-$ cell population (3.681%±2.113 vs 7.931%±3.923, $^{**}P<0.01$) and a higher population of TNF-α^+IFN-γ^-CD107a$^-$ (double negative) cell population (5.587%±3.589 vs 13.106±8.170, $^{**}P<0.01$) (Figure 40B). Moreover, similar results were shown upon Nalm6 stimulation (Figure 40C-D).

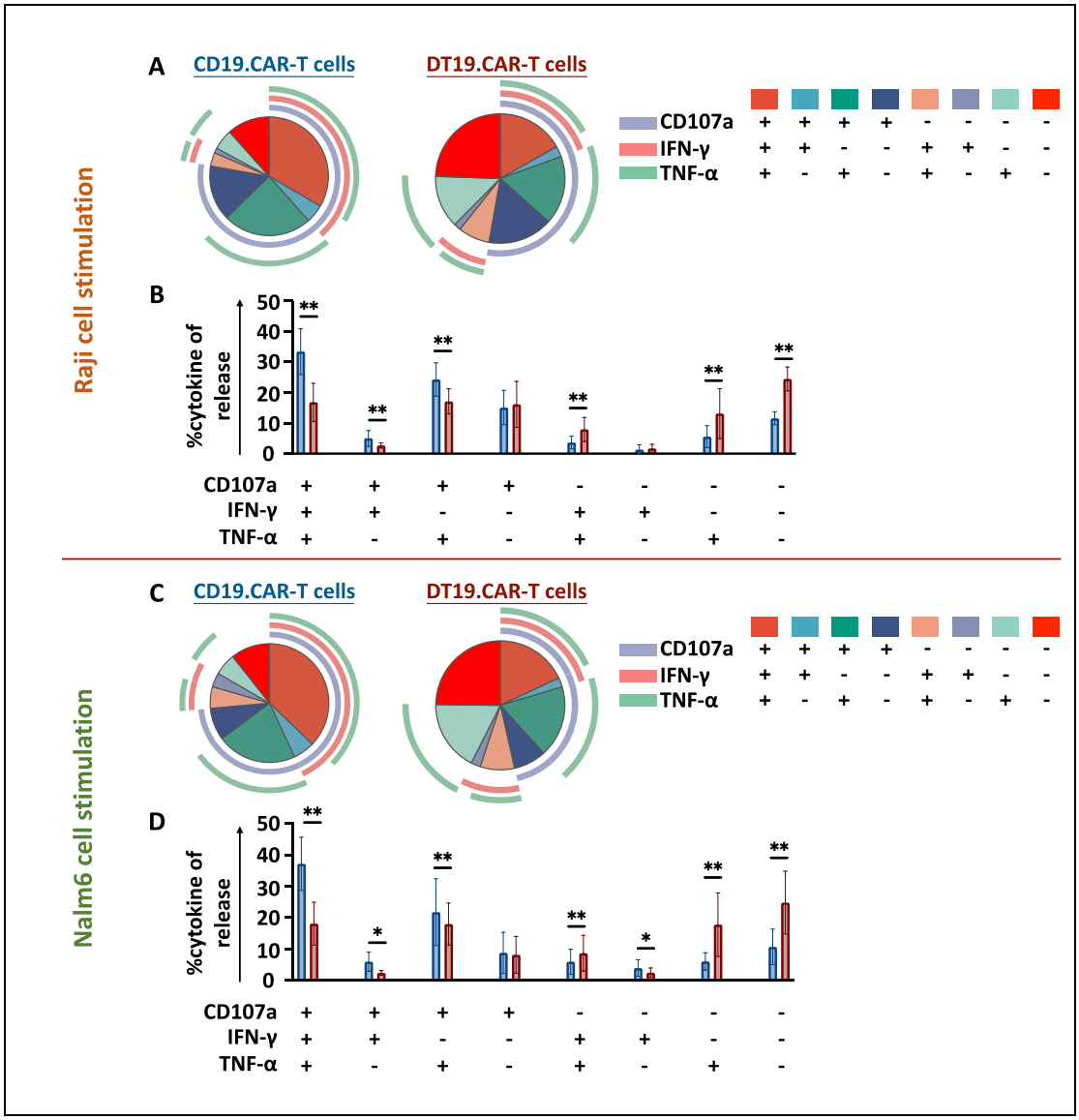

Figure 40: Effect of overexpression of TCF-1 on multi-functional CD19.CAR-T cells and DT19.CAR-T cells.

The polyfunctional CD19.CAR-T cells and DT19.CAR-T cells were analyzed using Boolean gating strategy. Raji cells were used as targeted cells (Figure 40A-B), and Nalm6 cells were used as targeted cells (Figure 40C-D). Nine individual donors were tested. A paired t-test was used for statistical analysis. (*P<0.05, **P<0.01, ***P<0.001, ****P<0.0001, *ns= no significant difference*)

Our findings, a low cytokine release capacity of CAR-T cells by additional TCF-1 transduction, was further strengthened by CD33.CAR-T cell model (Figure 41).

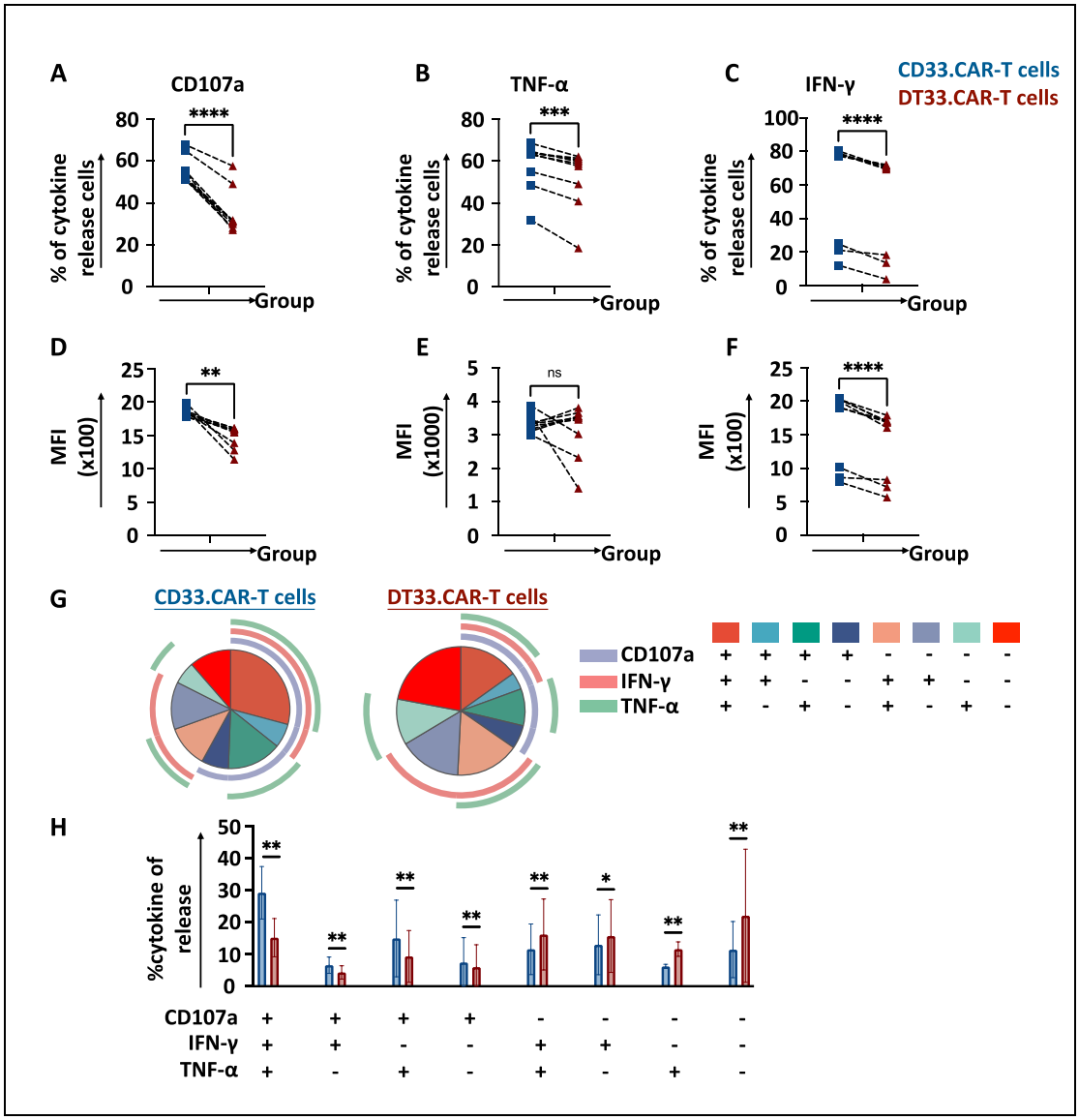

Figure 41: Statistical analysis of cytokine release of CD33.CAR-T cells and DT33.CAR-T cells. Effect of overexpression of TCF-1 on multi-functional CD33.CAR-T cells.

Statistical analysis of percentage of cytokine release of CD33.CAR-T cells and DT33.CAR-T cells (Figure 41A-C). Statistical analysis of MFI of cytokine release of CAR-T cells and DT.CAR-T cells (Figure 41D-F). The polyfunctional CD33.CAR-T cells and DT33.CAR-T cells were analyzed using Boolean gating strategy (Figure 41 G-H). TNF-α: Tumor Necrosis Factor-alpha; INF-γ: Interferon-gamma. Nine individual donors were tested. A paired t-test was used for statistical analysis. (*P<0.05, **P<0.01, ***P<0.001, ****P<0.0001, *ns= no significant difference*)

Since the magnitude of antigen receptor on T cells affect on the cytokine release, a correlation analysis between the MFI of CAR expression and the integrated MFI (iMFI) of cytokines in terms of CD107a, IFN-γ, and TNF-α was performed, showing significant positive correlations (Figure 42).

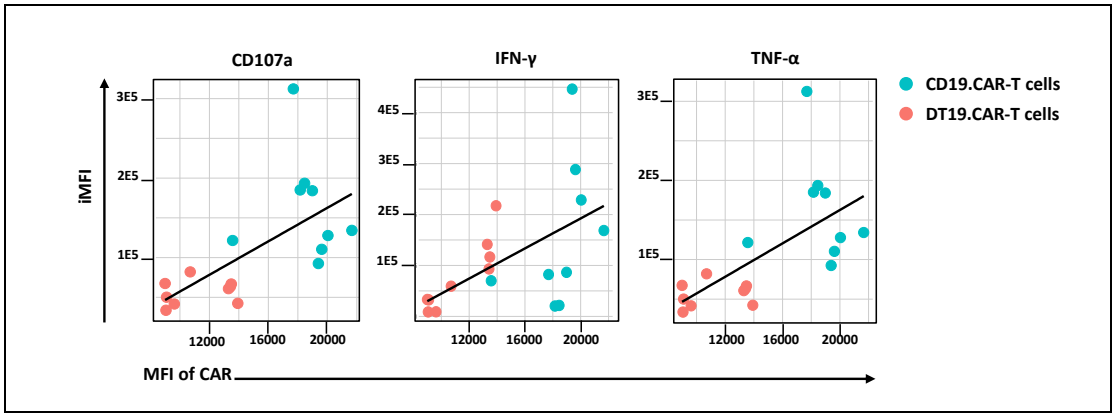

Figure 42: Statistical analysis of correlation of CAR expression density and quantity of cytokine production by CAR-T cells.

Integrated mean fluorescence intensity (iMFI) was calculated= (% percentage of cytokine production of CAR-T cells) * (MFI of cytokine production of CAR-T cells). Nine individual donors were tested.

3.6 Stable short-term killing capability of TCF-1 overexpressed CAR-T cells

The influence of TCF-1 on the short-term cytotoxicity of CD19.CAR-T cells was investigated by co-culturing CAR-T cells with different $CD19^+$ tumor cell lines (Raji and Nalm6 tumor cells) in different effector to target (E: T) ratios (1:1 and 1:2). The results obtained under the different scenarios were consistent and showed a comparable short-term killing efficiency between CD19.CAR-T and DT19.CAR-T cells (Figure 43), except co-culture of CAR-T cells with Raji cells in an E:T ratio of 1:1 (Figure 43B). A statistically significant higher number of residual Raji cells was found in DT19.CAR-T cell group (Figure 43B). Due to the low absolute number, however, we assumed there is no biological difference between these two groups.

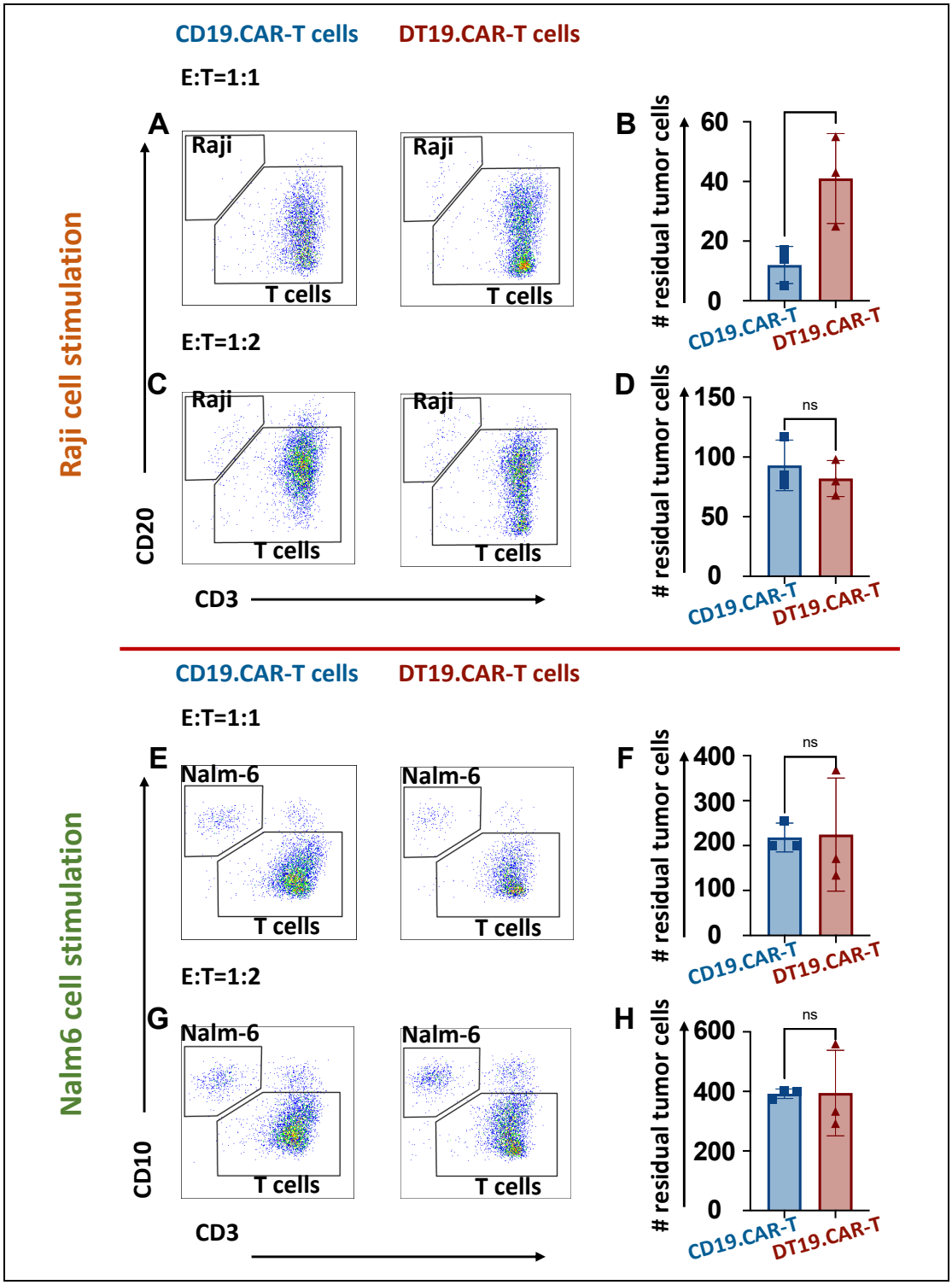

Figure 43: Representative dot plots and statistical analysis of killing efficiency of CD19.CAR-T cells and DT19.CAR-T cells after 24 hours in E:T ratio of 1:1 and 1:2.

Raji cells were used as targeted cells (Figure 43A-D), Nalm6 cells were used as targeted cells (Figure 43E-H). Effector cell: Target cells represented E:T. Three individual donors were tested. A paired t-test was used for statistical analysis. (*P<0.05, **P<0.01, ***P<0.001, ****P<0.0001, *ns= no significant difference*)

In accordance with the CD19.CAR model, a similar short-term killing capacity between CD33.CAR-T cells and DT33.CAR-T cells was observed (Figure 44).

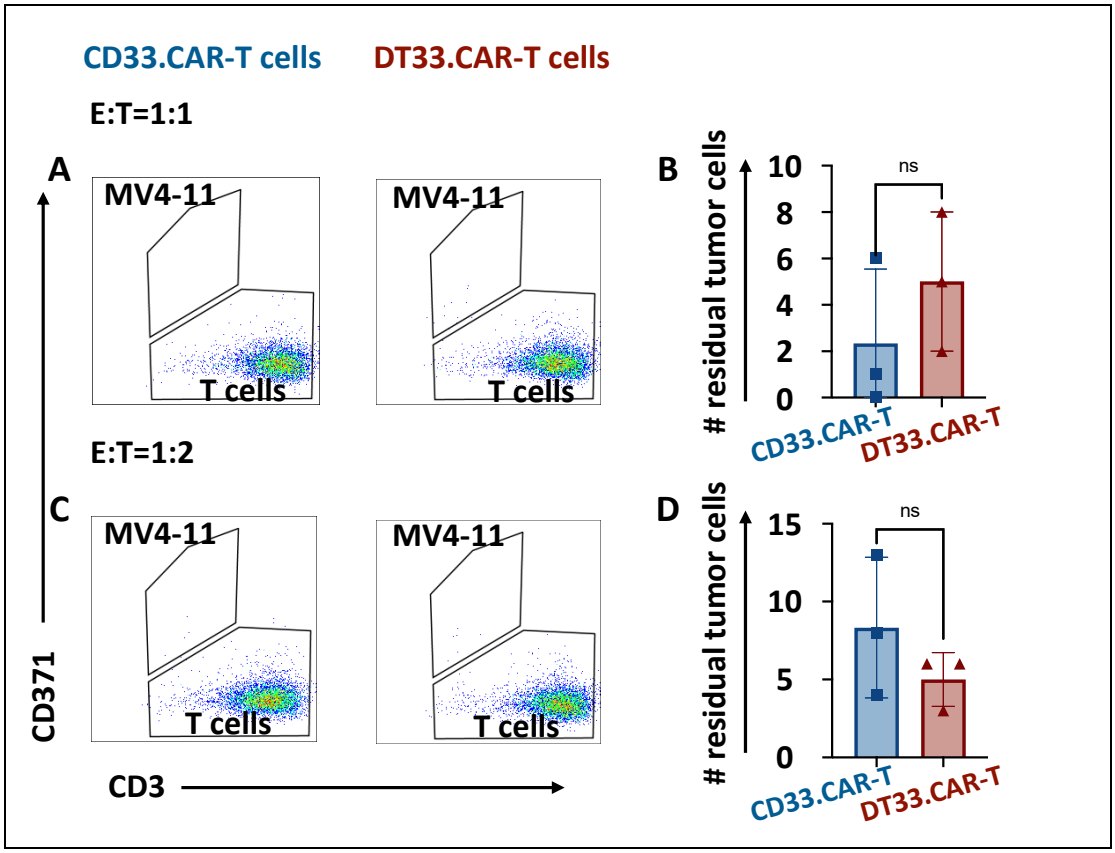

Figure 44: Representative dot plots and statistical analysis of killing efficiency of CD33.CAR-T cells and DT33.CAR-T cells after 24 hours at E:T ratio of 1:1 and 1:2.

MV4-11 cells were used as target cells. Effector cell: Target cells represented E:T. Three individual donors were tested. A paired t-test was used for statistical analysis. (*P<0.05, **P<0.01, ***P<0.001, ****P<0.0001, *ns= no significant difference*)

3.7 Superior persistence of TCF-1 overexpressed CAT-T cells

The long-term co-culture assay described in Figure 45 provides important information about the impact of TCF-1 overexpression on the long-term killing efficiency and persistence of CAR-T cells. In this assay, CAR-T cells and tumor cells are co-cultured at different E:T ratios (1:1 or 1:2) on day 1. Subsequently, the tumor cells are reseeded every day to stimulate CAR-T cells continuously. The purpose of reseeding tumor cells daily is to challenge the CAR-T cells and assess their ability to persist and maintain their killing efficiency over time, even in the presence of a growing tumor cell population.

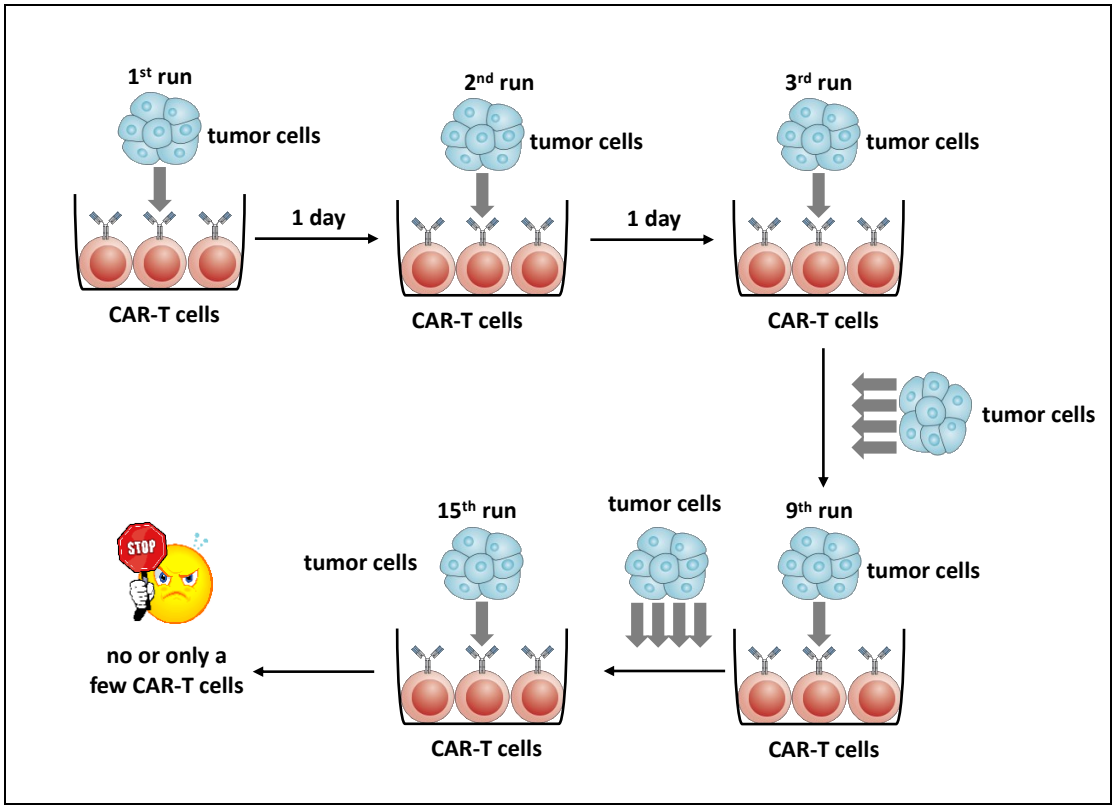

Figure 45: Workflow of long-term co-culture assay of CAR-T cells

$0.25x10^5$ of CAR-T cells or DT.CAR-T cells were seeded at day 1. $0.25x10^5$ (E:T=1:1) or $0.5x10^5$ (E:T=1:2) of tumor cells were seeded to challenge the CAR-T cells or DT.CAR-T cells every day until there is no or only few CAR-T cell or DT.CAR-T cell left. Flowcytometry was applied every 2 days to monitor the number of T cells and tumor cells, and the expression of CD4, CD8, PD-1 (Programmed Cell Death Protein 1), Tim3 (T-cell immunoglobulin and mucin domain-containing protein 3), Lag3 (Lymphocyte-activation gene 3).

In the long-term co-culture assay using healthy donor-derived CD19.CAR-T cells and DT19.CAR-T cells, the comparison between their killing efficiency and CAR-T cell persistence at different time points and E:T ratios reveals notable differences. DT19.CAR-T cells exhibited a better long-term cytotoxicity and persistence, showing more residual T cells and less tumor cells (Figure 46A-H).

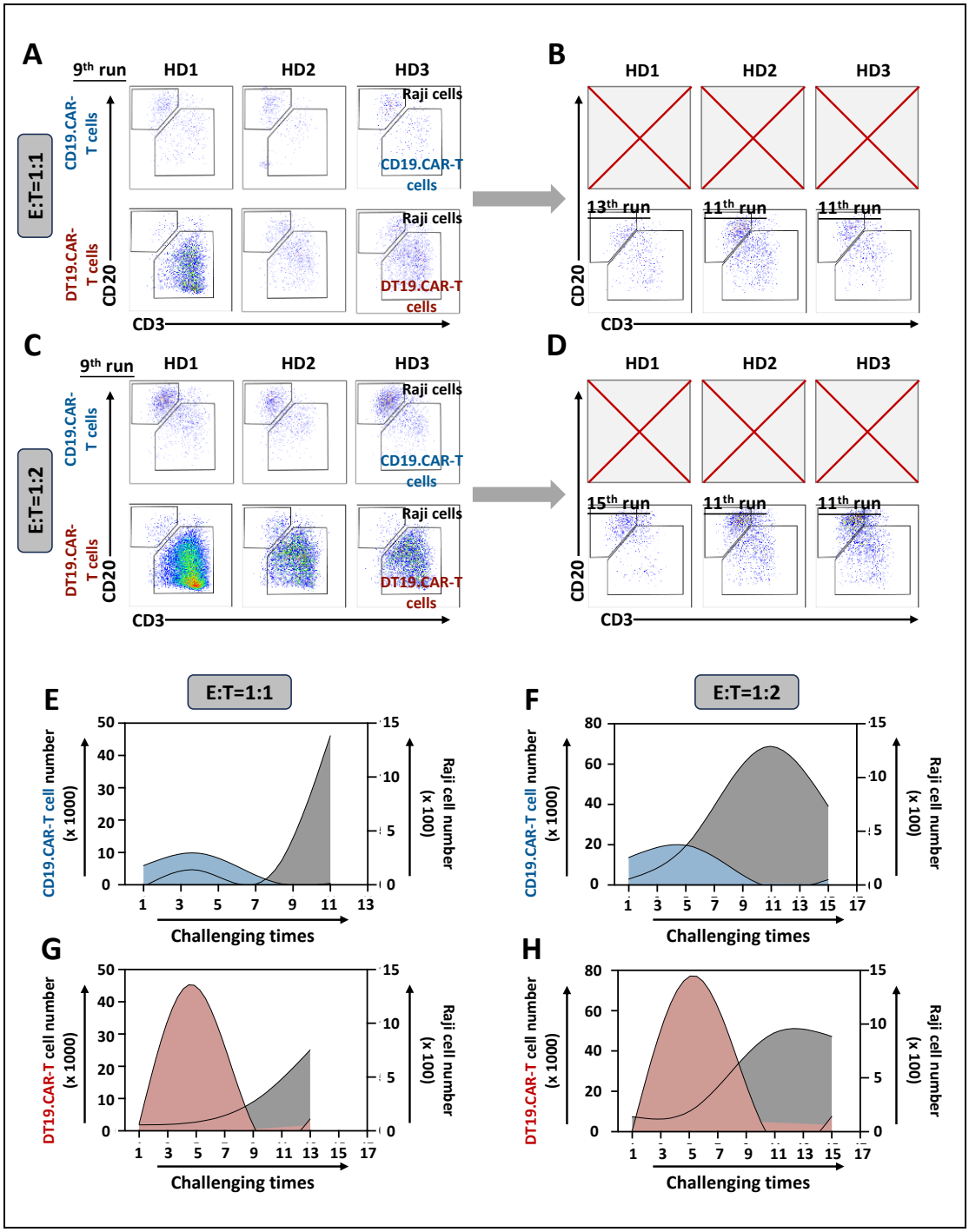

Figure 46: Statistical analysis of proliferation of CD19.CAR-T, DT19.CAR-T cells and Raji cells in co-culture assay at E:T ratio of 1:1 and 1:2.

Representative dot plots of co-culture assay of CD19.CAR-T cells and DT19.CAR-T cells at E:T ratio of 1:1 (Figure 46A-B), and 1:2 (Figure 46C-D). Dynamical cell expansion of CD19.CAR-T cells, DT19.CAR-T cells and Raji cells throughout the co-culture assay (Figure 46E-H). Raji cells were used as target cells. Effector cell: Target cells represented E: T. Three individual donors were tested. HD means healthy donor.

The consistent results were obtained by Nalm6 cell stimulation (Figure 47). Furthermore, CD33.CAT-T cell models showed similar results (Figure 48) which validate our results.

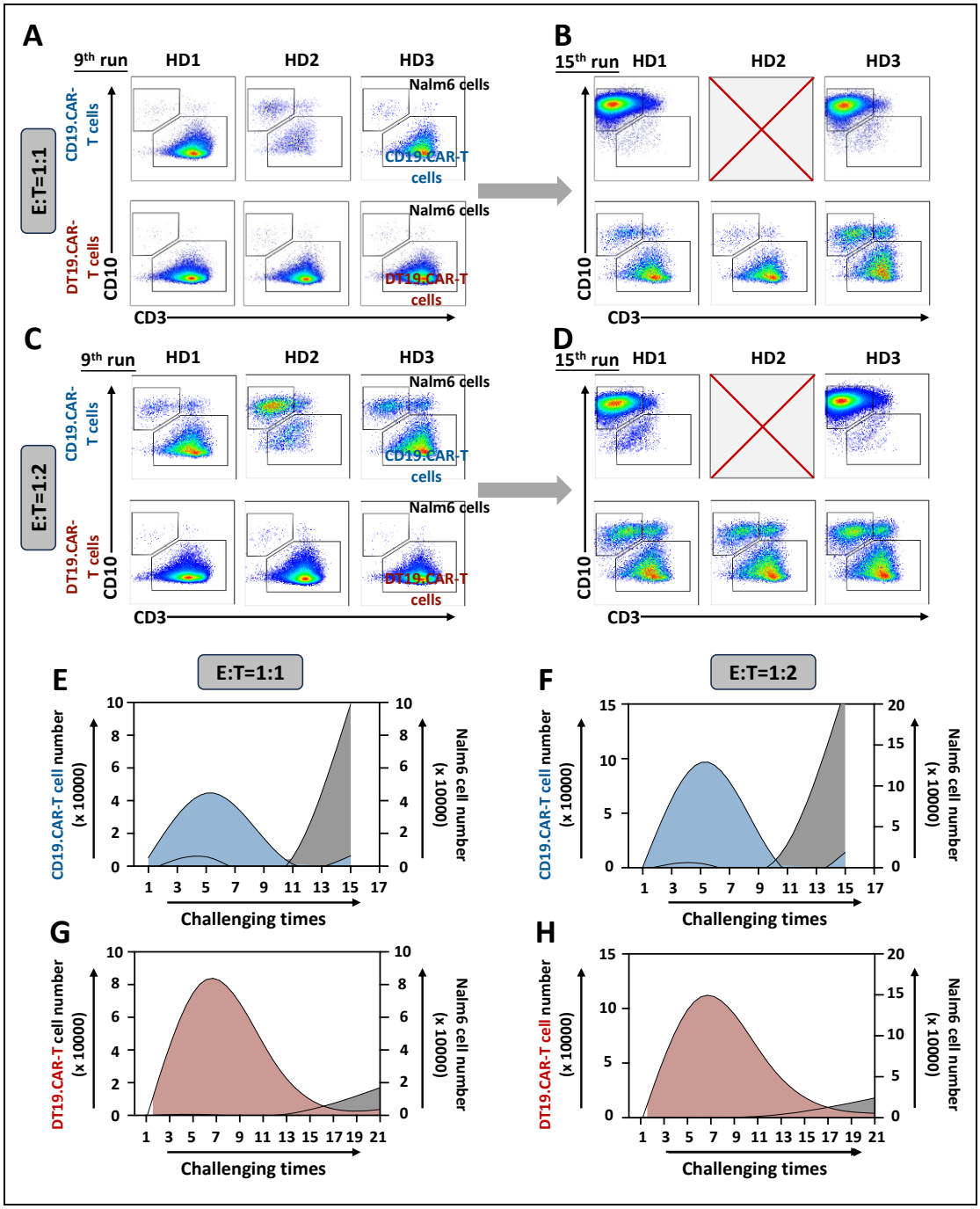

Figure 47: Statistical analysis of proliferation of CD19.CAR-T, DT19.CAR-T cells and Nalm6 cells in co-culture assay at E:T ratio of 1:1 and 1:2.

Representative dot plots of co-culture assay of CD19.CAR-T cells and DT19.CAR-T cells at E:T ratio of 1:1 (Figure 47A-B), and 1:2 (Figure 47C-D). Dynamical cell expansion of CD19.CAR-T cells, DT19.CAR-T cells and Nalm6 cells throughout the co-

culture assay (Figure 47E-H). Nalm6 cells were used as target cells. Effector cell: Target cells represented E: T. Three individual donors were tested. HD means healthy donor.

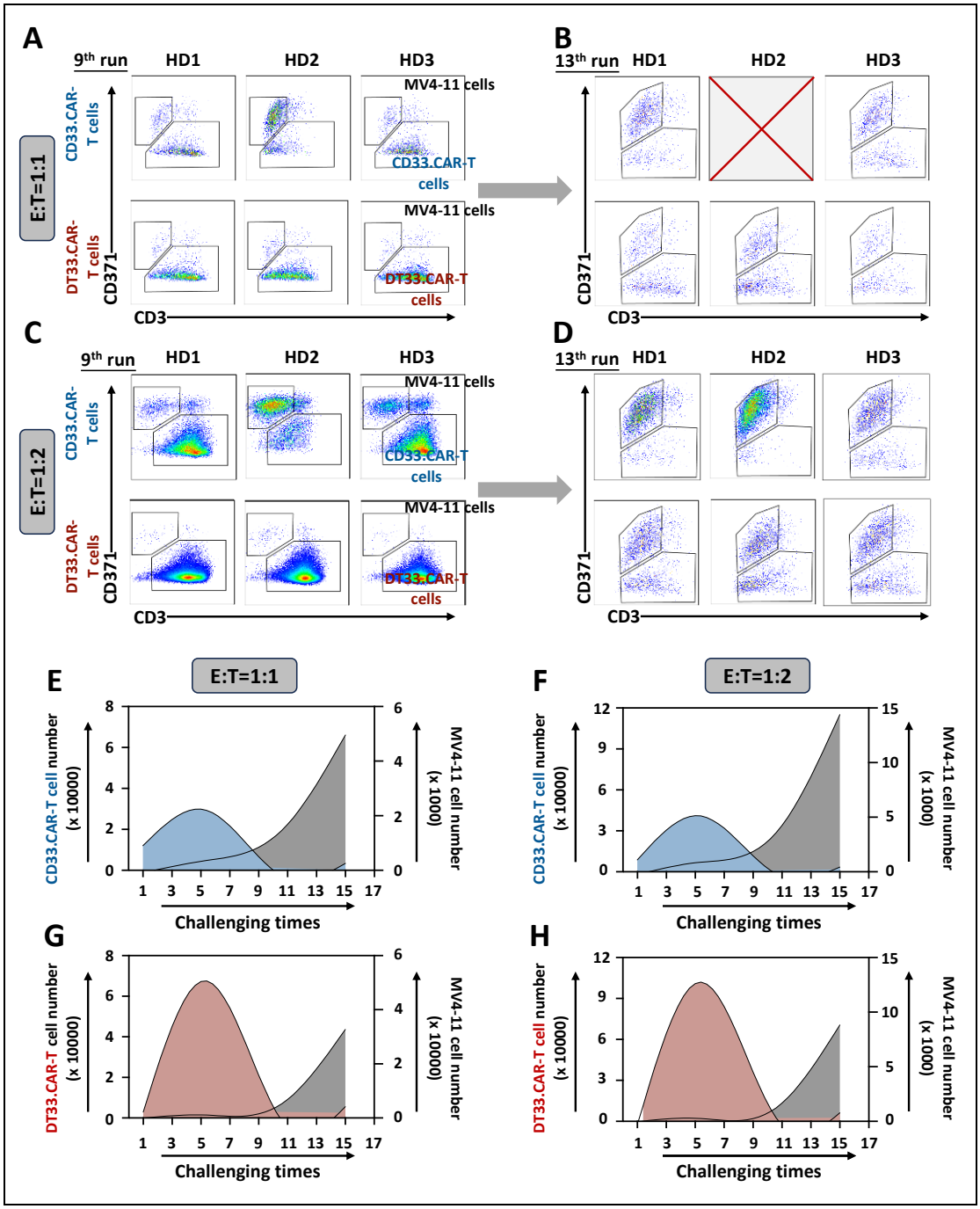

Figure 48: Statistical analysis of proliferation of CD33.CAR-T, DT33.CAR-T cells and Nalm6 cells in co-culture assay at E:T ratio of 1:1 and 1:2.

Representative dot plots of co-culture assay of CD33.CAR-T cells and DT33.CAR-T cells at E:T ratio of 1:1 (Figure 48A-B), and 1:2 (Figure 48C-D). Dynamical cell expansion of CD33.CAR-T cells, DT33.CAR-T cells, and MV4-11 cells throughout the co-culture assay (Figure 48E-H). MV4-11 cells were used as target cells. Effector cell: Target cells represented E:T. Three individual donors were tested. HD means healthy donor.

3.8 Upregulation of killing related cytokines by DT.CAR-T cells in long-term killing

To further investigate the cytokine release capability of DT.CAR-T cells in the long-time culture system, the supernatants in the co-culture assay were harvested at day 2, day 6 and day 10. Our data show that DT19.CAR-T cells exhibit a distinct cytokine profile compared to CD19.CAR-T cells. CD19.CAR-T cells showed a higher level of soluble Fas ligand (sFasL), granzyme A, perforin, and granulysin at the early stage of co-culture (day 2), but it was overtaken by DT19.CAR-T cells at the middle and late stages of co-culture (day 6 and day 10).

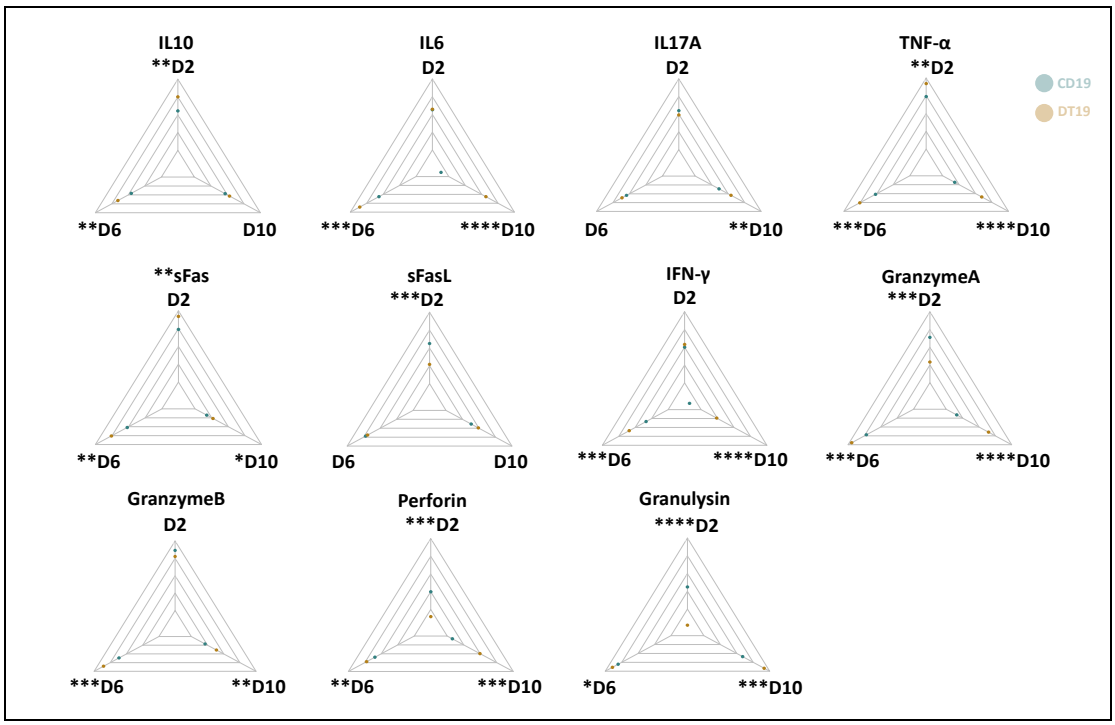

Figure 49: Radar plots of cytokines secretion in co-culture assay.

Raji cells were used as target cells. Interleukin-10 (IL10), Interleukin-6 (IL6), Interleukin-17A (IL17A), Tumor Necrosis Factor α (TNF-α), soluble Fas (sFas), soluble Fas ligand (sFasL), interferon γ (IFN-γ), granzyme A, granzyme B， perforin and granulysin from day 2, day 6 and day 10, were tested by LEGENDPlex™ analysis; D: Day. Three donors were tested. A paired t-test was used for statistical analysis. (*P<0.05, **P<0.01, ***P<0.001, ****P<0.0001, *ns= no significant difference*)

Notably, proinflammatory cytokines in the cell supernatant, such as IL6 and IL17A, demonstrated higher expression in DT19.CAR-T cells after the early stage of co-culture.

Conversely, the anti-inflammatory cytokine, interleukin-10 (IL10), showed higher expression at the early and middle stages in DT19.CAR-T cells, but not in the late stage. Furthermore, other critical effector cytokines, such as TNF-α, IFN-γ, and granzyme B, also displayed higher expression levels in DT19.CAR-T cells throughout the co-culture assay (Figure 49).

3.9 Reduction of multiple exhaustion markers in long-term killing

To investigate the interpretability of the clustering results, the protein expression profiles of detected clusters against reference populations was compared. Figure 50 showed an example of these results. The heatmap displayed median expression intensities for each protein markers, with hierarchical clustering to group rows and columns. The darker red indicates a higher level of expression, and the darker blue indicates a lower level of expression. Cluster analysis was then used to classify cell subpopulations with similar marker expression according to the level of expression of different markers (Figure 50A-B). Finally, 10 cell subpopulations were screened (Figure 50C).

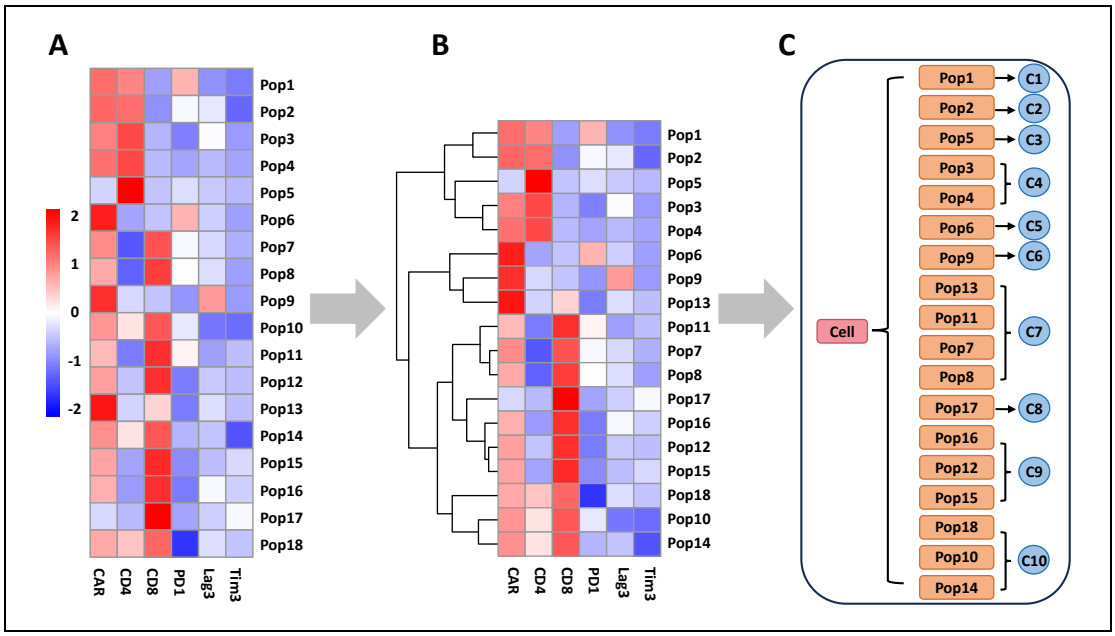

Figure 50: Workflow of cell clustering.

Expression profiles of detected populations by FlowSOM, a fast clustering and visualization technique for flow or mass cytometry data that builds self-organizing maps (SOM) to help visualize marker expression across cell subsets. Heatmap shows median expression intensities of each marker (column), for each detected population (row). Values are normalized and scaled between -2 to 2 for each marker (Figure 50A). Rows and columns are sorted by hierarchical clustering (Figure 50B). The summarized cell clusters are indicated in Figure 50C. Data set was from co-culture assay, effector cells were CD19.CAR-T cells and DT19.CAR-T cell, targeted cells were Raji cells; Pop: population; C: cluster; PD-1: Programmed Cell Death Protein 1; Tim3: T-cell immunoglobulin and mucin domain-containing protein 3; Lag3: Lymphocyte-activation gene 3.

To further detect the dynamic changes of those 10 cell clusters during the co-culture, the Locally Weighted Scatterplot Smoothing (LOESS) regression were applied. During the co-culture, the frequency of $CD8^+PD\text{-}1^-Tim3^+Lag3^+$ DT19.CAR-T cells was lower at the early stage of co-culture, while at the middle to late stage, this subpopulation was more than that in CD19.CAR-T cells (Figure 51A). $CD8^+PD\text{-}1^+Tim3^+Lag3^+$ subpopulation was a higher in CD19.CAR-T cells before the middle stage of co-culture, while it decreased rapidly later. This might be caused by low residual T cell number. $CD8^+PD\text{-}1^+Tim3^+Lag3^+$ subpopulation was higher in CD19.CAR-T cells before the middle stage of the co-culture, whereas it decreased rapidly later (Figure 51C).

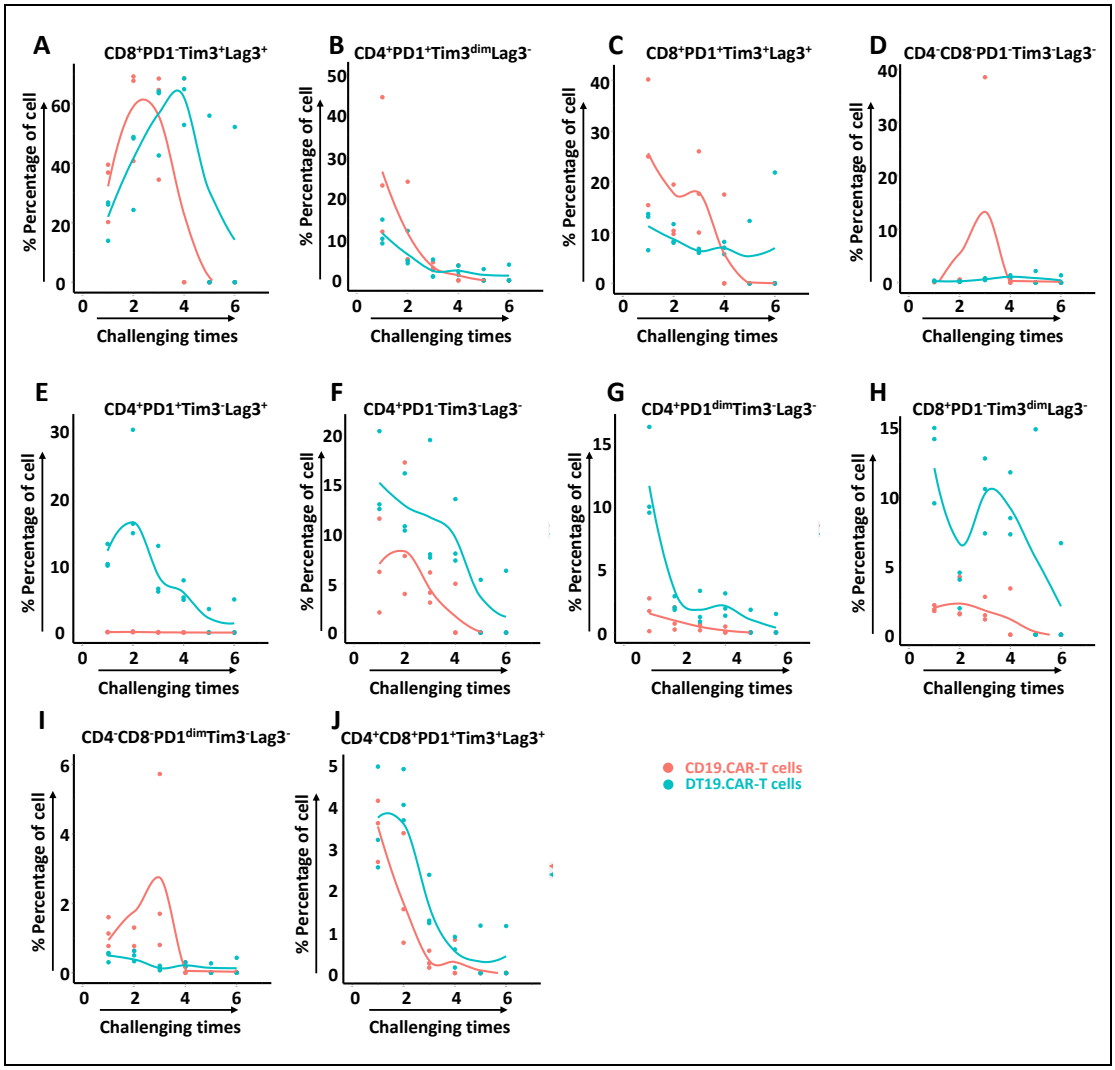

Figure 51: Locally estimated scatterplot smoothing (LOESS) regression line fitted to the data set from co-culture.

Data set was from co-culture assay, effector cells were CD19.CAR-T cells and DT19.CAR-T cell, targeted cells were Raji cells. PD-1: Programmed Cell Death Protein 1; Tim3: T cell immunoglobulin and mucin domain-containing protein 3; Lag3: Lymphocyte-activation gene 3; Dim: diminished.

A similar pattern was observed in $CD4^+PD1^+Tim3^{dim}Lag3^-$ subpopulation (Figure 51B). Comparing to that in CD19.CAR-T cells, $CD4^+PD1^+Tim3^-Lag3^+$, $CD4^+PD1^-Tim3^-Lag3^-$, $CD4^+PD1^{dim}Tim3^-Lag3^-$, $CD4^+CD8^+PD1^+Tim3^+Lag3^+$, and $CD8^+PD1^-Tim3^{dim}Lag3^-$ subpopulations showed higher frequency in DT19.CAR-T cells throughout the co-culture (Figure 51E-H, and J). It seems that $CD4^-CD8^-PD1^-Tim3^-Lag3^-$ and $CD4^-CD8^-PD1^{dim}Tim3^-Lag3^-$ cells reached a peak in the middle stage of co-

culture. It was caused by only one donor. Therefore, we assumed there was no biological difference between these two groups (Figure 51D and I).

The $CD19^+$ Nalm6 tumor cell line was further used to validate our findings. Eight cell clusters were identified (Figure 52A-C), and their dynamic changes are shown in Figure 52 D-N. The $CAR^+CD4^+PD\text{-}1^+Tim3^{dim}Lag3^{dim}$ subpopulation was higher in the early stage of co-culture (Figure 52D), whereas no difference was observed in the middle and late stage of co-culture in the CD19.CAR-T group. $CAR^+CD4^+PD\text{-}1^-Tim3^-Lag3^{dim}$ and $CAR^+CD8^+PD\text{-}1^-Tim3^+Lag3^+$ subpopulations showed higher proportions in DT19.CAR-T cells throughout the tumor challenge, while the proportion of $CAR^+CD8^+PD\text{-}1^-Tim3^+Lag3^+$ subpopulation was only about 0.5% (Figure 52E and I). Furthermore, $CAR^+CD4^-CD8^-PD\text{-}1^-Tim3^-Lag3^+$, $CAR^{dim}CD8^+PD\text{-}1^-Tim3^-Lag3^{dim}$, and $CAR^+CD8^+PD\text{-}1^{dim}Tim3^+Lag3^+$ subpopulations showed higher proportions of the CD19.CAR cell group at the very early stage, whereas DT19.CAR cells had more of these subpopulations at the middle and late stage (Figure 52F, H and K). In addition, the $CAR^+CD8^+PD\text{-}1^+Tim3^{dim}Lag3^+$ subpopulation in the DT19.CAR-T cell group had a low percentage during the co-culture assay in comparison to the CD19.CAR-T cell group (Figure 52G). $CAR^+CD8^+PD\text{-}1^-Tim3^+Lag3^-$ subpopulation showed higher percentage in CD19.CAR-T cell group, it increased gradually in the late stage, which is considered due to the reduced T cell residual. (Figure 52J).

Moreover, the dynamics of cell populations was monitored in experiments in which CD33.CAR-T cells were co-cultured with the MV4-11 tumor cell line and showed higher proportions of $CAR^+CD4^+PD\text{-}1^-Tim3^-Lag3^+$ and $CAR^+CD4^-CD8^-PD\text{-}1^-Tim3^-Lag3^+$ in DT33.CAR-T cells (Appendix Figure 9F and I). $CAR^+CD4^-CD8^-PD\text{-}1^-Tim3^-Lag3^-$ and $CAR^+CD8^+PD\text{-}1^-Tim3^-Lag3^{dim}$ cells were higher in CD33.CAR-T cell group at the late stage of co-culture. However, other six subpopulations ($CAR^{dim}CD4^+PD\text{-}1^-Tim3^-Lag3^-$, $CAR^+CD4^+PD\text{-}1^+Tim3^-Lag3^-$, $CAR^+CD4^+PD\text{-}1^-Tim3^-Lag3^-$,$CAR^{dim}CD4^-CD8^-PD\text{-}1^+Tim3^-Lag3^{dim}$, $CAR^+CD8^+PD1^+Tim3^+Lag3^+$, and $CAR^+CD4^+CD8^+PD\text{-}1^-$

Tim3^{dim}Lag3^{+}) did not show differences during the co-culture assay (Appendix Figure 9D, E, G, H, K, M).

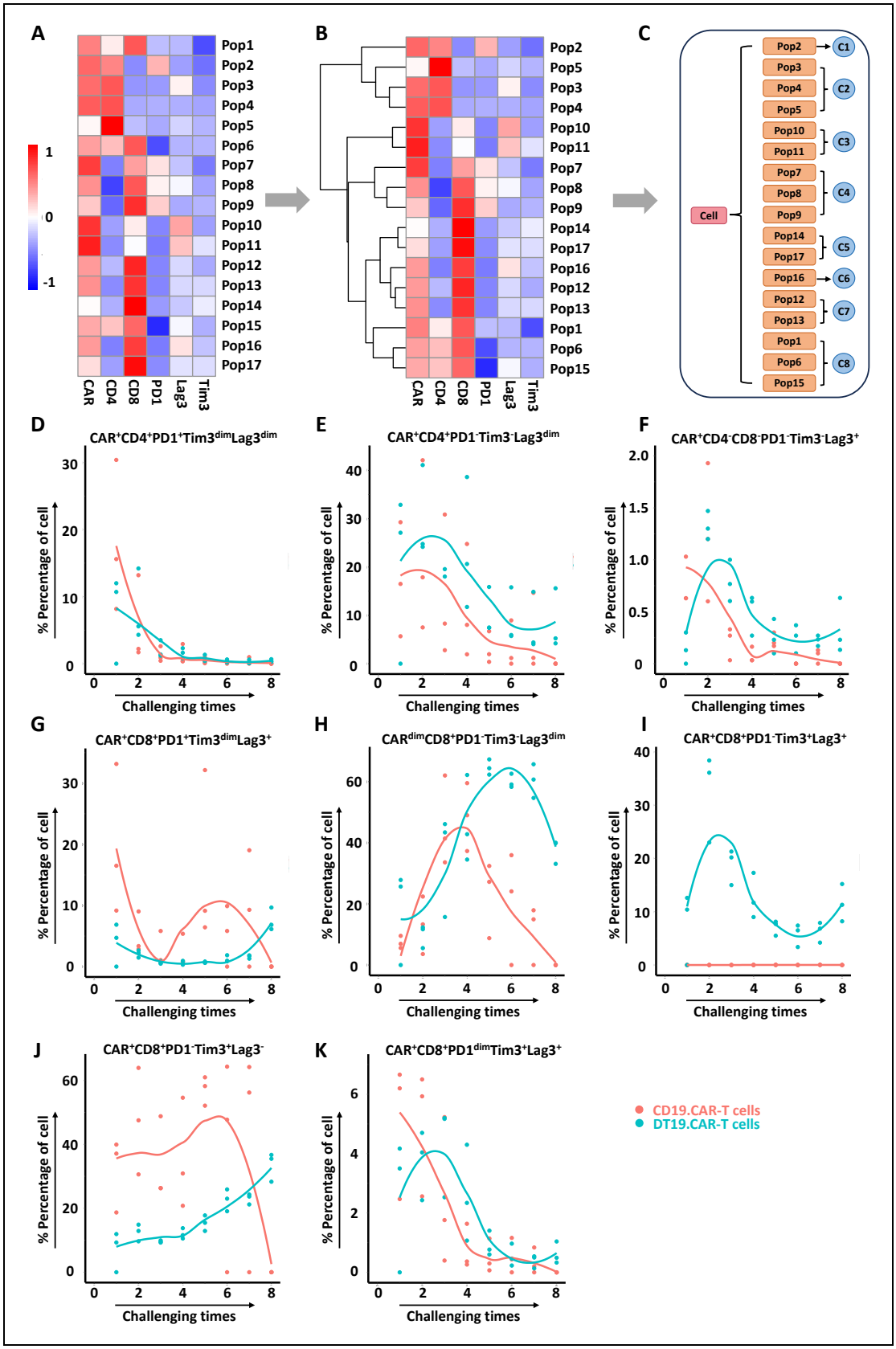

Figure 52: Workflow of cell clustering and locally estimated scatterplot smoothing (LOESS) regression line fitted to the data set from co-culture.

Expression profiles of detected populations by FlowSOM，a fast clustering and visualization technique for flow or mass cytometry data that builds self-organizing maps (SOM) to help visualize marker expression across cell subsets. Heatmap shows median expression intensities of each marker (column), for each detected population (row). Values are normalized and scaled between -1 to 1 for each marker (Figure 52A). Rows and columns are sorted by hierarchical clustering (Figure 52B). The summarized cell clusters are indicated in Figure 52C. Data set was from co-culture assay, effector cells were CD19.CAR-T cells and DT19.CAR-T cell, targeted cells were Nalm6 cells; Pop: population; C: cluster; PD-1: Programmed Cell Death Protein 1; Tim3: T-cell immunoglobulin and mucin domain-containing protein 3; Lag3: Lymphocyte-activation gene 3; Dim: diminished.

4. DISCUSSION

CAR-T cell therapy represents a revolutionary new pillar in the treatment of cancer. Although CAR-T cell treatment has produced remarkable clinical responses in certain subsets of B-cell leukemia or lymphoma, many challenges limit CAR-T therapeutic efficacy in solid tumors and hematological malignancies. A major challenge is the *in vivo* persistence of CAR-T cells. There is a need for innovative strategies and approaches for the development of more potent CAR-T cells. TCF-1, an important T-cell regulator, may be a therapeutic option to improve the persistence of CAR-T cells and lead to durable clinical responses.

In the present study, we successfully established a double transduction system a with third-generation CAR vector and an additional RV-SFG.Tcf-7.NGFR vector to CAR-T cells and DT.CAR-T cells. During the production process, we observed that DT.CAR-T cells obtained a lower expression of CAR. Several studies have suggested that the density of the CAR molecule in the membrane of the CAR-T cell may influence the CAR signaling pathway and thus affect its anti-tumor efficacy[130,131]. By generating BCMA CAR^{high} and CAR^{low} T cells, Prosper F and co-workers found CAR^{high} T cells can enhance tonic signaling, increase cell activation status, and drive T cells differentiation and induce an exhausted phenotype, characterized by high expression levels of PD-1, Tim3 and Lag3, which can limit the persistence of T cells and the outcome of clinic response [132]. Therefore, DT.CAR-T cells with lower expression of CAR might exert a better clinical response.

Using western blotting, CAR-T cells showed a lower level of TCF-1. In contrast, a high expression of TCF-1 was observed in DT.CAR-T cells. Interestingly, non-transduced T cells showed a similar level of TCF-1 expression when compared to DT.CAR-T cells. Those results suggest that TCF-1 expression was downregulated during CAR-T cell generation. TCF-1 expression could be rescued in DT.CAR-T cells by a knock-in strategy. TCF-1 can fuel functionality of exhausted $CD8^+$ T cells by promoting the

expression of an array of key effector function-associated transcription regulators, including Foxo1, Zeb2, Id2 and Eomes. Furthermore, TCF-1 deficiency could exacerbate $CD8^+$ T cell exhaustion and upregulation of TCF-1 and enhance $CD8^+$ T cell function in LCMV chronic infection [133]. In addition, TCF-1 expression is also correlated with memory marker expression and expansion capacity and declines with antigenic stimulation [134]. TCF-1 might counteract the differentiation of Tcf-7^{hi} cells and sustain the expression of conserved adult stem-cell genes that are critical for $CD8^+$ T cell stemness as shown by a recent study [135]. Therefore, keeping the expression of TCF-1 in CAR-T cells may prolong T cell persistence and enhance antitumor efficacy. Tonic CAR signaling, the intrinsic CAR activation in the absence of tumor antigen stimulation, is a pivotal event controlling CAR-T efficacy. It is evident that CAR-T cells exhaustion can be induced and maintain by tonic signaling, especially in the third-generation CAR structure, which contains an additional 4-1BB co-stimulatory domain [51,136,137]. In line with those results, the rest on tonic signaling CAR-T cells can reverse CAR-T cell exhaustion with decreased expression of the exhaustion-associated transcription factor TOX and increased expression of memory-associated transcription factors TCF-1 [138]. Our results also showed that non-transduced T cells displayed the same level expression of TCF-1 with DT.CAR-T cells. As non-transduced T cells were also manufactured with anti-CD3 and anti-CD8 antibodies, indicating they obtained same activation state, which suggested it is likely that the CAR structure, rather than the state of activation, is the main factor affecting TCF-1 expression.

Apoptosis, the process of programmed cell death, is essential for proper homeostatic maintenance and survival in multi-cellular organisms. The poly(ADP-ribose) polymerase (PARP-1), a 113 kDa nuclear enzyme, is cleaved by cleaved caspase 3 during apoptosis [139]. PARP can play a role in this process by promoting cell death if the DNA damage incurred during the process of CAR-T cell manufacturing or activation becomes overwhelming. This can lead to the activation of caspases, including cleaved-caspase-3, which then initiate the cascade of events that culminate in intrinsic apoptosis.

The higher expression of Ki67 in CAR-T cells might indicate an attempt at proliferation, but if the intrinsic apoptotic pathway is strongly activated, it could override the proliferation and result in limited expansion of CAR-T cells.

Activation-induced cell death (AICD) is one of the major reasons for CAR-T cell limited persistence. Several studies have reported that death receptor (DR) Fas (CD95) and its ligand FasL (CD95L) are important mediator of the DR-mediated AICD process in T cells. Consistent with previous research [140,141], we observed that the expression of CD95 (Fas) is downregulated on the DT.CAR-T cell surface. In addition, a downregulation of soluble FasL was also detected during the generation phase. Furthermore, the higher presence of $CD95^{+}CD253^{+}$ T cells in the CAR-T group suggests an increased propensity of these cells to undergo apoptosis. This may contribute to the observed differences in expansion between the two groups. The increased frequency of apotracker^{+} T cells in the CAR T-cell group further underlines the occurrence of apoptosis in these cells, irrespective of the pathway involved. The CD69 antigen, an early lymphocyte activation marker, belongs to the type II C-lectin membrane receptor family and is rapidly upregulated following leukocyte stimulation. Initial *in vitro* investigations of CD69 indicated its potential pro-inflammatory function [142]. A recent study found that after binding to oxidized low-density lipoprotein (oxLDL), the CD69-expressing cells showed an increased expression of PD-1, indicating that CD69 may contribute to the PD-1 induction in the modulation of inflammation [143]. Our results showed that downregulated expression of CD69, may enhance DT.CAR-T cell persistence by cooperating with CD95. In addition, the co-stimulator and cytokine signals are also reported to participate in regulating T cell AICD. Previous research has shown that 3rd generation CARs may be prone to AICD due to the intense stimulus [144]. Künkele et al. found that a third-generation CAR directed composing of CD28 and 4-1BB signal domains resulted in an increased cytolytic activity and greater CAR-T cell apoptosis than the second-generation CAR which contains only the 4-1BB signal domain upon *in vitro* tumor stimulation [145]. Despite CD40L-expressing CAR-T showed

an improved antitumor function *in vivo*, it can also induce the Fas-death receptor, which may limit the killing efficacy and persistence of CAR-T cells *ex vivo* [146]. Our results confirmed that reduced expression of activated co-stimulatory maker CD40L and ICOS, while upregulated expression of inhibitory co-stimulatory maker CTLA4 in DT.CAR-T cells. In addition, we found the secretion of proinflammatory cytokines of DT.CAR-T cells was reduced in the production phase, as well as by the tumor stimulation. Those results showed that overexpression of TCF-1 can reduce the cell apoptosis by inhibiting intrinsic and extrinsic apoptotic pathway. The overactivation of CAR-T cells may come at the expense of developmental and functional potential, which can limit the ability T cell to undergo expansion, persistence, and functionality after infusion into the patients. The efficacy of CAR-T cells is primarily influenced by the inherent characteristics of the T cells themselves and the composition of the infused T cell product [50,147]. T cells exhibit a broad spectrum of interrelated differentiation states that vary considerably in their ability to proliferate, self-renew and maintain long-term survival [148]. Substantial evidences from both murine and human studies suggest an inverse relationship between T cell differentiation and sustained antitumor efficacy, with early memory T cells exhibiting the most favorable properties [149]. Consequently, studies of patients with large B-cell lymphomas and CLL who responded positively to CD19.CAR-T cells revealed an enrichment of gene expression profiles associated with early memory T cells [127,150,151]. Casucci's group also found CAR-T cell manufacturing from naive/stem memory T lymphocytes can enhance antitumor responses while curtailing cytokine release syndrome [152]. As we mentioned, naïve T cells show a high expression of TCF-1, which keeps T cells with a stem-like characteristic. The final product of DT.CAR-T cells with an overexpression of TCF-1 leading to more naïve T cells might influence the CAR-T cell fate *in vivo*. As shown in our study, the high frequency of naïve T cell in final DT.CAR-T cell product may be related to the reduced cytokine release during the generation and the better killing efficacy in long-term killing *in vitro*. In addition, $CD4^+$ T_N cells in CAR-T cells expressed high $CD62L^+$ and CXCR3, indicating that this

subset already acquired the ability to recruit into the inflammatory sites (also tumor site). Those $CD62L^+CXCR3^+CD4^+$ T_N cells might have a less stem-like characteristic. In contrast, $CD62L^+CD4^+$ T_{CM} cell in DT.CAR-T cells with a lower expression of CXCR3 could help them to keep a better stemness and have more stronger antitumor functionality.

As we have shown, DT.CAR-T cells mediated a more durable antitumor response with an elevated expansion in co-culture assay compared with CAR-T cell products. It is noteworthy that despite contending with the tumor for several days, the highly proliferating DT.CAR-T cells exhibited constrained expression of multiple inhibitory receptors (IRs). In contrast, CAR-T cells exhibited the presence of IRs, indicating a trade-off with excessive activation. While these cells have identified the tumor and initiated activation, their capacity to effectively steer an antitumor response during the subsequent tumor challenge is somewhat restricted.

The activation induced expansion has been linked to a rise in both the frequency and intensity of CAR-T related CRS and ICANS in patients. [78,153,154]. Nevertheless, our observations suggest that DT.CAR-T cells are activated to a lesser extent than conventional CAR-T cells, leading to a reduction in the release of proinflammatory cytokines. The initiation of proinflammatory cell death can be facilitated by granzyme A and granzyme B, both of which are delivered into tumor cells via the perforin-mediated mechanism [155,156]. Notably, our results revealed a notable difference in that DT.CAR-T cells had significantly lower levels of granzyme A, granzyme B and perforin expression compared to conventional CAR-T cells. These observations suggest that this pathway may provide a partial explanation for the reduced toxic potential of DT.CAR-T cells compared to CAR-T cells. Recent data also suggest that attenuating the signaling strength in CAR-T cells could lead to reduced toxicity and increased efficacy in fighting tumors [53,157]. Based on their muted functionality, we hypothesized that TCF-1 could potentially modulate the processing of the signal strength transmitted by the CAR molecule in CAR-T cells, thereby leading to improved

efficacy and safety characteristics. Indeed, our investigations revealed a remarkable correlation that higher CAR expression correlated positively with cytokine release, while DT.CAR-T cells exhibited a more modulated activation profile across both the CD28 and 4-1BB costimulatory domains. As a result, the DT.CAR-T cell product exhibited superior expansion potential coupled with a reduced propensity to activate. This unique combination allows a finer calibration of the dynamic interplay between cellular and molecular factors that contribute to the development of CRS.

CD27, a member of the TNF receptor superfamily, is highly expressed on T cells. Its expression is upregulated in cases of increased lymphocyte activation [158]. Interestingly, a higher expression of CD27 was found on DT.CAR-T cells, suggesting that TCF-1 could selectively modulate CAR-T cell activation through different pathway and shape the central memory T cells to a less active potency. In addition, the overexpression of TCF-1 can increase $CD27^{+}TCF\text{-}1^{+}$ subset in Th17 cells, with inferred stemness feature and low anabolic metabolism. Thereafter, these $CD27^{+}TCF\text{-}1^{+}$ subset can develop into a terminally differentiated $CD27^{-}T\text{-}bet^{hi}$ subpopulation. In line with those results, overexpression of TCF-1 alters the final DT.CAR-T cell phenotype and drive CAR-T cells to obtain more naïve T cells. Our results suggest that overexpression of TCF-1 may preserve lineage identity and the stability of naïve/memory T cell lineage.

The outcome of CAR-T cell therapy is also influenced by the composition of products, such as the component of T memory cells [127,151,159] and the CD4/CD8 ratio [160,161]. Serval studies have found that $CD4^{+}$ CAR-T cells play a key role in exacerbating CRS, while maintaining long-term response [39,162,163]. Interestingly, in our study, the overexpression of TCF-1 has more impact on $CD4^{+}$ CAR-T cells rather than $CD8^{+}$ CAR-T cells in both the generation phase and co-culture assay. TCF-1 can drive the differentiation of early thymic progenitors and the commitment of $CD4^{+}$ T cells, therefore the final products have more potential to differentiate into $CD4^{+}$ high CAR-T cell after tumor stimulation. In addition, by overexpression of TCF-1, $CD27^{+}TCF\text{-}1^{+}$ also increased, which was consistent with increased CD27 expression in generation and reduced multiple IRs and

better killing efficacy during the co-culture assay. The short-term reduced cytokine release may relate not only the lower expression of CAR. Furthermore, despite TCF-1 is not essential for commitment to the CD8+ T cell lineage, but it still acts to maintain $CD8^+$ T cell stability and help it keep stem-like and self-renewal characteristics. The overexpression of TCF-1 could reduce the expression of multiple IRs on $CD8^+$ T cells and prolong the life of $CD8^+$ T cells by delaying the exhaustion of T cells, resulting in a more sustained cytotoxicity of $CD8^+$ T cells.

In conclusion, overexpression of TCF-1 in CAR-T cells prevents CAR-T cells from apoptosis, multiple inhibitory markers, keep T cell stem-like characteristic, and improves their persistence, resulting in enhanced antitumor efficacy of those DT.CAR-T cells *in vitro*. Thus, overexpression of TCF-1 might be an innovative approach for improving CAR-T cell persistence, thus reinforcing the clinic response of CAR-T cell therapy.

5. SUMMARY

Despite the remarkable success of CAR-T cell therapy in leukemia and lymphoma patients, lack of CAR-T cell persistence remains a significant clinical problem. In particular, CAR-T cells often exhibit a deficiency in TCF-1 expression, rendering cells susceptible to TCF-1-associated pathways and consequently to short survival in the host. Therefore, it is intriguing to modulate TCF-1 expression in CAR-T cells to address the challenge of CAR-T cell persistence and further improve therapeutic outcomes.

In this study, third generation CAR vectors were used, and a double transduction system was established. The effect of TCF-1 overexpression in CAR-T cells was comprehensively explored regarding various aspects. Given the phenotype and functionality of CAR-T cells after transduction, two different CAR models (CD19.CAR vector and CD33.CAR vector) were settled in the study to generalize the effect of overexpression of TCF-1. We found that (1) the overexpression of TCF-1 can enrich the naïve and stem cell-like CAR-T cells exhibiting a better killing efficacy; (2) the cytokine profile of CAR-T cells were switched from proinflammatory or killing related to inactive through overexpression of TCF-1; (3) the apoptotic status of CAR-T cells could be modulated by TCF-1 overexpression, thus resulting in a better long-term functionality in terms of repetitive tumor killing and reduced multiple inhibitory receptors.

In summary, overexpression of TCF-1 in CAR-T cells could reduce apoptosis, occurrence of CRS and improve their persistence, resulting in enhanced antitumor efficacy of CAR-T cells. Thus, overexpression of TCF-1 might improve CAR-T cell persistence *in vivo* and enhance the effect of CAR-T cell therapy in patients with relapsed/refractory hematologic malignancies.

6. DIE ZUSAMMENFASSUNG

Trotz des bemerkenswerten Erfolgs der CAR-T Zelltherapie bei Leukämie- und Lymphom Patienten bleibt der Mangel an CAR-T Zellpersistenz ein erhebliches klinisches Problem. Insbesondere weisen CAR-T Zellen häufig einen Mangel an TCF-1 Expression auf, wodurch die Zellen anfällig für TCF-1-assoziierte Signalwege werden und folglich im Wirt nur kurz überleben. Daher ist es interessant, die TCF-1 Expression in CAR-T Zellen zu modulieren, um das Problem der CAR-T Zellpersistenz anzugehen und die therapeutischen Ergebnisse weiter zu verbessern.

In dieser Studie wurden CAR-Vektoren der dritten Generation verwendet und ein Doppel Transduktion System etabliert. Die Wirkung der TCF-1-Überexpression in CAR-T-Zellen wurde umfassend in Bezug auf verschiedene Aspekte untersucht. Angesichts des Phänotyps und der Funktionalität von CAR-T Zellen nach der Transduktion wurden in der Studie zwei verschiedene CAR-Modelle (CD19.CAR Vektor und CD33.CAR Vektor) verwendet, um die Wirkung der TCF-1-Überexpression zu verallgemeinern. Wir fanden heraus, dass (1) die Überexpression von TCF-1 naive und stammzellähnliche CAR-T Zellen anreichern kann, die eine bessere Abtötungseffizienz aufweisen; (2) das Zytokin Profil der CAR-T Zellen durch die Überexpression von TCF-1 von proinflammatorisch oder abtötungsbezogen auf inaktiv umgeschaltet wurde; (3) der apoptotische Status von CAR-T Zellen durch die Überexpression von TCF-1 moduliert werden konnte, was zu einer besseren Langzeitfunktionalität in Bezug auf wiederholte Tumor Lyse und reduzierte multiple inhibitorische Rezeptoren führte.

Zusammenfassend kann die Überexpression von TCF-1 in CAR-T Zellen Apoptose und Auftreten von CRS reduzieren und deren Persistenz verbessern kann, was zu einer verbesserten Antitumor-Wirksamkeit von CAR-T Zellen führt. Somit könnte die Überexpression von TCF-1 die Persistenz von CAR-T Zellen *in vivo* verbessern und die Wirkung der CAR-T Zelltherapie bei Verstärken.

7. REFERENCES

1. Brudno, J.N., and Kochenderfer, J.N. (2019). Recent advances in CAR T-cell toxicity: Mechanisms, manifestations and management. Blood Rev *34*, 45-55. 10.1016/j.blre.2018.11.002.
2. Zhang, X., Zhu, L., Zhang, H., Chen, S., and Xiao, Y. (2022). CAR-T Cell Therapy in Hematological Malignancies: Current Opportunities and Challenges. Front Immunol *13*, 927153. 10.3389/fimmu.2022.927153.
3. Manier, S., Ingegnere, T., Escure, G., Prodhomme, C., Nudel, M., Mitra, S., and Facon, T. (2022). Current state and next-generation CAR-T cells in multiple myeloma. Blood Rev *54*, 100929. 10.1016/j.blre.2022.100929.
4. Bao, C., Gao, Q., Li, L.L., Han, L., Zhang, B., Ding, Y., Song, Z., Zhang, R., Zhang, J., and Wu, X.H. (2021). The Application of Nanobody in CAR-T Therapy. Biomolecules *11*. 10.3390/biom11020238.
5. Watanabe, N., Mo, F., and McKenna, M.K. (2022). Impact of Manufacturing Procedures on CAR T Cell Functionality. Front Immunol *13*, 876339. 10.3389/fimmu.2022.876339.
6. Marple, A.H., Bonifant, C.L., and Shah, N.N. (2020). Improving CAR T-cells: The next generation. Semin Hematol *57*, 115-121. 10.1053/j.seminhematol.2020.07.002.
7. Zhang, C., Liu, J., Zhong, J.F., and Zhang, X. (2017). Engineering CAR-T cells. Biomark Res *5*, 22. 10.1186/s40364-017-0102-y.
8. Huang, R., Li, X., He, Y., Zhu, W., Gao, L., Liu, Y., Gao, L., Wen, Q., Zhong, J.F., Zhang, C., and Zhang, X. (2020). Recent advances in CAR-T cell engineering. J Hematol Oncol *13*, 86. 10.1186/s13045-020-00910-5.
9. Labanieh, L., Majzner, R.G., and Mackall, C.L. (2018). Programming CAR-T cells to kill cancer. Nat Biomed Eng *2*, 377-391. 10.1038/s41551-018-0235-9.
10. De Bousser, E., Callewaert, N., and Festjens, N. (2021). T Cell Engaging Immunotherapies, Highlighting Chimeric Antigen Receptor (CAR) T Cell Therapy. Cancers (Basel) *13*. 10.3390/cancers13236067.
11. Lee, Y.H., and Kim, C.H. (2019). Evolution of chimeric antigen receptor (CAR) T cell therapy: current status and future perspectives. Arch Pharm Res *42*, 607-616. 10.1007/s12272-019-01136-x.
12. Hughes-Parry, H.E., Cross, R.S., and Jenkins, M.R. (2019). The Evolving Protein Engineering in the Design of Chimeric Antigen Receptor T Cells. Int J Mol Sci *21*. 10.3390/ijms21010204.
13. Vishwasrao, P., Li, G., Boucher, J.C., Smith, D.L., and Hui, S.K. (2022). Emerging CAR T Cell Strategies for the Treatment of AML. Cancers (Basel) *14*. 10.3390/cancers14051241.
14. Luo, L., Zhou, X., Zhou, L., Liang, Z., Yang, J., Tu, S., and Li, Y. (2022). Current state of CAR-T therapy for T-cell malignancies. Ther Adv Hematol *13*, 20406207221143025. 10.1177/20406207221143025.

15. Locke, F.L., Ghobadi, A., Jacobson, C.A., Miklos, D.B., Lekakis, L.J., Oluwole, O.O., Lin, Y., Braunschweig, I., Hill, B.T., Timmerman, J.M., et al. (2019). Long-term safety and activity of axicabtagene ciloleucel in refractory large B-cell lymphoma (ZUMA-1): a single-arm, multicentre, phase 1-2 trial. Lancet Oncol *20*, 31-42. 10.1016/s1470-2045(18)30864-7.
16. Schuster, S.J., Bishop, M.R., Tam, C.S., Waller, E.K., Borchmann, P., McGuirk, J.P., Jäger, U., Jaglowski, S., Andreadis, C., Westin, J.R., et al. (2019). Tisagenlecleucel in Adult Relapsed or Refractory Diffuse Large B-Cell Lymphoma. N Engl J Med *380*, 45-56. 10.1056/NEJMoa1804980.
17. Si Lim, S.J., Grupp, S.A., and DiNofia, A.M. (2021). Tisagenlecleucel for treatment of children and young adults with relapsed/refractory B-cell acute lymphoblastic leukemia. Pediatr Blood Cancer *68*, e29123. 10.1002/pbc.29123.
18. Guedan, S., Chen, X., Madar, A., Carpenito, C., McGettigan, S.E., Frigault, M.J., Lee, J., Posey, A.D., Jr., Scholler, J., Scholler, N., et al. (2014). ICOS-based chimeric antigen receptors program bipolar TH17/TH1 cells. Blood *124*, 1070-1080. 10.1182/blood-2013-10-535245.
19. Song, D.G., Ye, Q., Poussin, M., Harms, G.M., Figini, M., and Powell, D.J., Jr. (2012). CD27 costimulation augments the survival and antitumor activity of redirected human T cells in vivo. Blood *119*, 696-706. 10.1182/blood-2011-03-344275.
20. Kawalekar, O.U., RS, O.C., Fraietta, J.A., Guo, L., McGettigan, S.E., Posey, A.D., Jr., Patel, P.R., Guedan, S., Scholler, J., Keith, B., et al. (2016). Distinct Signaling of Coreceptors Regulates Specific Metabolism Pathways and Impacts Memory Development in CAR T Cells. Immunity *44*, 712. 10.1016/j.immuni.2016.02.023.
21. Chmielewski, M., and Abken, H. (2015). TRUCKs: the fourth generation of CARs. Expert Opin Biol Ther *15*, 1145-1154. 10.1517/14712598.2015.1046430.
22. Hawkins, E.R., D'Souza, R.R., and Klampatsa, A. (2021). Armored CAR T-Cells: The Next Chapter in T-Cell Cancer Immunotherapy. Biologics *15*, 95-105. 10.2147/btt.S291768.
23. Lanitis, E., Rota, G., Kosti, P., Ronet, C., Spill, A., Seijo, B., Romero, P., Dangaj, D., Coukos, G., and Irving, M. (2021). Optimized gene engineering of murine CAR-T cells reveals the beneficial effects of IL-15 coexpression. J Exp Med *218*. 10.1084/jem.20192203.
24. Duan, D., Wang, K., Wei, C., Feng, D., Liu, Y., He, Q., Xu, X., Wang, C., Zhao, S., Lv, L., et al. (2021). The BCMA-Targeted Fourth-Generation CAR-T Cells Secreting IL-7 and CCL19 for Therapy of Refractory/Recurrent Multiple Myeloma. Front Immunol *12*, 609421. 10.3389/fimmu.2021.609421.
25. Tokarew, N., Ogonek, J., Endres, S., von Bergwelt-Baildon, M., and Kobold, S. (2019). Teaching an old dog new tricks: next-generation CAR T cells. Br J Cancer *120*, 26-37. 10.1038/s41416-018-0325-1.

26. Zhylko, A., Winiarska, M., and Graczyk-Jarzynka, A. (2020). The Great War of Today: Modifications of CAR-T Cells to Effectively Combat Malignancies. Cancers (Basel) *12*. 10.3390/cancers12082030.
27. You, F., Wang, Y., Jiang, L., Zhu, X., Chen, D., Yuan, L., An, G., Meng, H., and Yang, L. (2019). A novel CD7 chimeric antigen receptor-modified NK-92MI cell line targeting T-cell acute lymphoblastic leukemia. Am J Cancer Res *9*, 64-78.
28. Duan, H., Huang, H., and Jing, G. (2019). An Antibody Fab Fragment-based Chimeric Antigen Receptor Could Efficiently Eliminate Human Thyroid Cancer Cells. J Cancer *10*, 1890-1895. 10.7150/jca.30163.
29. Balakrishnan, A., Rajan, A., Salter, A.I., Kosasih, P.L., Wu, Q., Voutsinas, J., Jensen, M.C., Plückthun, A., and Riddell, S.R. (2019). Multispecific Targeting with Synthetic Ankyrin Repeat Motif Chimeric Antigen Receptors. Clin Cancer Res *25*, 7506-7516. 10.1158/1078-0432.Ccr-19-1479.
30. McCue, A.C., Yao, Z., and Kuhlman, B. (2022). Advances in modular control of CAR-T therapy with adapter-mediated CARs. Adv Drug Deliv Rev *187*, 114358. 10.1016/j.addr.2022.114358.
31. Minutolo, N.G., Hollander, E.E., and Powell, D.J., Jr. (2019). The Emergence of Universal Immune Receptor T Cell Therapy for Cancer. Front Oncol *9*, 176. 10.3389/fonc.2019.00176.
32. Borrok, M.J., Li, Y., Harvilla, P.B., Vellalore Maruthachalam, B., Tamot, N., Prokopowitz, C., Chen, J., Venkataramani, S., Grewal, I.S., Ganesan, R., and Singh, S. (2022). Conduit CAR: Redirecting CAR T-Cell Specificity with A Universal and Adaptable Bispecific Antibody Platform. Cancer Res Commun *2*, 146-157. 10.1158/2767-9764.Crc-21-0150.
33. Albinger, N., Hartmann, J., and Ullrich, E. (2021). Current status and perspective of CAR-T and CAR-NK cell therapy trials in Germany. Gene Ther *28*, 513-527. 10.1038/s41434-021-00246-w.
34. Gee, A.P. (2018). GMP CAR-T cell production. Best Pract Res Clin Haematol *31*, 126-134. 10.1016/j.beha.2018.01.002.
35. Blache, U., Popp, G., Dünkel, A., Koehl, U., and Fricke, S. (2022). Potential solutions for manufacture of CAR T cells in cancer immunotherapy. Nat Commun *13*, 5225. 10.1038/s41467-022-32866-0.
36. Maude, S.L., Laetsch, T.W., Buechner, J., Rives, S., Boyer, M., Bittencourt, H., Bader, P., Verneris, M.R., Stefanski, H.E., Myers, G.D., et al. (2018). Tisagenlecleucel in Children and Young Adults with B-Cell Lymphoblastic Leukemia. N Engl J Med *378*, 439-448. 10.1056/NEJMoa1709866.
37. Fowler, N.H., Dickinson, M., Dreyling, M., Martinez-Lopez, J., Kolstad, A., Butler, J., Ghosh, M., Popplewell, L., Chavez, J.C., Bachy, E., et al. (2022). Tisagenlecleucel in adult relapsed or refractory follicular lymphoma: the phase 2 ELARA trial. Nat Med *28*, 325-332. 10.1038/s41591-021-01622-0.
38. Wang, M., Munoz, J., Goy, A., Locke, F.L., Jacobson, C.A., Hill, B.T., Timmerman, J.M., Holmes, H., Jaglowski, S., Flinn, I.W., et al. (2020). KTE-X19 CAR T-Cell

Therapy in Relapsed or Refractory Mantle-Cell Lymphoma. N Engl J Med *382*, 1331-1342. 10.1056/NEJMoa1914347.

39. Abramson, J.S., Palomba, M.L., Gordon, L.I., Lunning, M.A., Wang, M., Arnason, J., Mehta, A., Purev, E., Maloney, D.G., Andreadis, C., et al. (2020). Lisocabtagene maraleucel for patients with relapsed or refractory large B-cell lymphomas (TRANSCEND NHL 001): a multicentre seamless design study. Lancet *396*, 839-852. 10.1016/s0140-6736(20)31366-0.
40. Berdeja, J.G., Madduri, D., Usmani, S.Z., Jakubowiak, A., Agha, M., Cohen, A.D., Stewart, A.K., Hari, P., Htut, M., Lesokhin, A., et al. (2021). Ciltacabtagene autoleucel, a B-cell maturation antigen-directed chimeric antigen receptor T-cell therapy in patients with relapsed or refractory multiple myeloma (CARTITUDE-1): a phase 1b/2 open-label study. Lancet *398*, 314-324. 10.1016/s0140-6736(21)00933-8.
41. Munshi, N.C., Anderson, L.D., Jr., Shah, N., Madduri, D., Berdeja, J., Lonial, S., Raje, N., Lin, Y., Siegel, D., Oriol, A., et al. (2021). Idecabtagene Vicleucel in Relapsed and Refractory Multiple Myeloma. N Engl J Med *384*, 705-716. 10.1056/NEJMoa2024850.
42. Kandra, P., Nandigama, R., Eul, B., Huber, M., Kobold, S., Seeger, W., Grimminger, F., and Savai, R. (2022). Utility and Drawbacks of Chimeric Antigen Receptor T Cell (CAR-T) Therapy in Lung Cancer. Front Immunol *13*, 903562. 10.3389/fimmu.2022.903562.
43. Liu, Y., An, L., Huang, R., Xiong, J., Yang, H., Wang, X., and Zhang, X. (2022). Strategies to enhance CAR-T persistence. Biomark Res *10*, 86. 10.1186/s40364-022-00434-9.
44. Chohan, K.L., Siegler, E.L., and Kenderian, S.S. (2023). CAR-T Cell Therapy: the Efficacy and Toxicity Balance. Curr Hematol Malig Rep *18*, 9-18. 10.1007/s11899-023-00687-7.
45. Wang, J.Y., and Wang, L. (2023). CAR-T cell therapy: Where are we now, and where are we heading? Blood Sci *5*, 237-248. 10.1097/bs9.0000000000000173.
46. Shah, N.N., and Fry, T.J. (2019). Mechanisms of resistance to CAR T cell therapy. Nat Rev Clin Oncol *16*, 372-385. 10.1038/s41571-019-0184-6.
47. Lee, D.W., Kochenderfer, J.N., Stetler-Stevenson, M., Cui, Y.K., Delbrook, C., Feldman, S.A., Fry, T.J., Orentas, R., Sabatino, M., Shah, N.N., et al. (2015). T cells expressing CD19 chimeric antigen receptors for acute lymphoblastic leukaemia in children and young adults: a phase 1 dose-escalation trial. Lancet *385*, 517-528. 10.1016/s0140-6736(14)61403-3.
48. Singh, N., Perazzelli, J., Grupp, S.A., and Barrett, D.M. (2016). Early memory phenotypes drive T cell proliferation in patients with pediatric malignancies. Sci Transl Med *8*, 320ra323. 10.1126/scitranslmed.aad5222.
49. Maude, S.L., Frey, N., Shaw, P.A., Aplenc, R., Barrett, D.M., Bunin, N.J., Chew, A., Gonzalez, V.E., Zheng, Z., Lacey, S.F., et al. (2014). Chimeric antigen receptor T cells for sustained remissions in leukemia. N Engl J Med *371*, 1507-1517. 10.1056/NEJMoa1407222.

50. Turtle, C.J., Hanafi, L.A., Berger, C., Gooley, T.A., Cherian, S., Hudecek, M., Sommermeyer, D., Melville, K., Pender, B., Budiarto, T.M., et al. (2016). CD19 CAR-T cells of defined CD4+:CD8+ composition in adult B cell ALL patients. J Clin Invest *126*, 2123-2138. 10.1172/jci85309.
51. Long, A.H., Haso, W.M., Shern, J.F., Wanhainen, K.M., Murgai, M., Ingaramo, M., Smith, J.P., Walker, A.J., Kohler, M.E., Venkateshwara, V.R., et al. (2015). 4-1BB costimulation ameliorates T cell exhaustion induced by tonic signaling of chimeric antigen receptors. Nat Med *21*, 581-590. 10.1038/nm.3838.
52. Wittibschlager, V., Bacher, U., Seipel, K., Porret, N., Wiedemann, G., Haslebacher, C., Hoffmann, M., Daskalakis, M., Akhoundova, D., and Pabst, T. (2023). CAR T-Cell Persistence Correlates with Improved Outcome in Patients with B-Cell Lymphoma. Int J Mol Sci *24*. 10.3390/ijms24065688.
53. Feucht, J., Sun, J., Eyquem, J., Ho, Y.J., Zhao, Z., Leibold, J., Dobrin, A., Cabriolu, A., Hamieh, M., and Sadelain, M. (2019). Calibration of CAR activation potential directs alternative T cell fates and therapeutic potency. Nat Med *25*, 82-88. 10.1038/s41591-018-0290-5.
54. Sadelain, M., Brentjens, R., and Rivière, I. (2013). The basic principles of chimeric antigen receptor design. Cancer Discov *3*, 388-398. 10.1158/2159-8290.Cd-12-0548.
55. Maus, M.V., and June, C.H. (2016). Making Better Chimeric Antigen Receptors for Adoptive T-cell Therapy. Clin Cancer Res *22*, 1875-1884. 10.1158/1078-0432.Ccr-15-1433.
56. Ma, S., Li, X., Wang, X., Cheng, L., Li, Z., Zhang, C., Ye, Z., and Qian, Q. (2019). Current Progress in CAR-T Cell Therapy for Solid Tumors. Int J Biol Sci *15*, 2548-2560. 10.7150/ijbs.34213.
57. Larson, R.C., Kann, M.C., Bailey, S.R., Haradhvala, N.J., Llopis, P.M., Bouffard, A.A., Scarfó, I., Leick, M.B., Grauwet, K., Berger, T.R., et al. (2022). CAR T cell killing requires the IFNγR pathway in solid but not liquid tumours. Nature *604*, 563-570. 10.1038/s41586-022-04585-5.
58. Martinez, M., and Moon, E.K. (2019). CAR T Cells for Solid Tumors: New Strategies for Finding, Infiltrating, and Surviving in the Tumor Microenvironment. Front Immunol *10*, 128. 10.3389/fimmu.2019.00128.
59. Nguyen, D.T., Ogando-Rivas, E., Liu, R., Wang, T., Rubin, J., Jin, L., Tao, H., Sawyer, W.W., Mendez-Gomez, H.R., Cascio, M., et al. (2022). CAR T Cell Locomotion in Solid Tumor Microenvironment. Cells *11*. 10.3390/cells11121974.
60. Liu, G., Rui, W., Zhao, X., and Lin, X. (2021). Enhancing CAR-T cell efficacy in solid tumors by targeting the tumor microenvironment. Cell Mol Immunol *18*, 1085-1095. 10.1038/s41423-021-00655-2.
61. Wik, J.A., and Skålhegg, B.S. (2022). T Cell Metabolism in Infection. Front Immunol *13*, 840610. 10.3389/fimmu.2022.840610.
62. Crespo, J., Sun, H., Welling, T.H., Tian, Z., and Zou, W. (2013). T cell anergy, exhaustion, senescence, and stemness in the tumor microenvironment. Curr Opin Immunol *25*, 214-221. 10.1016/j.coi.2012.12.003.

63. Depil, S., Duchateau, P., Grupp, S.A., Mufti, G., and Poirot, L. (2020). 'Off-the-shelf' allogeneic CAR T cells: development and challenges. Nat Rev Drug Discov *19*, 185-199. 10.1038/s41573-019-0051-2.
64. Ma, L., Dichwalkar, T., Chang, J.Y.H., Cossette, B., Garafola, D., Zhang, A.Q., Fichter, M., Wang, C., Liang, S., Silva, M., et al. (2019). Enhanced CAR-T cell activity against solid tumors by vaccine boosting through the chimeric receptor. Science *365*, 162-168. 10.1126/science.aav8692.
65. Abreu, T.R., Fonseca, N.A., Gonçalves, N., and Moreira, J.N. (2020). Current challenges and emerging opportunities of CAR-T cell therapies. J Control Release *319*, 246-261. 10.1016/j.jconrel.2019.12.047.
66. Sotillo, E., Barrett, D.M., Black, K.L., Bagashev, A., Oldridge, D., Wu, G., Sussman, R., Lanauze, C., Ruella, M., Gazzara, M.R., et al. (2015). Convergence of Acquired Mutations and Alternative Splicing of CD19 Enables Resistance to CART-19 Immunotherapy. Cancer Discov *5*, 1282-1295. 10.1158/2159-8290.Cd-15-1020.
67. Fischer, J., Paret, C., El Malki, K., Alt, F., Wingerter, A., Neu, M.A., Kron, B., Russo, A., Lehmann, N., Roth, L., et al. (2017). CD19 Isoforms Enabling Resistance to CART-19 Immunotherapy Are Expressed in B-ALL Patients at Initial Diagnosis. J Immunother *40*, 187-195. 10.1097/cji.0000000000000169.
68. Jabbour, E., Düll, J., Yilmaz, M., Khoury, J.D., Ravandi, F., Jain, N., Einsele, H., Garcia-Manero, G., Konopleva, M., Short, N.J., et al. (2018). Outcome of patients with relapsed/refractory acute lymphoblastic leukemia after blinatumomab failure: No change in the level of CD19 expression. Am J Hematol *93*, 371-374. 10.1002/ajh.24987.
69. Mejstríková, E., Hrusak, O., Borowitz, M.J., Whitlock, J.A., Brethon, B., Trippett, T.M., Zugmaier, G., Gore, L., von Stackelberg, A., and Locatelli, F. (2017). CD19-negative relapse of pediatric B-cell precursor acute lymphoblastic leukemia following blinatumomab treatment. Blood Cancer J *7*, 659. 10.1038/s41408-017-0023-x.
70. Bhojwani, D., Sposto, R., Shah, N.N., Rodriguez, V., Yuan, C., Stetler-Stevenson, M., O'Brien, M.M., McNeer, J.L., Quereshi, A., Cabannes, A., et al. (2019). Inotuzumab ozogamicin in pediatric patients with relapsed/refractory acute lymphoblastic leukemia. Leukemia *33*, 884-892. 10.1038/s41375-018-0265-z.
71. Piccaluga, P.P., Arpinati, M., Candoni, A., Laterza, C., Paolini, S., Gazzola, A., Sabattini, E., Visani, G., and Pileri, S.A. (2011). Surface antigens analysis reveals significant expression of candidate targets for immunotherapy in adult acute lymphoid leukemia. Leuk Lymphoma *52*, 325-327. 10.3109/10428194.2010.529206.
72. Nagel, I., Bartels, M., Duell, J., Oberg, H.H., Ussat, S., Bruckmueller, H., Ottmann, O., Pfeifer, H., Trautmann, H., Gökbuget, N., et al. (2017). Hematopoietic stem cell involvement in BCR-ABL1-positive ALL as a potential mechanism of resistance to blinatumomab therapy. Blood *130*, 2027-2031. 10.1182/blood-2017-05-782888.
73. Raponi, S., De Propris, M.S., Intoppa, S., Milani, M.L., Vitale, A., Elia, L., Perbellini, O., Pizzolo, G., Foá, R., and Guarini, A. (2011). Flow cytometric study of potential target antigens (CD19, CD20, CD22, CD33) for antibody-based

immunotherapy in acute lymphoblastic leukemia: analysis of 552 cases. Leuk Lymphoma *52*, 1098-1107. 10.3109/10428194.2011.559668.

74. Chevallier, P., Robillard, N., Houille, G., Ayari, S., Guillaume, T., Delaunay, J., Harousseau, J.L., Avet-Loiseau, H., Mohty, M., and Garand, R. (2009). Simultaneous study of five candidate target antigens (CD20, CD22, CD33, CD52, HER2) for antibody-based immunotherapy in B-ALL: a monocentric study of 44 cases. Leukemia *23*, 806-807. 10.1038/leu.2008.303.
75. Fry, T.J., Shah, N.N., Orentas, R.J., Stetler-Stevenson, M., Yuan, C.M., Ramakrishna, S., Wolters, P., Martin, S., Delbrook, C., Yates, B., et al. (2018). CD22-targeted CAR T cells induce remission in B-ALL that is naive or resistant to CD19-targeted CAR immunotherapy. Nat Med *24*, 20-28. 10.1038/nm.4441.
76. Obstfeld, A.E., Frey, N.V., Mansfield, K., Lacey, S.F., June, C.H., Porter, D.L., Melenhorst, J.J., and Wasik, M.A. (2017). Cytokine release syndrome associated with chimeric-antigen receptor T-cell therapy: clinicopathological insights. Blood *130*, 2569-2572. 10.1182/blood-2017-08-802413.
77. Sheth, V.S., and Gauthier, J. (2021). Taming the beast: CRS and ICANS after CAR T-cell therapy for ALL. Bone Marrow Transplant *56*, 552-566. 10.1038/s41409-020-01134-4.
78. Schubert, M.L., Schmitt, M., Wang, L., Ramos, C.A., Jordan, K., Müller-Tidow, C., and Dreger, P. (2021). Side-effect management of chimeric antigen receptor (CAR) T-cell therapy. Ann Oncol *32*, 34-48. 10.1016/j.annonc.2020.10.478.
79. Neelapu, S.S. (2019). Managing the toxicities of CAR T-cell therapy. Hematol Oncol *37 Suppl 1*, 48-52. 10.1002/hon.2595.
80. Gust, J., Ponce, R., Liles, W.C., Garden, G.A., and Turtle, C.J. (2020). Cytokines in CAR T Cell-Associated Neurotoxicity. Front Immunol *11*, 577027. 10.3389/fimmu.2020.577027.
81. Hou, A.J., Chen, L.C., and Chen, Y.Y. (2021). Navigating CAR-T cells through the solid-tumour microenvironment. Nat Rev Drug Discov *20*, 531-550. 10.1038/s41573-021-00189-2.
82. Allen, G.M., Frankel, N.W., Reddy, N.R., Bhargava, H.K., Yoshida, M.A., Stark, S.R., Purl, M., Lee, J., Yee, J.L., Yu, W., et al. (2022). Synthetic cytokine circuits that drive T cells into immune-excluded tumors. Science *378*, eaba1624. 10.1126/science.aba1624.
83. Newick, K., O'Brien, S., Moon, E., and Albelda, S.M. (2017). CAR T Cell Therapy for Solid Tumors. Annu Rev Med *68*, 139-152. 10.1146/annurev-med-062315-120245.
84. Luo, Z., Yao, X., Li, M., Fang, D., Fei, Y., Cheng, Z., Xu, Y., and Zhu, B. (2022). Modulating tumor physical microenvironment for fueling CAR-T cell therapy. Adv Drug Deliv Rev *185*, 114301. 10.1016/j.addr.2022.114301.
85. Marofi, F., Motavalli, R., Safonov, V.A., Thangavelu, L., Yumashev, A.V., Alexander, M., Shomali, N., Chartrand, M.S., Pathak, Y., Jarahian, M., et al. (2021).

CAR T cells in solid tumors: challenges and opportunities. Stem Cell Res Ther *12*, 81. 10.1186/s13287-020-02128-1.

86. Rodriguez-Garcia, A., Lynn, R.C., Poussin, M., Eiva, M.A., Shaw, L.C., O'Connor, R.S., Minutolo, N.G., Casado-Medrano, V., Lopez, G., Matsuyama, T., and Powell, D.J., Jr. (2021). CAR-T cell-mediated depletion of immunosuppressive tumor-associated macrophages promotes endogenous antitumor immunity and augments adoptive immunotherapy. Nat Commun *12*, 877. 10.1038/s41467-021-20893-2.
87. Shalabi, H., Kraft, I.L., Wang, H.W., Yuan, C.M., Yates, B., Delbrook, C., Zimbelman, J.D., Giller, R., Stetler-Stevenson, M., Jaffe, E.S., et al. (2018). Sequential loss of tumor surface antigens following chimeric antigen receptor T-cell therapies in diffuse large B-cell lymphoma. Haematologica *103*, e215-e218. 10.3324/haematol.2017.183459.
88. Yu, H., Sotillo, E., Harrington, C., Wertheim, G., Paessler, M., Maude, S.L., Rheingold, S.R., Grupp, S.A., Thomas-Tikhonenko, A., and Pillai, V. (2017). Repeated loss of target surface antigen after immunotherapy in primary mediastinal large B cell lymphoma. Am J Hematol *92*, E11-e13. 10.1002/ajh.24594.
89. Gounari, F., and Khazaie, K. (2022). TCF-1: a maverick in T cell development and function. Nat Immunol *23*, 671-678. 10.1038/s41590-022-01194-2.
90. Raghu, D., Xue, H.H., and Mielke, L.A. (2019). Control of Lymphocyte Fate, Infection, and Tumor Immunity by TCF-1. Trends Immunol *40*, 1149-1162. 10.1016/j.it.2019.10.006.
91. Ma, J., Wang, R., Fang, X., and Sun, Z. (2012). β-catenin/TCF-1 pathway in T cell development and differentiation. J Neuroimmune Pharmacol *7*, 750-762. 10.1007/s11481-012-9367-y.
92. Xing, S., Li, F., Zeng, Z., Zhao, Y., Yu, S., Shan, Q., Li, Y., Phillips, F.C., Maina, P.K., Qi, H.H., et al. (2016). Tcf1 and Lef1 transcription factors establish CD8(+) T cell identity through intrinsic HDAC activity. Nat Immunol *17*, 695-703. 10.1038/ni.3456.
93. Johnson, J.L., Georgakilas, G., Petrovic, J., Kurachi, M., Cai, S., Harly, C., Pear, W.S., Bhandoola, A., Wherry, E.J., and Vahedi, G. (2018). Lineage-Determining Transcription Factor TCF-1 Initiates the Epigenetic Identity of T Cells. Immunity *48*, 243-257.e210. 10.1016/j.immuni.2018.01.012.
94. Choi, Y.S., Gullicksrud, J.A., Xing, S., Zeng, Z., Shan, Q., Li, F., Love, P.E., Peng, W., Xue, H.H., and Crotty, S. (2015). LEF-1 and TCF-1 orchestrate T(FH) differentiation by regulating differentiation circuits upstream of the transcriptional repressor Bcl6. Nat Immunol *16*, 980-990. 10.1038/ni.3226.
95. Yu, S., Zhou, X., Steinke, F.C., Liu, C., Chen, S.C., Zagorodna, O., Jing, X., Yokota, Y., Meyerholz, D.K., Mullighan, C.G., et al. (2012). The TCF-1 and LEF-1 transcription factors have cooperative and opposing roles in T cell development and malignancy. Immunity *37*, 813-826. 10.1016/j.immuni.2012.08.009.
96. Famili, F., Wiekmeijer, A.S., and Staal, F.J. (2017). The development of T cells from stem cells in mice and humans. Future Sci OA *3*, Fso186. 10.4155/fsoa-2016-0095.

97. Germar, K., Dose, M., Konstantinou, T., Zhang, J., Wang, H., Lobry, C., Arnett, K.L., Blacklow, S.C., Aifantis, I., Aster, J.C., and Gounari, F. (2011). T-cell factor 1 is a gatekeeper for T-cell specification in response to Notch signaling. Proc Natl Acad Sci U S A *108*, 20060-20065. 10.1073/pnas.1110230108.
98. Weber, B.N., Chi, A.W., Chavez, A., Yashiro-Ohtani, Y., Yang, Q., Shestova, O., and Bhandoola, A. (2011). A critical role for TCF-1 in T-lineage specification and differentiation. Nature *476*, 63-68. 10.1038/nature10279.
99. Steinke, F.C., Yu, S., Zhou, X., He, B., Yang, W., Zhou, B., Kawamoto, H., Zhu, J., Tan, K., and Xue, H.H. (2014). TCF-1 and LEF-1 act upstream of Th-POK to promote the CD4(+) T cell fate and interact with Runx3 to silence Cd4 in CD8(+) T cells. Nat Immunol *15*, 646-656. 10.1038/ni.2897.
100. Emmanuel, A.O., Arnovitz, S., Haghi, L., Mathur, P.S., Mondal, S., Quandt, J., Okoreeh, M.K., Maienschein-Cline, M., Khazaie, K., Dose, M., and Gounari, F. (2018). TCF-1 and HEB cooperate to establish the epigenetic and transcription profiles of CD4(+)CD8(+) thymocytes. Nat Immunol *19*, 1366-1378. 10.1038/s41590-018-0254-4.
101. Zhang, J., He, Z., Sen, S., Wang, F., Zhang, Q., and Sun, Z. (2018). TCF-1 Inhibits IL-17 Gene Expression To Restrain Th17 Immunity in a Stage-Specific Manner. J Immunol *200*, 3397-3406. 10.4049/jimmunol.1800193.
102. Mielke, L.A., Liao, Y., Clemens, E.B., Firth, M.A., Duckworth, B., Huang, Q., Almeida, F.F., Chopin, M., Koay, H.F., Bell, C.A., et al. (2019). TCF-1 limits the formation of Tc17 cells via repression of the MAF-RORγt axis. J Exp Med *216*, 1682-1699. 10.1084/jem.20181778.
103. Hu, G., Cui, K., Fang, D., Hirose, S., Wang, X., Wangsa, D., Jin, W., Ried, T., Liu, P., Zhu, J., et al. (2018). Transformation of Accessible Chromatin and 3D Nucleome Underlies Lineage Commitment of Early T Cells. Immunity *48*, 227-242.e228. 10.1016/j.immuni.2018.01.013.
104. Zhou, X., Yu, S., Zhao, D.M., Harty, J.T., Badovinac, V.P., and Xue, H.H. (2010). Differentiation and persistence of memory CD8(+) T cells depend on T cell factor 1. Immunity *33*, 229-240. 10.1016/j.immuni.2010.08.002.
105. Zhu, J., Yamane, H., and Paul, W.E. (2010). Differentiation of effector CD4 T cell populations (*). Annu Rev Immunol *28*, 445-489. 10.1146/annurev-immunol-030409-101212.
106. Zhang, Y., Zhang, Y., Gu, W., and Sun, B. (2014). TH1/TH2 cell differentiation and molecular signals. Adv Exp Med Biol *841*, 15-44. 10.1007/978-94-017-9487-9_2.
107. Crotty, S. (2011). Follicular helper CD4 T cells (TFH). Annu Rev Immunol *29*, 621-663. 10.1146/annurev-immunol-031210-101400.
108. Nakayamada, S., Kanno, Y., Takahashi, H., Jankovic, D., Lu, K.T., Johnson, T.A., Sun, H.W., Vahedi, G., Hakim, O., Handon, R., et al. (2011). Early Th1 cell differentiation is marked by a Tfh cell-like transition. Immunity *35*, 919-931. 10.1016/j.immuni.2011.11.012.

109. Qiu, H., Wu, H., Chan, V., Lau, C.S., and Lu, Q. (2017). Transcriptional and epigenetic regulation of follicular T-helper cells and their role in autoimmunity. Autoimmunity *50*, 71-81. 10.1080/08916934.2017.1284821.
110. Yu, D., and Ye, L. (2018). A Portrait of CXCR5(+) Follicular Cytotoxic CD8(+) T cells. Trends Immunol *39*, 965-979. 10.1016/j.it.2018.10.002.
111. Xue, H.H., and Zhao, D.M. (2012). Regulation of mature T cell responses by the Wnt signaling pathway. Ann N Y Acad Sci *1247*, 16-33. 10.1111/j.1749-6632.2011.06302.x.
112. Karmaus, P.W.F., Chen, X., Lim, S.A., Herrada, A.A., Nguyen, T.M., Xu, B., Dhungana, Y., Rankin, S., Chen, W., Rosencrance, C., et al. (2019). Metabolic heterogeneity underlies reciprocal fates of T(H)17 cell stemness and plasticity. Nature *565*, 101-105. 10.1038/s41586-018-0806-7.
113. Schmetterer, K.G., Neunkirchner, A., and Pickl, W.F. (2012). Naturally occurring regulatory T cells: markers, mechanisms, and manipulation. Faseb j *26*, 2253-2276. 10.1096/fj.11-193672.
114. Ziegler, S.F., and Buckner, J.H. (2009). FOXP3 and the regulation of Treg/Th17 differentiation. Microbes Infect *11*, 594-598. 10.1016/j.micinf.2009.04.002.
115. Rothenberg, E.V. (2019). Programming for T-lymphocyte fates: modularity and mechanisms. Genes Dev *33*, 1117-1135. 10.1101/gad.327163.119.
116. Shevach, E.M., and Thornton, A.M. (2014). tTregs, pTregs, and iTregs: similarities and differences. Immunol Rev *259*, 88-102. 10.1111/imr.12160.
117. Sage, P.T., and Sharpe, A.H. (2016). T follicular regulatory cells. Immunol Rev *271*, 246-259. 10.1111/imr.12411.
118. Reina-Campos, M., Scharping, N.E., and Goldrath, A.W. (2021). CD8(+) T cell metabolism in infection and cancer. Nat Rev Immunol *21*, 718-738. 10.1038/s41577-021-00537-8.
119. Wen, S., Lu, H., Wang, D., Guo, J., Dai, W., and Wang, Z. (2021). TCF-1 maintains CD8(+) T cell stemness in tumor microenvironment. J Leukoc Biol *110*, 585-590. 10.1002/jlb.5mr1120-778r.
120. Kratchmarov, R., Magun, A.M., and Reiner, S.L. (2018). TCF1 expression marks self-renewing human CD8(+) T cells. Blood Adv *2*, 1685-1690. 10.1182/bloodadvances.2018016279.
121. Danilo, M., Chennupati, V., Silva, J.G., Siegert, S., and Held, W. (2018). Suppression of Tcf1 by Inflammatory Cytokines Facilitates Effector CD8 T Cell Differentiation. Cell Rep *22*, 2107-2117. 10.1016/j.celrep.2018.01.072.
122. Man, K., Gabriel, S.S., Liao, Y., Gloury, R., Preston, S., Henstridge, D.C., Pellegrini, M., Zehn, D., Berberich-Siebelt, F., Febbraio, M.A., et al. (2017). Transcription Factor IRF4 Promotes CD8(+) T Cell Exhaustion and Limits the Development of Memory-like T Cells during Chronic Infection. Immunity *47*, 1129-1141.e1125. 10.1016/j.immuni.2017.11.021.
123. Leong, Y.A., Chen, Y., Ong, H.S., Wu, D., Man, K., Deleage, C., Minnich, M., Meckiff, B.J., Wei, Y., Hou, Z., et al. (2016). CXCR5(+) follicular cytotoxic T cells

control viral infection in B cell follicles. Nat Immunol *17*, 1187-1196. 10.1038/ni.3543.

124. Jung, S., and Baek, J.H. (2021). The Potential of T Cell Factor 1 in Sustaining CD8(+) T Lymphocyte-Directed Anti-Tumor Immunity. Cancers (Basel) *13*. 10.3390/cancers13030515.
125. Sade-Feldman, M., Yizhak, K., Bjorgaard, S.L., Ray, J.P., de Boer, C.G., Jenkins, R.W., Lieb, D.J., Chen, J.H., Frederick, D.T., Barzily-Rokni, M., et al. (2019). Defining T Cell States Associated with Response to Checkpoint Immunotherapy in Melanoma. Cell *176*, 404. 10.1016/j.cell.2018.12.034.
126. Miller, B.C., Sen, D.R., Al Abosy, R., Bi, K., Virkud, Y.V., LaFleur, M.W., Yates, K.B., Lako, A., Felt, K., Naik, G.S., et al. (2019). Subsets of exhausted CD8(+) T cells differentially mediate tumor control and respond to checkpoint blockade. Nat Immunol *20*, 326-336. 10.1038/s41590-019-0312-6.
127. Fraietta, J.A., Lacey, S.F., Orlando, E.J., Pruteanu-Malinici, I., Gohil, M., Lundh, S., Boesteanu, A.C., Wang, Y., O'Connor, R.S., Hwang, W.T., et al. (2018). Determinants of response and resistance to CD19 chimeric antigen receptor (CAR) T cell therapy of chronic lymphocytic leukemia. Nat Med *24*, 563-571. 10.1038/s41591-018-0010-1.
128. Zangari, B., Tsuji, T., Matsuzaki, J., Mohammadpour, H., Eppolito, C., Battaglia, S., Ito, F., Chodon, T., Koya, R., Robert McGray, A.J., and Odunsi, K. (2022). Tcf-1 protects anti-tumor TCR-engineered CD8(+) T-cells from GzmB mediated self-destruction. Cancer Immunol Immunother *71*, 2881-2898. 10.1007/s00262-022-03197-2.
129. Osman, A., Yan, B., Li, Y., Pavelko, K.D., Quandt, J., Saadalla, A., Singh, M.P., Kazemian, M., Gounari, F., and Khazaie, K. (2021). TCF-1 controls T(reg) cell functions that regulate inflammation, CD8(+) T cell cytotoxicity and severity of colon cancer. Nat Immunol *22*, 1152-1162. 10.1038/s41590-021-00987-1.
130. Ho, J.Y., Wang, L., Liu, Y., Ba, M., Yang, J., Zhang, X., Chen, D., Lu, P., and Li, J. (2021). Promoter usage regulating the surface density of CAR molecules may modulate the kinetics of CAR-T cells in vivo. Mol Ther Methods Clin Dev *21*, 237-246. 10.1016/j.omtm.2021.03.007.
131. Walker, A.J., Majzner, R.G., Zhang, L., Wanhainen, K., Long, A.H., Nguyen, S.M., Lopomo, P., Vigny, M., Fry, T.J., Orentas, R.J., and Mackall, C.L. (2017). Tumor Antigen and Receptor Densities Regulate Efficacy of a Chimeric Antigen Receptor Targeting Anaplastic Lymphoma Kinase. Mol Ther *25*, 2189-2201. 10.1016/j.ymthe.2017.06.008.
132. Rodriguez-Marquez, P., Calleja-Cervantes, M.E., Serrano, G., Oliver-Caldes, A., Palacios-Berraquero, M.L., Martin-Mallo, A., Calviño, C., Español-Rego, M., Ceballos, C., Lozano, T., et al. (2022). CAR density influences antitumoral efficacy of BCMA CAR T cells and correlates with clinical outcome. Sci Adv *8*, eabo0514. 10.1126/sciadv.abo0514.

133. Wang, Y., Hu, J., Li, Y., Xiao, M., Wang, H., Tian, Q., Li, Z., Tang, J., Hu, L., Tan, Y., et al. (2019). The Transcription Factor TCF1 Preserves the Effector Function of Exhausted CD8 T Cells During Chronic Viral Infection. Front Immunol *10*, 169. 10.3389/fimmu.2019.00169.
134. Rutishauser, R.L., Deguit, C.D.T., Hiatt, J., Blaeschke, F., Roth, T.L., Wang, L., Raymond, K.A., Starke, C.E., Mudd, J.C., Chen, W., et al. (2021). TCF-1 regulates HIV-specific CD8+ T cell expansion capacity. JCI Insight *6*. 10.1172/jci.insight.136648.
135. Pais Ferreira, D., Silva, J.G., Wyss, T., Fuertes Marraco, S.A., Scarpellino, L., Charmoy, M., Maas, R., Siddiqui, I., Tang, L., Joyce, J.A., et al. (2020). Central memory CD8(+) T cells derive from stem-like Tcf7(hi) effector cells in the absence of cytotoxic differentiation. Immunity *53*, 985-1000.e1011. 10.1016/j.immuni.2020.09.005.
136. Frigault, M.J., Lee, J., Basil, M.C., Carpenito, C., Motohashi, S., Scholler, J., Kawalekar, O.U., Guedan, S., McGettigan, S.E., Posey, A.D., Jr., et al. (2015). Identification of chimeric antigen receptors that mediate constitutive or inducible proliferation of T cells. Cancer Immunol Res *3*, 356-367. 10.1158/2326-6066.Cir-14-0186.
137. Gomes-Silva, D., Mukherjee, M., Srinivasan, M., Krenciute, G., Dakhova, O., Zheng, Y., Cabral, J.M.S., Rooney, C.M., Orange, J.S., Brenner, M.K., and Mamonkin, M. (2017). Tonic 4-1BB Costimulation in Chimeric Antigen Receptors Impedes T Cell Survival and Is Vector-Dependent. Cell Rep *21*, 17-26. 10.1016/j.celrep.2017.09.015.
138. Weber, E.W., Parker, K.R., Sotillo, E., Lynn, R.C., Anbunathan, H., Lattin, J., Good, Z., Belk, J.A., Daniel, B., Klysz, D., et al. (2021). Transient rest restores functionality in exhausted CAR-T cells through epigenetic remodeling. Science *372*. 10.1126/science.aba1786.
139. D'Amours, D., Desnoyers, S., D'Silva, I., and Poirier, G.G. (1999). Poly(ADP-ribosyl)ation reactions in the regulation of nuclear functions. Biochem J *342 (Pt 2)*, 249-268.
140. Varadhachary, A.S., and Salgame, P. (1998). CD95 mediated T cell apoptosis and its relevance to immune deviation. Oncogene *17*, 3271-3276. 10.1038/sj.onc.1202572.
141. Johann, L., and Waisman, A. (2021). The astrocyte LAMP lights a T cell TRAIL of death. Neuron *109*, 1423-1425. 10.1016/j.neuron.2021.04.009.
142. Cebrián, M., Yagüe, E., Rincón, M., López-Botet, M., de Landázuri, M.O., and Sánchez-Madrid, F. (1988). Triggering of T cell proliferation through AIM, an activation inducer molecule expressed on activated human lymphocytes. J Exp Med *168*, 1621-1637. 10.1084/jem.168.5.1621.
143. Jiménez-Fernández, M., Rodríguez-Sinovas, C., Cañes, L., Ballester-Servera, C., Vara, A., Requena, S., de la Fuente, H., Martínez-González, J., and Sánchez-Madrid, F. (2022). CD69-oxLDL ligand engagement induces Programmed Cell Death 1 (PD-1) expression in human CD4 + T lymphocytes. Cell Mol Life Sci *79*, 468. 10.1007/s00018-022-04481-1.

144. Ramos, C.A., Rouce, R., Robertson, C.S., Reyna, A., Narala, N., Vyas, G., Mehta, B., Zhang, H., Dakhova, O., Carrum, G., et al. (2018). In Vivo Fate and Activity of Second- versus Third-Generation CD19-Specific CAR-T Cells in B Cell Non-Hodgkin's Lymphomas. Mol Ther *26*, 2727-2737. 10.1016/j.ymthe.2018.09.009.

145. Künkele, A., Johnson, A.J., Rolczynski, L.S., Chang, C.A., Hoglund, V., Kelly-Spratt, K.S., and Jensen, M.C. (2015). Functional Tuning of CARs Reveals Signaling Threshold above Which CD8+ CTL Antitumor Potency Is Attenuated due to Cell Fas-FasL-Dependent AICD. Cancer Immunol Res *3*, 368-379. 10.1158/2326-6066.Cir-14-0200.

146. Curran, K.J., Seinstra, B.A., Nikhamin, Y., Yeh, R., Usachenko, Y., van Leeuwen, D.G., Purdon, T., Pegram, H.J., and Brentjens, R.J. (2015). Enhancing antitumor efficacy of chimeric antigen receptor T cells through constitutive CD40L expression. Mol Ther *23*, 769-778. 10.1038/mt.2015.4.

147. Sabatino, M., Hu, J., Sommariva, M., Gautam, S., Fellowes, V., Hocker, J.D., Dougherty, S., Qin, H., Klebanoff, C.A., Fry, T.J., et al. (2016). Generation of clinical-grade CD19-specific CAR-modified CD8+ memory stem cells for the treatment of human B-cell malignancies. Blood *128*, 519-528. 10.1182/blood-2015-11-683847.

148. Gattinoni, L., Speiser, D.E., Lichterfeld, M., and Bonini, C. (2017). T memory stem cells in health and disease. Nat Med *23*, 18-27. 10.1038/nm.4241.

149. Flynn, J.K., and Gorry, P.R. (2014). Stem memory T cells (TSCM)-their role in cancer and HIV immunotherapies. Clin Transl Immunology *3*, e20. 10.1038/cti.2014.16.

150. Majzner, R.G., and Mackall, C.L. (2019). Clinical lessons learned from the first leg of the CAR T cell journey. Nat Med *25*, 1341-1355. 10.1038/s41591-019-0564-6.

151. Deng, Q., Han, G., Puebla-Osorio, N., Ma, M.C.J., Strati, P., Chasen, B., Dai, E., Dang, M., Jain, N., Yang, H., et al. (2020). Characteristics of anti-CD19 CAR T cell infusion products associated with efficacy and toxicity in patients with large B cell lymphomas. Nat Med *26*, 1878-1887. 10.1038/s41591-020-1061-7.

152. Arcangeli, S., Bove, C., Mezzanotte, C., Camisa, B., Falcone, L., Manfredi, F., Bezzecchi, E., El Khoury, R., Norata, R., Sanvito, F., et al. (2022). CAR T cell manufacturing from naive/stem memory T lymphocytes enhances antitumor responses while curtailing cytokine release syndrome. J Clin Invest *132*. 10.1172/jci150807.

153. Hay, K.A., Gauthier, J., Hirayama, A.V., Voutsinas, J.M., Wu, Q., Li, D., Gooley, T.A., Cherian, S., Chen, X., Pender, B.S., et al. (2019). Factors associated with durable EFS in adult B-cell ALL patients achieving MRD-negative CR after CD19 CAR T-cell therapy. Blood *133*, 1652-1663. 10.1182/blood-2018-11-883710.

154. Santomasso, B., Bachier, C., Westin, J., Rezvani, K., and Shpall, E.J. (2019). The Other Side of CAR T-Cell Therapy: Cytokine Release Syndrome, Neurologic Toxicity, and Financial Burden. Am Soc Clin Oncol Educ Book *39*, 433-444. 10.1200/edbk_238691.

155. Liu, Y., Fang, Y., Chen, X., Wang, Z., Liang, X., Zhang, T., Liu, M., Zhou, N., Lv, J., Tang, K., et al. (2020). Gasdermin E-mediated target cell pyroptosis by CAR T cells triggers cytokine release syndrome. Sci Immunol *5*. 10.1126/sciimmunol.aax7969.

156. Zhou, Z., He, H., Wang, K., Shi, X., Wang, Y., Su, Y., Wang, Y., Li, D., Liu, W., Zhang, Y., et al. (2020). Granzyme A from cytotoxic lymphocytes cleaves GSDMB to trigger pyroptosis in target cells. Science *368*. 10.1126/science.aaz7548.

157. Ghorashian, S., Kramer, A.M., Onuoha, S., Wright, G., Bartram, J., Richardson, R., Albon, S.J., Casanovas-Company, J., Castro, F., Popova, B., et al. (2019). Enhanced CAR T cell expansion and prolonged persistence in pediatric patients with ALL treated with a low-affinity CD19 CAR. Nat Med *25*, 1408-1414. 10.1038/s41591-019-0549-5.

158. Buchan, S.L., Rogel, A., and Al-Shamkhani, A. (2018). The immunobiology of CD27 and OX40 and their potential as targets for cancer immunotherapy. Blood *131*, 39-48. 10.1182/blood-2017-07-741025.

159. Gattinoni, L., Lugli, E., Ji, Y., Pos, Z., Paulos, C.M., Quigley, M.F., Almeida, J.R., Gostick, E., Yu, Z., Carpenito, C., et al. (2011). A human memory T cell subset with stem cell-like properties. Nat Med *17*, 1290-1297. 10.1038/nm.2446.

160. Davila, M.L., Riviere, I., Wang, X., Bartido, S., Park, J., Curran, K., Chung, S.S., Stefanski, J., Borquez-Ojeda, O., Olszewska, M., et al. (2014). Efficacy and toxicity management of 19-28z CAR T cell therapy in B cell acute lymphoblastic leukemia. Sci Transl Med *6*, 224ra225. 10.1126/scitranslmed.3008226.

161. Kalos, M., Levine, B.L., Porter, D.L., Katz, S., Grupp, S.A., Bagg, A., and June, C.H. (2011). T cells with chimeric antigen receptors have potent antitumor effects and can establish memory in patients with advanced leukemia. Sci Transl Med *3*, 95ra73. 10.1126/scitranslmed.3002842.

162. Bove, C., Arcangeli, S., Falcone, L., Camisa, B., El Khoury, R., Greco, B., De Lucia, A., Bergamini, A., Bondanza, A., Ciceri, F., et al. (2023). CD4 CAR-T cells targeting CD19 play a key role in exacerbating cytokine release syndrome, while maintaining long-term responses. J Immunother Cancer *11*. 10.1136/jitc-2022-005878.

163. Ogasawara, K., Lymp, J., Mack, T., Dell'Aringa, J., Huang, C.P., Smith, J., Peiser, L., and Kostic, A. (2022). In Vivo Cellular Expansion of Lisocabtagene Maraleucel and Association With Efficacy and Safety in Relapsed/Refractory Large B-Cell Lymphoma. Clin Pharmacol Ther *112*, 81-89. 10.1002/cpt.2561.

8. APPENDIX

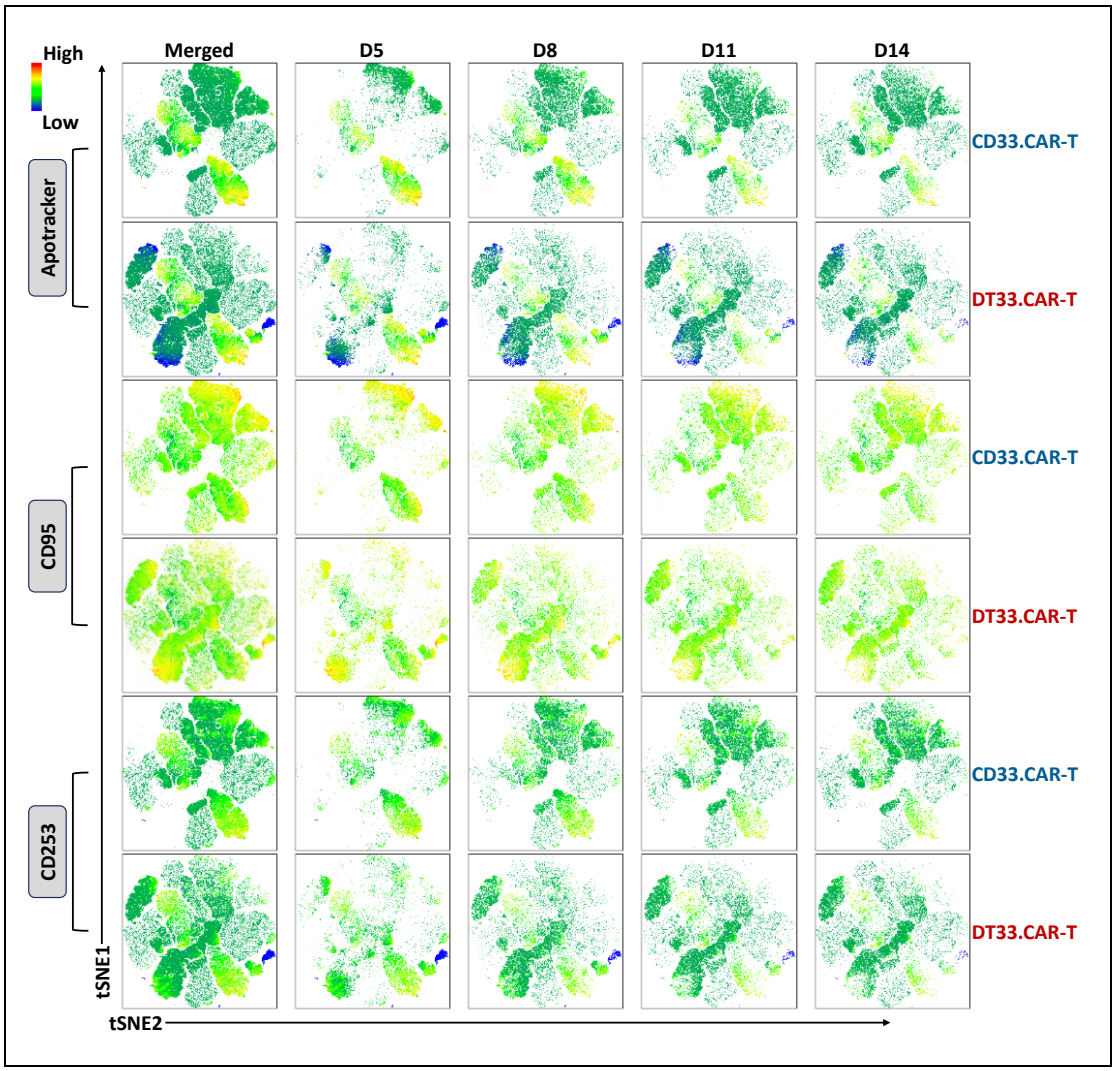

Appendix Figure 1: The intensity of apoptosis related proteins on CD33.CAR-T cells and DT33.CAR-T cells in t-SNE plot.

Merged: t-SNE figures from day 5 to day 14 were combined; D5: marker expression on t-SNE from generation day 5; D8: marker expression on t-SNE from generation day 8; D11: marker expression on t-SNE from generation day 11; D14; marker expression on t-SNE from generation day 14.

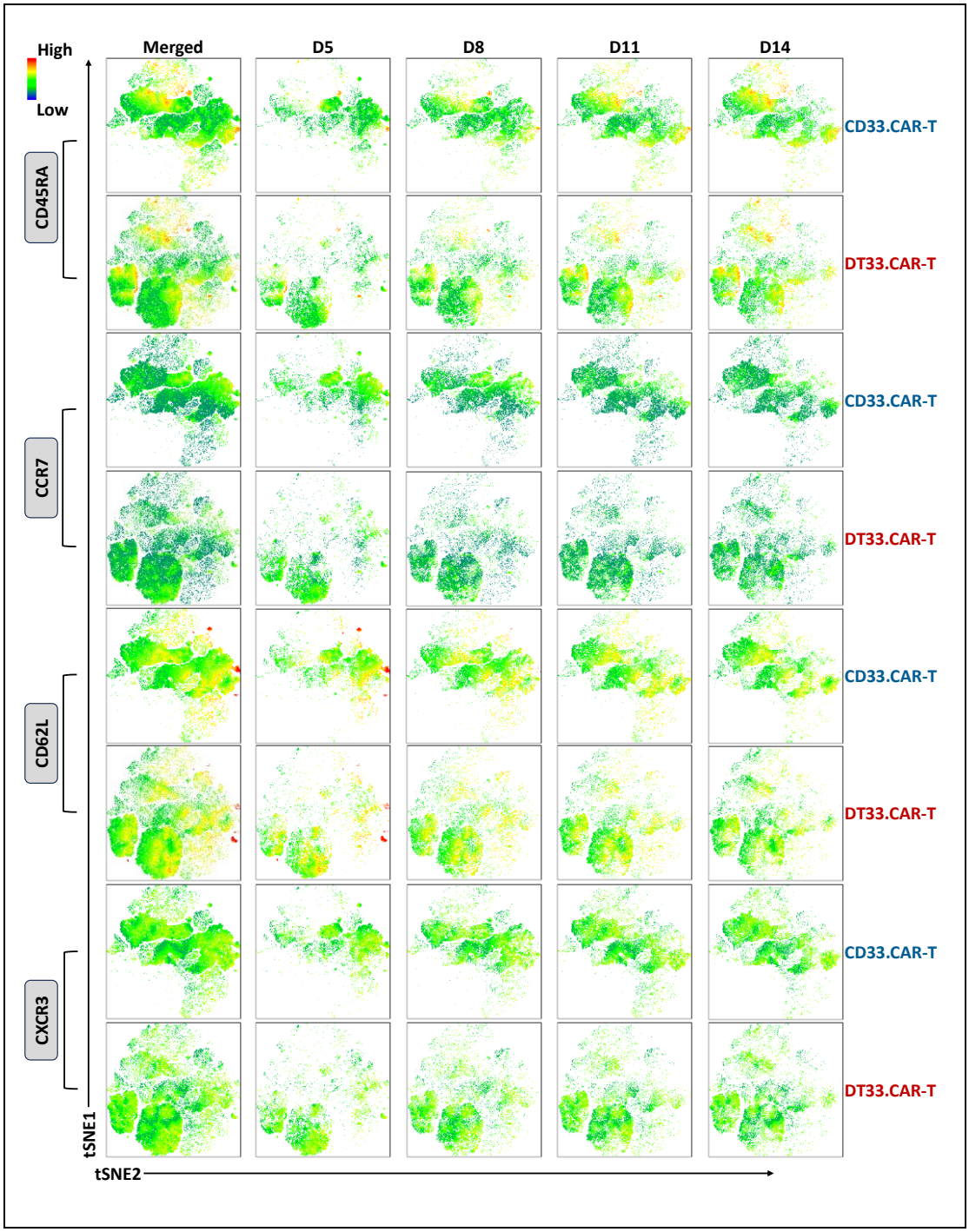

Appendix Figure 2: The intensity of differentiation markers on CD33.CAR-T cells and DT33.CAR-T cells in t-SNE plot.

Merged: t-SNE figures from day 5 to day 14 were combined; D5: marker expression on t-SNE from generation day 5; D8: marker expression on t-SNE from generation day 8; D11: marker expression on t-SNE from generation day 11; D14; marker expression on t-SNE from generation day 14.

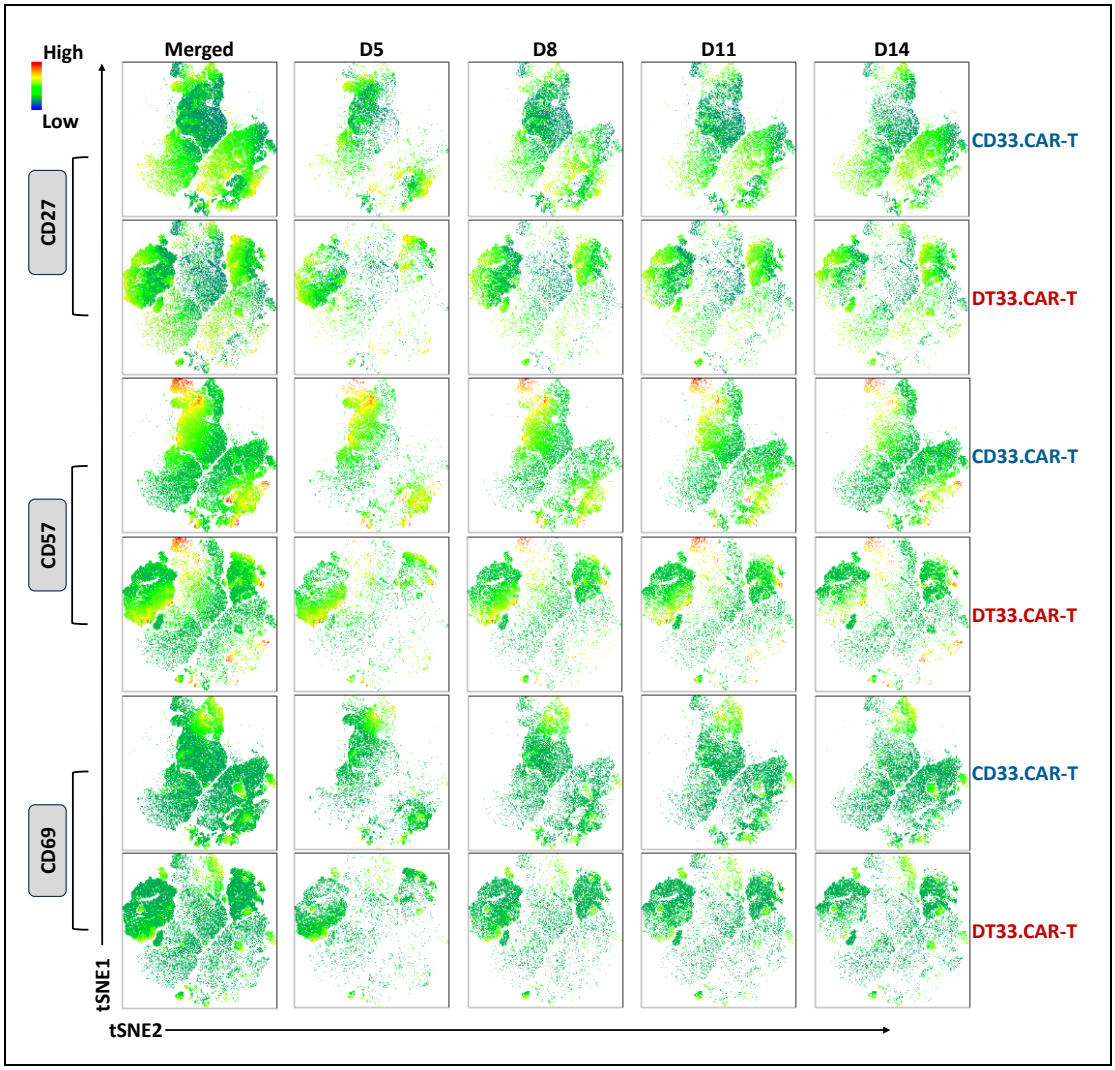

Appendix Figure 3: The intensity of activation markers on CD33.CAR-T cells and DT33.CAR-T cells in t-SNE plot.

Merged: t-SNE figures from day 5 to day 14 were combined; D5: marker expression on t-SNE from generation day 5; D8: marker expression on t-SNE from generation day 8; D11: marker expression on t-SNE from generation day 11; D14; marker expression on t-SNE from generation day 14.

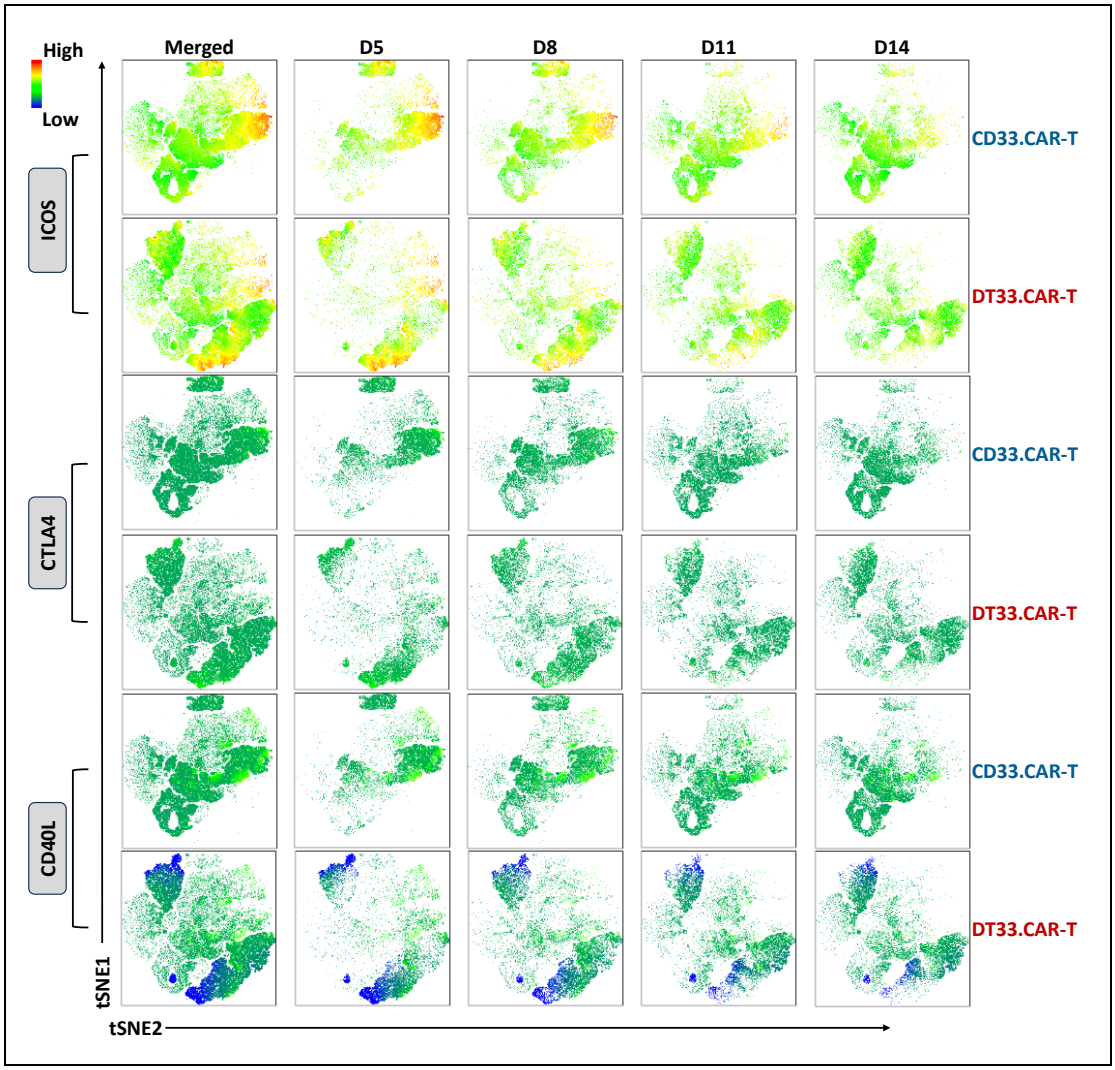

Appendix Figure 4: The intensity of co-stimulatory markers on CD33.CAR-T cells and DT33.CAR-T cells in t-SNE plot.

Merged: t-SNE figures from day 5 to day 14 were combined; D5: marker expression on t-SNE from generation day 5; D8: marker expression on t-SNE from generation day8; D11: marker expression on t-SNE from generation day 11; D14; marker expression on t-SNE from generation day 14.

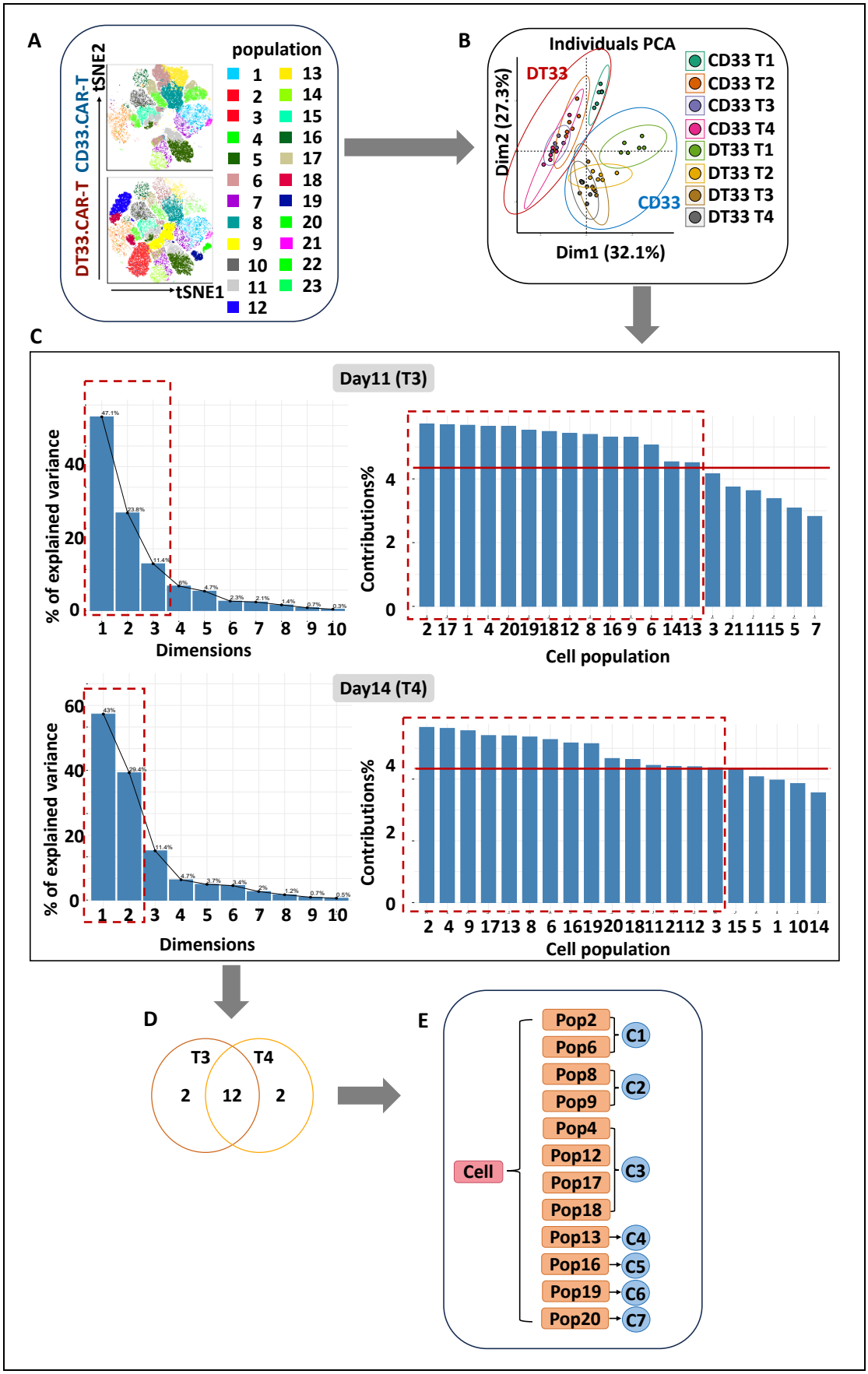

Appendix Figure 5: Cell clusters and filtering of apoptotic markers.

A: Cell clustering and PCA: t-SNE plot pf phonograph identified cell clusters. B: Evaluation of distinguishing capability of cell clusters by PCA. C : Dimension reduction by PCA: Elbow-shaped scree plot to determine the number of factors to retain in an exploratory principal component (left panel). Contribution of rows to the dimensions (right panel), Rows that contribute the most to dimension 1 and dimension 2, or/and dimension 3, in total >70%, are the most important in explaining the variability in the data set. Rows that do not contribute much to any dimension or that contribute to the last dimensions are less important. D: The relationships between most important cell populations at day 11 and day 14 by Venn diagram. Figure B: Manual classification of common cell populations by flowcytometry dot plots (Pop: cell population, C: cell cluster).

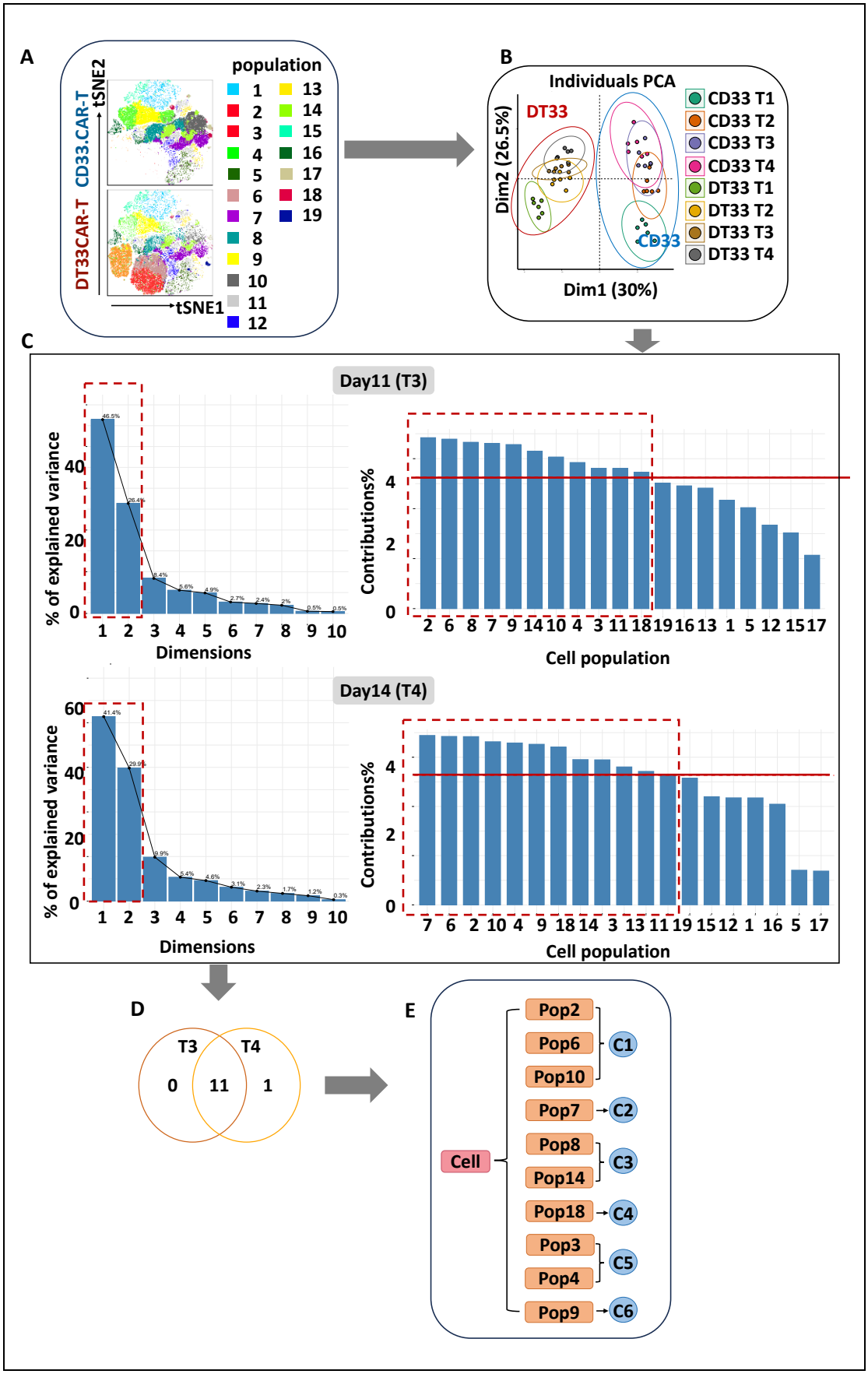

Appendix Figure 6: Cell clusters and filtering of differentiation markers.

A: Cell clustering and PCA: t-SNE plot pf phonograph identified cell clusters. B: Evaluation of distinguishing capability of cell clusters by PCA. C: Dimension reduction by PCA: Elbow-shaped scree plot to determine the number of factors to retain in an exploratory principal component (left panel). Contribution of rows to the dimensions (right panel), Rows that contribute the most to dimension 1 and dimension 2, or/and dimension 3, in total >70%, are the most important in explaining the variability in the data set. Rows that do not contribute much to any dimension or that contribute to the last dimensions are less important. D: The relationships between most important cell populations at day 11 and day 14 by Venn diagram. Figure B: Manual classification of common cell populations by flowcytometry dot plots (Pop: cell population, C: cell cluster).

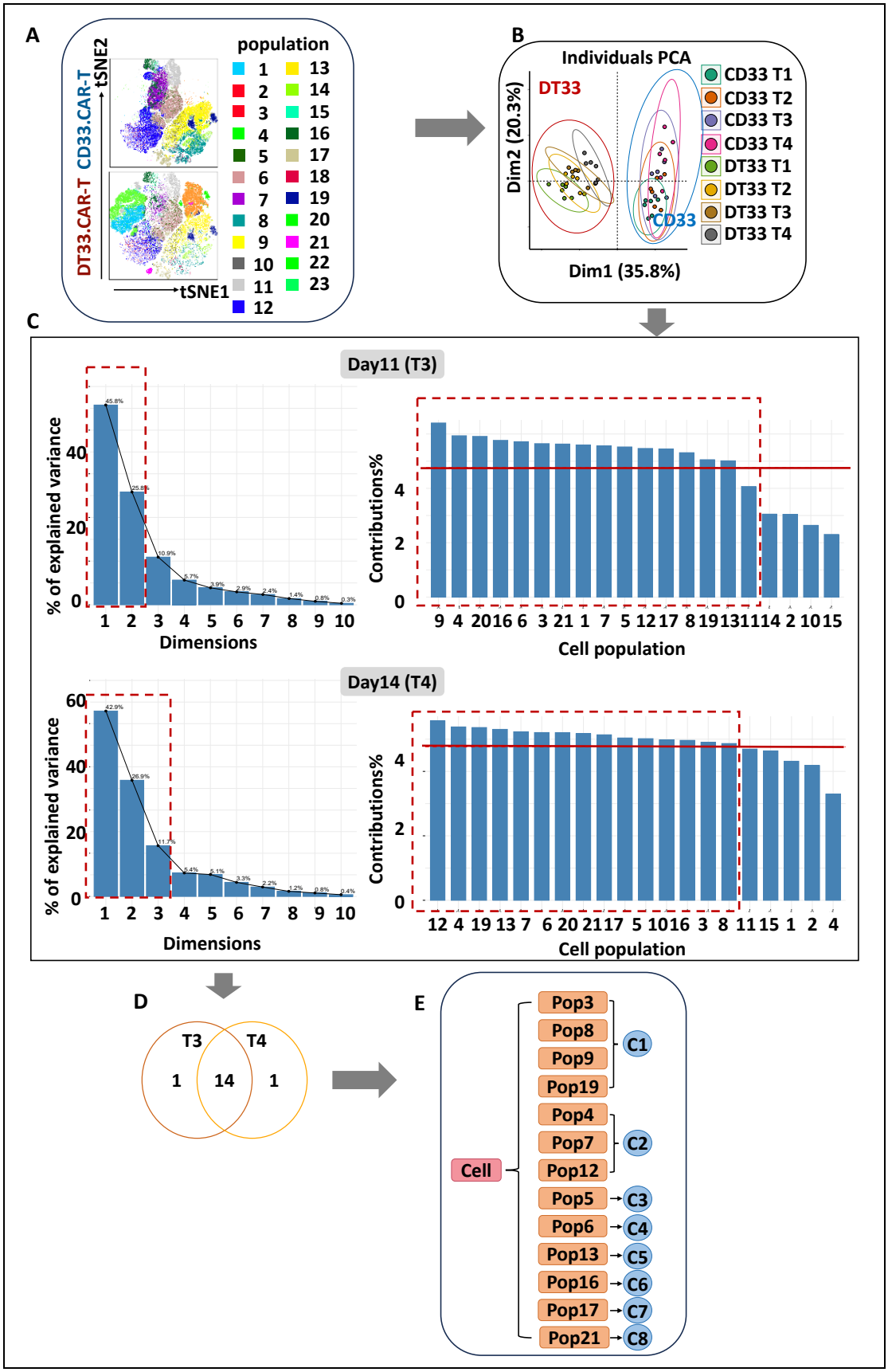

Appendix Figure 7: Cell clusters and filtering of activation markers

A: Cell clustering and PCA: t-SNE plot pf phonograph identified cell clusters. B: Evaluation of distinguishing capability of cell clusters by PCA. C : Dimension reduction by PCA: Elbow-shaped scree plot to determine the number of factors to retain in an exploratory principal component (left panel). Contribution of rows to the dimensions (right panel), Rows that contribute the most to dimension 1 and dimension 2, or/and dimension 3, in total >70%, are the most important in explaining the variability in the data set. Rows that do not contribute much to any dimension or that contribute to the last dimensions are less important. D: The relationships between most important cell populations at day 11 and day 14 by Venn diagram. Figure B: Manual classification of common cell populations by flowcytometry dot plots (Pop: cell population, C: cell cluster).

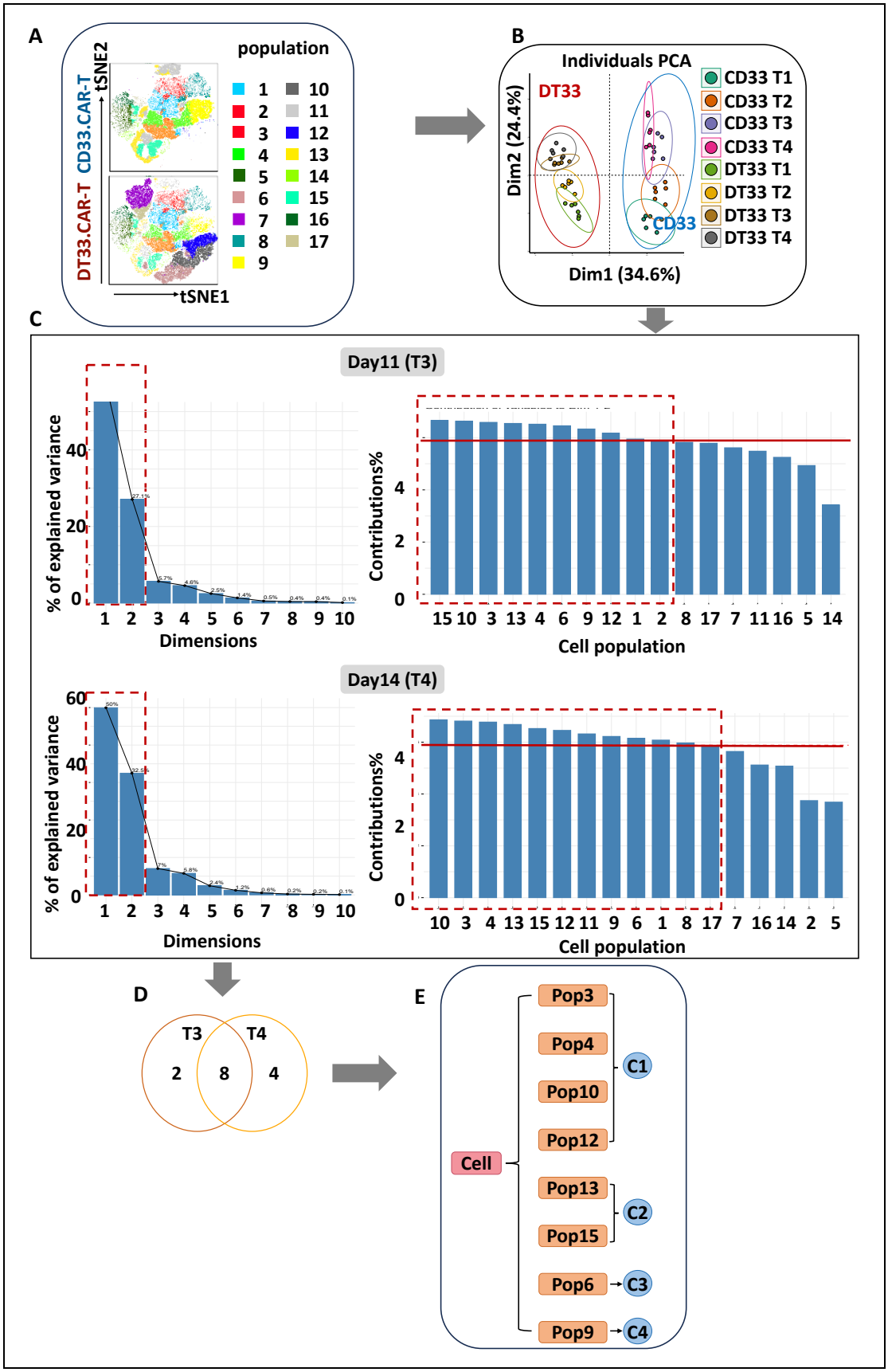

Appendix Figure 8: Cell clusters and filtering of co-stimulatory markers

A: Cell clustering and PCA: t-SNE plot pf phonograph identified cell clusters. B: Evaluation of distinguishing capability of cell clusters by PCA. C : Dimension reduction by PCA: Elbow-shaped scree plot to determine the number of factors to retain in an exploratory principal component (left panel). Contribution of rows to the dimensions (right panel), Rows that contribute the most to dimension 1 and dimension 2, or/and dimension 3, in total >70%, are the most important in explaining the variability in the data set. Rows that do not contribute much to any dimension or that contribute to the last dimensions are less important. D: The relationships between most important cell populations at day 11 and day 14 by Venn diagram. Figure B: Manual classification of common cell populations by flowcytometry dot plots (Pop: cell population, C: cell cluster).

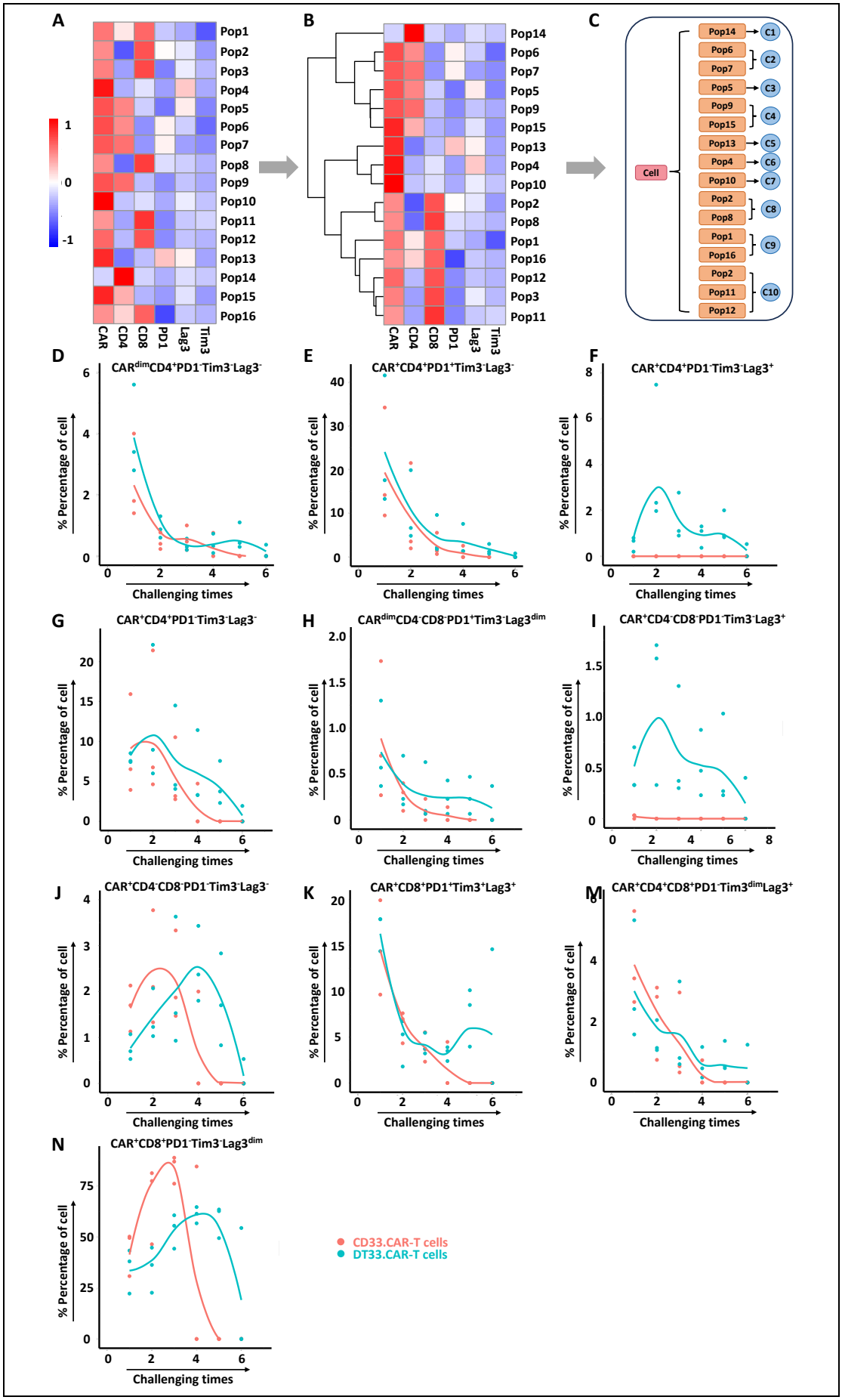
A
Pop1
Pop2
Pop3
Pop4
Pop5
Pop6
Pop7
Pop8
Pop9
Pop10
Pop11
Pop12
Pop13
Pop14
Pop15
Pop16
CAR
CD4
CD8
PD1
Lag3
Tim3
1
0
-1
B
Pop14
Pop6
Pop7
Pop5
Pop9
Pop15
Pop13
Pop4
Pop10
Pop2
Pop8
Pop1
Pop16
Pop12
Pop3
Pop11
C
Cell
Pop14
Pop6
Pop7
Pop5
Pop9
Pop15
Pop13
Pop4
Pop10
Pop2
Pop8
Pop1
Pop16
Pop2
Pop11
Pop12
C1
C2
C3
C4
C5
C6
C7
C8
C9
C10
D
CAR^dimCD4^+PD1^-Tim3^-Lag3^-
E
CAR^+CD4^+PD1^+Tim3^-Lag3^-
F
CAR^+CD4^+PD1^-Tim3^-Lag3^+
G
CAR^+CD4^+PD1^-Tim3^-Lag3^-
H
CAR^dimCD4^-CD8^-PD1^+Tim3^-Lag3^dim
I
CAR^+CD4^-CD8^-PD1^-Tim3^-Lag3^+
J
CAR^+CD4^-CD8^-PD1^-Tim3^-Lag3^-
K
CAR^+CD8^+PD1^+Tim3^+Lag3^+
M
CAR^+CD4^+CD8^+PD1^-Tim3^dimLag3^+
N
CAR^+CD8^+PD1^-Tim3^-Lag3^dim
% Percentage of cell
Challenging times
CD33.CAR-T cells
DT33.CAR-T cells

Appendix Figure 9: Workflow of cell clustering and locally estimated scatterplot smoothing (LOESS) regression line fitted to the data set from co-culture.

Expression profiles of detected populations by FlowSOM， a fast clustering and visualization technique for flow or mass cytometry data that builds self-organizing maps (SOM) to help visualize marker expression across cell subsets. Heatmap shows median expression intensities of each marker (column), for each detected population (row). Values are normalized and scaled between -1 to 1 for each marker (Figure 9A). Rows and columns are sorted by hierarchical clustering (Figure 9B). The summarized cell clusters are indicated in Figure 9C. Data set was from co-culture assay, effector cells were CD33.CAR-T cells and DT33.CAR-T cell, targeted cells were MV4-11 cells; Pop: population; C: cluster; PD-1: Programmed Cell Death Protein 1; Tim3: T-cell immunoglobulin and mucin domain-containing protein 3; Lag3: Lymphocyte-activation gene 3; Dim: diminished.

CURRICULUM VITAE

Hao Yao
Fritz-Frey.Str.11, Heidelberg, 69121
+49 152 07460547 | haoyao1228@gmail.com

Experience

PhD candidate,Cellular Immunotherapy *11/2019 - Now*
***University of Heideiberg**, Heidelberg, Germany*

- Established a retroviral-based double transduction system for improvement of CAR-T cells with a factor of interest
- Invented a new application of a factor not only to reduce side effects of CAR-T cells but also improve their persistence and killing efficiency
- Collaborated with Karlsruhe Institute of Technology to establish a 3D CAR-T cell culture model
- Performed various immunological assays to analyze CAR-T cells

Resident Doctor, Department of Hematology *06/2017-06/2019*
***Jiangsu Province Hospitalof Chinese Medicine**, Nanjing, China*

- Provided emergency, inpatient and outpatient care and was in charge of medical history acquisition
- Collected and organized over 50 clinical cases of thrombocytopenia and over 30 clinical cases of aplastic anemia
- In charge of a research project on ART induced apoptosis and autophagy via PI3K/Akt/mTOR pathway *in vitro*
- Performed mouse experiments
- Supervised young fellows in the lab

Medical Intern on Rotation *06/2016 – 05/2017*
***Jiangsu Province Hospital of Chinese Medicine**, Nanjing, China*

Education

PhD candidate, Cellular Immunotherapy, Dr. sc. hum *11/2019 – Now*
***University of Heidelberg**, Heidelberg, Germany*

Master of Chinese Medicine in Hematology *09/2016 – 06/2019*
***Nanjing University of Chinese Medicine**, Nanjing, China*

Bachelor of Chinese Medicine *09/2011 – 06/2016*
***Nanjing University of Chinese Medicine**, Nanjing, China*

Skills

Certificates: Chinese medicine doctor license

Experimental skills: CAR-T cell related experimental skill sets, cell culture, cell transfection, CAR-T cell generation, *in vitro* CAR-T cell killing assay, CRISPR-CAS9

RNP, cloning, bacterial work, PCR, western blot, advanced flow cytometry, ELISpot, ELISA

Software skills: R language, SPSS, Flowjo, Prism, Microsoft Office Suite

Languages: Mandarin (mother language), English (IELTS – C1), German (A1)

Awards

48th EBMT (European Society for Blood & Marrow Transplantation) Best Young Poster Abstract *03/2022*

48th EBMT *Springer Award for the Best Basic Science Poster* *03/2022*

Award for Outstanding Graduate Thesis *06/2019*

Multiple-Author Publications

1.CD33-directed immunotherapy with third-generation chimeric antigen receptor T cells and gemtuzumab ozogamicin in intact and CD33-edited acute myeloid leukemia and hematopoietic stem and progenitor cells. *Int J Cancer. 2022*

2. Targeting autophagy in multiple myeloma. *Leuk Res. 2017*

ACKNOWLEDGMENT

No matter how tightly I hold my hands, I cannot grasp the time that flows away like water. My story here began in the fall of 2019 and ended in the summer of 2024. Although COVID-19 has taken over almost four years on campus, I have secretly saved lots of growth and emotions.

Foremost and of utmost importance, I extend my heartfelt gratitude to my esteemed doctoral advisor, Prof. Dr. med. Michael Schmitt, whose unwavering support, invaluable guidance, and constant encouragement have illuminated every step of this profound journey. His expertise and dedication have not only enriched my academic pursuits but have also shaped me into a more capable and confident individual. His mentorship will forever stand as a beacon of inspiration in my scholarly and personal endeavors.

I extend my deepest and most sincere appreciation to my dedicated supervisor Dr. med Lei Wang, whose unwavering commitment to my academic journey has been nothing short of inspiring. His guidance has not only enriched my academic understanding but has also fueled my motivation to strive for excellence. His mentorship has been a guiding light through the intricacies of research, propelling me towards innovative thinking and a deeper understanding of my field. I am truly fortunate to have had the privilege of his guidance and mentorship.

My heartfelt thanks also go to the diligent technicians in the laboratory, Dr.sc.hum Brigitte Neuber, Stefanie Grimm, Birgit Michels, Mandy Hinkelbein, Ann-Kathrin Bauer, and Madelaine Jansen, whose technical assistance and collaborative spirit greatly facilitated my experiment. Your dedication to maintaining a conducive research environment is truly commendable.

Of course, I would like to give my sincere thanks to my dear friends Dr. med. Sanmei Wang, Dr. sc. hum. Bailin He, Dr. med. Lin Min, Dr.med Huixiu Han, Dr.med Yuntian

Ding, Cand.Med Genqiao Jiang, Cand.Med David Sedloev. Their unwavering support, shared laughter, and genuine concern have not only lightened the burdens but have also reminded me of the importance of maintaining a balanced and fulfilling life. In addition, I would give my special thanks to Cand.Med Qian Chen and Dr.rer.nat Alejandro Hernandez Sanchez. As I reflect upon this chapter of my life, I am acutely aware of how those two people have left an indelible imprint on my memories and experiences. Their presence has been a reminder that amidst the rigors of academia, meaningful connections and shared moments are what truly color the tapestry of life. For their enduring friendship and the unwavering support, they've provided, I am truly thankful.

I extend my gratitude to my master's degree supervisor Prof. Dr. Qun Shen, whose guidance and mentorship during my earlier academic pursuit laid the foundation for the skills and knowledge I applied in this research.

Furthermore, to my beloved parents! Their boundless love, unwavering support, and countless sacrifices have formed the bedrock upon which my accomplishments stand. Their sacrifices, often unseen but deeply felt, have enabled me to pursue my dreams with dedication and determination. Through their selfless efforts, they have provided me with opportunities that have shaped my journey and nurtured my growth. As I stand on the threshold of new horizons, I carry with me the values, lessons, and unwavering love that they have bestowed upon me. I am forever grateful for their presence, their guidance, and the immeasurable impact they've had on shaping who I am today.

As a Chinese saying, “If life is just like the first sight, why sad farewell”. Each of person has contributed in their own unique way, and I am honored to have them as part of this journey. Thank you for being instrumental in my academic and personal growth.

Hao YAO

Heidelberg University, Germany, April. 2024

EIDESSTATTLICHE VERSICHERUNG

1. Bei der eingereichten Dissertation zu dem Thema

   Reshape of CAR-T cells by overexpression of TCF-1

   handelt es sich um meine eigenständig erbrachte Leistung.

2. Ich habe nur die angegebenen Quellen und Hilfsmittel benutzt und mich keiner unzulässigen Hilfe Dritter bedient. Insbesondere habe ich wörtlich oder sinngemäß aus anderen Werken übernommene Inhalte als solche kenntlich gemacht.

3. Die Arbeit oder Teile davon habe ich bislang nicht an einer Hochschule des In- oder Auslands als Bestandteil einer Prüfungs- oder Qualifikationsleistung vorgelegt.

4. Die Richtigkeit der vorstehenden Erklärungen bestätige ich. Die Bedeutung der eidesstattlichen Versicherung und die strafrechtlichen Folgen einer unrichtigen oder unvollständigen eidesstattlichen Versicherung sind mir bekannt. Ich versichere an Eides statt, dass ich nach bestem Wissen die reine Wahrheit erklärt und nichts verschwiegen habe.

Ort und Datum Unterschrift